TU WIEN

TECHNISCHE
UNIVERSITÄT
WIEN

DIPLOMARBEIT

Modeling Aortic Blood Pressure with Difference Equations

Ausgeführt zur Erlangung des akademischen Grades

Diplom-Ingenieurin

am

Institut für Analysis und Scientific Computing

der Technischen Universität Wien

unter der Anleitung von

Ao.Univ.Prof. i.R. Dipl.-Ing. Dr.techn. Felix Breitenecker

und

Univ.Lektor Dipl.-Ing. Dr.techn. Bernhard Hametner

durch

Laura Christine Lotteraner, B.Sc.

Matrikelnummer: 1225397

Glockengasse 21/4a

1020 Wien

Ort, Datum	Felix Breitenecker	Laura Lotteraner

Simplicity is the ultimate sophistication.

Leonardo Da Vinci, 1452–1519

Everything should be made as simple as possible,

but not simpler.

Albert Einstein, 1879–1955

Eidesstattliche Erklärung

Ich erkläre an Eides statt, dass ich die vorliegende Diplomarbeit selbstständig und ohne fremde Hilfe verfasst, andere als die angegebenen Quellen und Hilfsmittel nicht benutzt bzw. die wörtlich oder sinngemäß entnommenen Stellen als solche kenntlich gemacht habe.

_____	_____
Ort, Datum	Laura Lotteraner

Kurzfassung

Bluthochdruck ist weltweit ein bedeutender Risikofaktor für Todesfälle. Um Diagnose- und Präventionsmaßnahmen zu verbessern, ist es notwendig, die zugrundeliegenden Dynamiken des Herzkreislaufsystems zu verstehen, wobei mathematische Modelle hilfreich sein können. Während viele Aspekte des Blutdrucks in früheren Modellen diskutiert wurden, wird das Konzept der Re-Reflexionen von Blutdruckwellen am Herzen bisher kaum berücksichtigt.

In dieser Arbeit wird ein einfaches Differenzengleichungsmodell entwickelt und präsentiert, welches die zeitlichen Veränderungen des Blutdrucks in der Aorta, der größten Arterie des menschlichen Körpers, beschreibt. Das Modell behandelt Reflexionen von Blutdruckwellen im arteriellen System sowie Re-Reflexionen am Herzen. Dabei wird die Anzahl der Reflexionsstellen im arteriellen System variiert, sodass verschiedene Versionen des Modells entstehen. Die Reflexion am Herzen wird als konstant, aber auch, motiviert durch das periodische Öffnen und Schließen der Aortenklappe, als zeitabhängig angenommen.

Weitere Parameter sind die Geschwindigkeit der Pulswelle, die Entfernung zu den Reflexionsstellen, die Stärke der Reflexion an diesen sowie die Herzrate. Da die Modellparameter physiologischen Parametern entsprechen, können Referenzwerte aus der Literatur angegeben werden.

Die Eigenschaften des Modells werden ausführlich diskutiert, sowohl analytisch als auch numerisch. Für die analytische Diskussion wird auf Theorie über Differenzengleichungen zurückgegriffen, die für das Modell mit einer Reflexionsstelle auch eine explizite Lösung liefert. Die Modellgleichungen werden dann in MATLAB implementiert. Der Vergleich von Blutdruckkurven, die durch die Modellgleichungen generiert wurden, mit einer bei Patienten gemessenen zeigt die Eignung des Modells zur Beschreibung von Blutdruckdynamiken, abhängig von der Wahl der Parameter.

Die Analyse des Einflusses der verschiedenen Parameter auf Form und Größenordnung der

erzeugten Kurven zeigt viele Parallelen zu früheren Resultaten auf, was die Brauchbarkeit des Modells untermauert. Jene Beobachtungen, die keine Entsprechung in der Literatur haben, helfen beim Verständnis des Modells. Es zeigt sich, dass die Resultate verbessert werden können, wenn das Modell verfeinert wird, was weitere Forschung auf dem Gebiet motiviert. Eine solche Verfeinerung kann durch die Hinzunahme weiterer Reflexionsstellen, aber auch durch die genauere Modellierung der Reflexion am Herzen erzielt werden.

Abstract

Elevated blood pressure is a major cause of death not only in developed countries. In order to improve diagnosis and prevention it is crucial to understand the underlying dynamics. Mathematical models can help with this. While many aspects of blood pressure have been considered by previous researchers, the concept of re-reflections of blood pressure waves at the heart has been neglected in most models.

In this thesis a simple difference equation model is developed and presented. It describes blood pressure development over time in the aorta, the largest artery of the human body, depending on parameters that characterize both the heart and the arterial system. Reflections both at one and more sites in the arterial system as well as re-reflections at the heart are considered. Different versions of the model are obtained by varying the number of reflection sites in the arterial system. Reflection at the heart is assumed both constant and time-dependent, motivated by the periodic behavior of the aortic valve.

Further parameters include pulse wave velocity, distance to the reflection sites, reflection magnitudes and heart rate. Since the model parameters are linked to physiological parameters, reference values can be found in literature.

The model is discussed thoroughly, both analytically, using difference equation theory, and numerically. For the simplest versions of the model, considering only one reflection site, it is possible to solve the equations directly. To conduct numerical analysis the model is implemented in MATLAB. Comparison of blood pressure curves generated by the model and blood pressure curves measured in patients demonstrates that the model is able to represent reality to some extent, depending on the choice of parameters.

Studying the influence of different parameters on shape and magnitude of modeled curves reveals parallels to previous results which confirms the model's usefulness. Some observations, however, do not have a counterpart in literature. They increase understanding of the model. It is shown that results can be improved by refining the model, motivating

further research in the field. Refinement can be obtained by increasing the number of reflection sites and by a more detailed description of reflections at the heart.

Acknowledgements

First of all I want to thank Bernhard Hametner from the *Austrian Institute of Technology* for supervising this thesis. Thank you for your input and many fruitful discussions. I really appreciate the opportunity to work on a topic that combines my mathematical background with my interest in medicine.

I am grateful to Felix Breitenecker for enabling me to write this thesis in cooperation with the AIT. A big thank you also goes to my colleagues at the AIT who made long days of (not always successful) research much more enjoyable.

This thesis is the last step in a journey that took almost six years. I would like to acknowledge everyone who has been part of this journey. Without the help of my colleagues and friends I would not be where I am now. Thank you for six great years.

Special thanks go to my boyfriend who has not left my side since the first semester at university. I deeply appreciate your ongoing belief in me, even when I was in doubt.

Last but not least I wish to express my deepest gratitude for my parents. They have always supported me in every possible way. Thank you!

Contents

Introduction

1.1 Motivation

Cardiovascular diseases are a group of diseases affecting the heart and the vascular system, that is, the system of blood vessels. They are the main cause of death in many developed countries. Statistik Austria [42], for example, reports that 41.2% of all deaths in Austria were caused by cardiovascular diseases in 2016. One of the major risk factors for many types of cardiovascular diseases is hypertension, that is, elevated blood pressure. According to the World Health Organization [22] hypertension alone accounts for about 12.8% of the annual deaths worldwide.

For this reason it is important to understand how blood pressure dynamics in the cardiovascular system work. Researchers from a wide range of scientific fields such as medicine, computer science and mathematics have been working on this problem for centuries. Mathematical blood pressure models can help understand the dynamics and be used to interpret data obtained from patients.

In order to highlight different aspects of blood pressure dynamics, different types of models have been developed. Many of them include wave reflections [31], a concept that was first mentioned in the seventeenth century [27]. The idea is that blood pressure waves coming from the heart (*forward waves*) are reflected at certain sites in the arterial system and produce *backward waves*. Some researchers [4, 53] extended this idea and argued that these backward waves are re-reflected when they arrive at the heart. However, only very few models exist that address this issue and therefore it is only poorly understood so far.

1.2   Aim of the Thesis

The aim of this thesis is to develop a mathematical model of blood pressure dynamics that includes the concept of re-reflected pressure waves. It is desirable to use a model that is as simple as possible while at the same time including all the information necessary to describe wave reflections.

Difference equations are a useful tool for simple descriptions of time-discrete dynamical systems. They link the state of the system (which in the present case is blood pressure) at any point in time with the states at a finite number of previous points in time. The easiest type of difference equations are linear difference equations of the form

$$x_k = \begin{cases} \sum_{j=1}^{N} a_{kj} x_{k-j} + b_k, & k \in \mathbb{N}_{>N} \\ y_k, & k = 1, \ldots, N \end{cases}$$

with prescribed coefficients $a_{kj} \in \mathbb{R}$, inhomogeneities $b_k \in \mathbb{R}$ and initial values $y_k \in \mathbb{R}$. They have been studied extensively [1, 11] and solution techniques have been developed [21].

Even though blood pressure dynamics are time-continuous, difference equations can be used to describe them. We will fix a measuring site in the aorta and consider the development of blood pressure over time. Blood pressure at a fixed point in time can then be calculated as the sum of blood pressure values at previous times, determined by the choice of a finite number of reflection sites.

Besides formulating the model, the goal of the thesis is to analyze and present its properties such as the influence of various parameters on results. The model parameters and properties can be grouped in three types as follows:

- Technical properties that do not have any physiological equivalent,

- changes in the arterial system and

- changes in the heart.

1.3   Thesis Outline

The thesis consists of five chapters. In chapter 1 motivation for and the aim of the thesis are presented. Chapter 2 gives an overview of anatomy and physiology of the cardiovascular system and introduces terminology that will be used later on as well as the most important types of blood pressure models. In chapter 3 we will formulate the model, considering only one reflection site. We will then analyze its properties and the influence of parameters. Chapter 4 introduces more reflection sites and studies how this improves results. In chapter 5 the results are discussed and applications of the model are suggested.

An appendix provides material on linear difference equations and supplementary data for chapter 4.

Pressure Waves in the Arterial System

In order for the models developed in chapters 3 and 4 to make sense it is crucial to know about the functioning of the cardiovascular system. It is also important to understand the technical terminology that will be used later on. This chapter aims to explain both as well as give an overview of the models of the cardiovascular system that are currently in use.

2.1 Anatomy and Physiology of the Cardiovascular System

Information about anatomy and physiology of the cardiovascular system can be found in various medical and biomedical engineering textbooks [10, 13, 27, 32]. The role of the cardiovascular system is to supply body cells with oxygen, nutrients and other substances such as hormones, to cart off waste products and to maintain a stable body temperature. It consists of two interconnected parts, the heart as the pumping motor and the vascular system as a network for distribution. The carrier liquid is blood.

2.1.1 The Heart

Anatomy of the Heart. Even though mostly considered "the pump" of the cardiovascular system the heart consists of two pumps working in parallel. The right side pumps deoxygenated blood into the lung (*pulmonary circulation*) where it is reoxygenated and carried back to the left side of the heart. Oxygenated blood is distributed in the body (*systemic circulation*) by the left side of the heart, returning to the right side to complete the circle.

The heart is a hollow muscle with muscle tissue consisting of a special type of muscle cells, *cardiomyocytes*, that together form the *myocardium*. Cardiomyocytes mainly differ from skeletal muscles in two aspects: their contractibility is lower but at the same time they are more resistant to fatigue [13]. Pumping is performed by rhythmic contractions of the myocardium that lead to a change in size of the cavities of the heart.

Each of the two sides of the heart is comprised of two cavities, the *atrium* and the *ventricle*. The atria, positioned in the upper half of the heart, collect the blood from their respective veins, the *venae cavae* for the right and the *pulmonary vein* for the left atrium. From the atria the blood is transported to the ventricles through the *tricuspid valve* and *mitral valve*, respectively. The valves prevent blood from flowing back to the atria from the ventricles. The ventricles are positioned in the lower part of the heart and contract to push the blood into their respective arteries, the *pulmonary artery* for the right and the *aorta* for the left side. At the exit of each ventricle a second valve, the *pulmonary valve* for the right and *aortic valve* for the left side, prevents blood to flow back into the ventricle. Since the systemic circulation is much larger than the pulmonary circulation the left ventricle needs more pumping power to supply it. Therefore the muscle tissue is much stronger in the left ventricle compared to the right one.

A schematic illustration of the anatomy of the human heart is presented in figure 2.1. The sides are reversed with respect to their names due to the position of the observer.
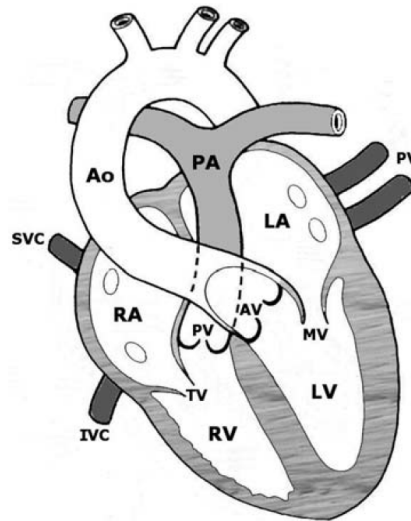
Figure 2.1: Schematic cross section of the heart, from [13]. **Cavities**: RA - right atrium, LA - left atrium, RV - right ventricle, LV - left ventricle. **Valves**: TV - tricuspid valve, MV - mitral valve, PV - pulmonary valve, AV - aortic valve. **Vessels**: SVC - superior vena cava, IVC - inferior vena cava, PV - pulmonary vein, PA - pulmonary artery, AO - aorta.

Electromechanical Properties of the Heart. The rhythmic pumping of the heart is regulated by an electrical impulse system. The primary pacemaker of the heart is the *sino-atrial node*, a bundle of nervous tissue located in the wall of the right atrium. Through

its automatic self-excitation a electrochemical signal is produced at a rate of about 1 sec^{-1}. The signal spreads through the myocardium as a depolarization wave, distributed by so-called *nodal myocytes*. First the wave reaches the atria and causes them to contract. From the atria the wave proceeds to the *atrio-ventricular node* that is located at the lower part of the interatrial wall. This atrio-ventricular node works as a propagator for the signal but can also take the role of a secondary pacemaker. At the atrio-ventricular node the depolarization wave experiences a delay of around 100 ms before it proceeds to the ventricles, causing them to contract almost synchronously. Recording the depolarization wave produces an *electrocardiogram* (ECG). Opening and closing of the four valves is controlled by blood pressure changes in the vessels and heart cavities due to contractions. While the rhythm of excitation of the sino-atrial node is about 1 sec^{-1}, corresponding to a heart rate of 60 beats per minute (bpm), it is not steady. The body has a variety of control mechanisms to influence the heart rate according to its needs, mainly the central nervous system and the release of hormones into the blood. A resting athlete's heart may have only 45 bpm while under physical exercise the heart rate can reach up to 200 bpm.

The Cardiac Cycle. A cardiac cycle consists of two phases, *systole* and *diastole*. There are various definitions for both phases that differ slightly. Systole is generally defined as the time between closing of the mitral valve and closing of the aortic valve. Another definition uses the electric activity of the myocardium, detected by the ECG. For the purpose of this thesis it will be safe to define systole as the period of ventricular ejection [13]. Diastole will be accordingly defined as the rest of the cardiac cycle, either using the closing times of the valves or myocardial activity. At rest, when the heart rate is around $60 - 70$ bpm, the diastole takes up about two thirds of the cardiac cycle. An increase in heart rate mostly implies a decrease in diastole length while systole length remains almost constant. Only at very high heart rates systole length decreases too [13].

2.1.2 The Vascular System

In analogy to the heart's two sides the vascular system consists of two separate circulations. The *pulmonary circulation* is supplied with deoxygenated blood by the right ventricle and transports it through the lung. Reoxygenated blood is carried back to the left atrium. The *systemic circulation* provides the body cells with oxygenated blood and carts off deoxygenated blood. It is supplied by the left ventricle and leads into the right atrium.

Each of the two circulations is a closed system that can be divided into three compartments: arteries, *microcirculation* and veins. Both networks consist of branching and merging vessels of varying elasticity and decreasing size distal to the heart with around twenty generations of bifurcations from the heart to the most distal vessels. Arteries and veins transport blood from and to the heart, respectively. In between them are the capillaries, arterioles and venules, also referred to as *microcirculation*, and responsible for various exchange processes between blood and body cells.

In this thesis the focus will lie on the behavior of large arteries in the systemic circulation. We will therefore concentrate on their properties and only give a short overview of the nature of other vessels. From the left ventricle blood is pumped into the aorta, the largest artery.
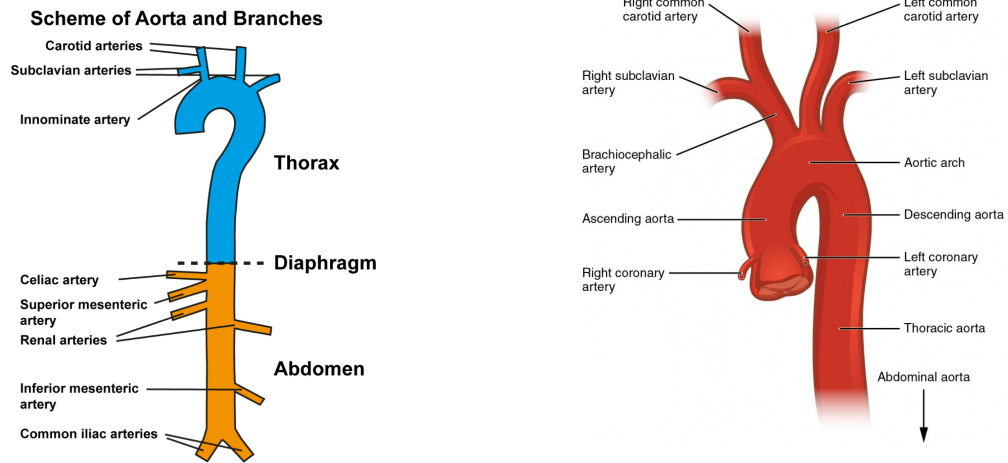
(a) Schematic image of the aorta and its branches. Thoracic and abdominal aorta are separated by the diaphragm. From [24].

(b) Schematic image of the thoracic aorta and its branches. Separation into ascending aorta, aortic arch and descending aorta. From [28].

Figure 2.2: Schematic images of different parts of the aorta and their branches.

The Arterial System.   The aorta not only is the main distributing artery with branches to all the different areas of the body, it also serves as a so-called *Windkessel*. Blood is ejected from the ventricle in a discrete way. Because the aorta, in particular in regions proximal to the heart, is more distensible than more distal arteries it can extend during systole to store blood, thus acting as a reservoir. During diastole the aorta contracts, releasing the stored blood. This process smooths out the change of blood flow and blood pressure throughout the cardiac cycle, similar to the way an air chamber (German: Windkessel) transforms pulsatile flow to a steady one.

Stretching along the entire torso with a length of about 50 cm in a human adult, the aorta can be divided into segments with respect to different properties. One classification is into *thoracic* and *abdominal* aorta, separated by the *diaphragm*, see figure 2.2 (a). These two segments can be further divided into the *aortic root* at the opening of the aortic valve, the *ascending aorta* immediately after it, the *aortic arch* and the *descending aorta*, see figure 2.2 (b). The coronary arteries, supplying the heart, originate at the aortic root. Arteries branching off in the aortic arch supply the upper half of the body (arms, neck, head) while the arteries for all the abdominal organs originate in the abdominal aorta. At the *aortic bifurcation* the aorta terminates and splits up into the *common iliac arteries* that supply the pelvis and the lower limbs. From origin to termination aortic diameter decreases.

Even though the Windkessel effect of the large arteries weakens the differences in pressure and flow in the arterial system between systole and diastole, both pressure and flow fluc-

tuate throughout the cardiac cycle. Since the object of this thesis is aortic blood pressure we will omit further information about blood flow. Blood pressure is oscillating between a minimum (*diastolic pressure*, DBP) and a maximum (*systolic pressure*, SBP) value. Their difference is named *pulse pressure* (PP). By convention, blood pressure is expressed in millimeters of mercury, mmHg. In a healthy human adolescent the values are

$$DBP \approx 80 \text{ mmHg}, \qquad SBP \approx 120 \text{ mmHg}, \qquad PP \approx 40 \text{ mmHg}$$

in the ascending aorta (*central aortic pressure*).

The Microcirculation.   With each bifurcation of arteries the size decreases until they are called *arterioles*. The distinction between arteries and arterioles according to the vessels' sizes is made at rather arbitrary values. From the arterioles blood is transported to the *capillaries*, the vessels where the exchange of oxygen and nutrients between blood and body cells takes place. Analogously to arterioles, the smallest vessels leading away from capillaries are named *venules*. Their size increases as they lead back towards the heart until, at a rather arbitrary threshold, they are called veins.

The Venous System.   In most parts of the body, apart from the skull, the venous network mirrors the arterial one. Many large arteries and their corresponding veins run together with nerves surrounded by connective tissue. While blood flow in arteries is connected directly to the cardiac cycle and thus quite regular, blood flow in veins depends on other factors such as muscle contractions and respiration and displays significant irregularities. To prevent backflow, large and medium sized veins have valves. Blood pressure in veins is considerably lower than in arteries.

Wave Reflection.   Both blood flow and blood pressure in arteries display one-dimensional wave-like behavior, propagating along the arterial system. Pressure waves can propagate in either direction of the artery. At any site in the system where properties such as elasticity of the vessel wall change, at every bifurcation and also at the terminations of the arterial system reflected flow and pressure waves arise, see figure 2.3.
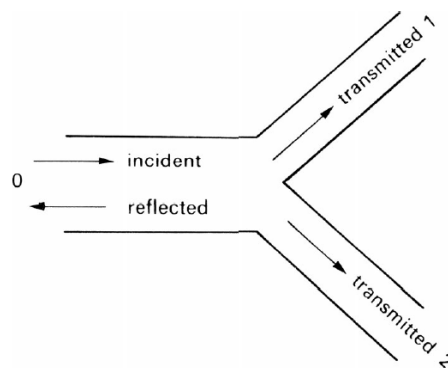
Figure 2.3: Schematic image of flow and pressure wave reflection at an arterial bifurcation. From [10].

Thus, at any site in the arterial system measured flow (Q, liters per minute) and pressure (P, mmHg) can be split up into their forward (i.e. away from the heart) and backward (i.e. towards the heart) component,

$$Q = Q^f + Q^b \qquad \text{and} \qquad P = P^f + P^b.$$

The reflected waves are responsible for the difference in shape between flow and pressure waves, compare figures 2.4 (a) and (b). They display the development of flow and pressure at a fixed measuring site in the ascending aorta over time.

(a) Aortic flow　　　　　　　　**(b)** Aortic pressure
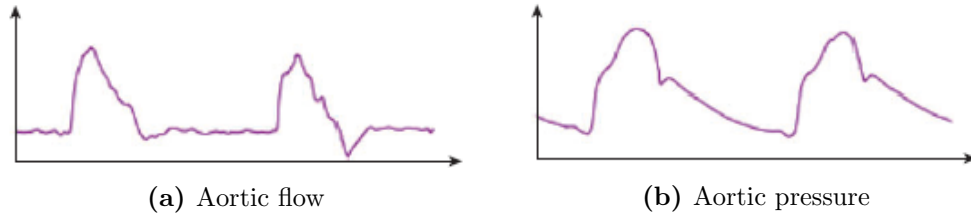
Figure 2.4: Pressure and flow wave in the ascending aorta. From [48].

While reflected pressure waves add up with the original forward traveling wave, reflected flow waves are subtracted from the original wave. Both amplitude and timing of reflected waves depend on various parameters such as the number and location of reflection sites, pulse wave velocity and damping effects. Even though the role wave reflections play in physiology and pathology of the cardiovascular system has been discussed controversially [31] most researchers have reached the conclusion that they must be included in models and analysis of the cardiovascular system [27]. The concept of wave reflection can be extended by including reflections at the heart. Each of forward and backward flow and pressure would therefore be composed of multiple waves. Evidence for the occurence of these *re-reflections* can be found in the shape of the forward flow wave [4].

2.1.3 Blood

Blood is a suspension of blood cells (45% of volume) in blood plasma (55% of volume). The relative contribution of blood cells to blood volume is called *hematocrit*. 92% of blood plasma are water while the rest is comprised of proteins, small molecules and ions. Red blood cells (*erythrocytes*) are mainly responsible for the transport of oxygen in the blood and represent 97% of blood cell volume. The rest consists of white blood cells (*leukocytes*) that are important for the immune system of the body and platelets (*thrombocytes*), essential for blood coagulation at sites of injury.

In the following we will be interested in the viscosity of blood a detailed definition and description of which can be found in literature [54]. The viscosity of blood depends on both the viscosity of the plasma and the hematocrit. Unfortunately it is not constant but also subject to size, shape and flexibility of the red blood cells, blood velocity, the size of

the blood vessel and temperature. In large arteries, however, these influences are of little importance and can be neglected [47], leading to the assumption of a constant viscosity value η.

2.2 Modeling the Cardiovascular System

Applying mathematical methods in cardiovascular research can serve different purposes. Some mathematical models aim to interpret measured blood pressure (and flow) values with respect to their influence on cardiovascular disease. Other models aim to find a way of calculating blood pressure (and flow) values depending on parameters of the system. In this section we will give an overview of previously developed models of both types. First, however, the characteristic features of a blood pressure curve and some parameters of the cardiovascular system will be introduced.

2.2.1 Characteristics of a Blood Pressure Curve

Even though measured blood pressure curves differ from person to person, they all display characteristic features. The shape also depends on the position within the vascular system where the pressure is measured. Since we will concentrate on the aorta in this thesis, we will also present the features of an aortic blood pressure wave, see figure 2.5.
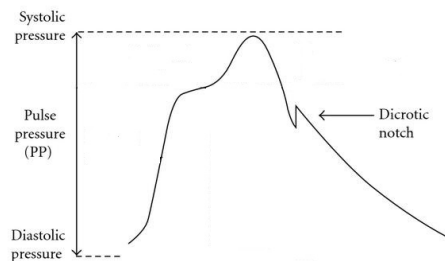
Figure 2.5: Characteristic features of a blood pressure wave, including shoulder point and dicrotic notch. Modified from [44].

In systole an aortic blood pressure wave consists of a steep systolic upstroke, usually a shoulder point (see section 2.2.4) and a systolic peak. The end of systole is marked by an incision, the *dicrotic notch*, that can be more ore less distinct. During diastole blood pressure declines slowly and resembles an exponential decay.

2.2.2 Terminology

Impedance. It has been found [45, 46] that an analogy between electrical transmission line theory and pulse wave propagation can be drawn where pressure corresponds to voltage and flow to current [13]. Thus, also the term *impedance*, originally describing a relation

between voltage and current, can be used to describe the arterial system. Since both pressure and flow are propagated through the arterial system as waves they can be analysed in the frequency domain and separated into their harmonics by Fourier analysis [54]. Then, for each harmonic, *input impedance* at a specific site in the arterial system is defined as

$$Z = \frac{P}{Q} \quad \in \mathbb{C}, \tag{2.1}$$

i.e. the fraction of pressure and flow at the given site [31]. This complex number gives information about the ratio of amplitudes as well as on the phase difference between the two harmonics [54]. Analogously, *characteristic impedance* is defined as the ratio

$$Z_0 = \frac{P_0}{Q_0} \quad \in \mathbb{C} \tag{2.2}$$

where P_0 and Q_0 refer to pressure and flow in a setting where no reflections are present [31]. The calculation of impedance gives meaningful results only under certain conditions such as linearity and time invariance that the arterial system at least approximates [54]. If blood viscosity and viscoelasticity of the wall are neglected, which is a good approximation in large arteries, it is possible to approximate characteristic impedance by the real number

$$Z_0 = \frac{\rho \cdot c_0}{A_c} \quad \in \mathbb{R}, \tag{2.3}$$

where ρ denotes the density of blood, c_0 is the pulse wave velocity (see below) and A_c is the cross-sectional area of the vessel [54].

Compliance.   To describe the Windkessel effect of large arteries it is necessary to know how much the arteries extend when pressure rises during systole. This information is expressed by *compliance*, defined by

$$C = \frac{\Delta V}{\Delta P} \quad \in \mathbb{R},$$

i.e. the ratio of change in volume and change in pressure. Its inverse is called *arterial stiffness* [27]. Because the relationship between pressure and volume is nonlinear, the value of C depends on the value of P around which change is considered [54], see figure 2.6. Since in blood vessels with their approximately cylindrical shape change in volume is proportional to change in cross-sectional area, the use of *area compliance*

$$C_A = \frac{\Delta A_c}{\Delta P} \quad \in \mathbb{R},$$

where A_c denotes cross-sectional area, instead of C makes sense [54].

Pulse Wave Velocity.   The velocity with which a blood pressure wave (*pulse wave*) propagates through the arterial system is called *pulse wave velocity* (PWV) and generally denoted by c_0. It has been established as a marker of arterial stiffness and cardiovascular
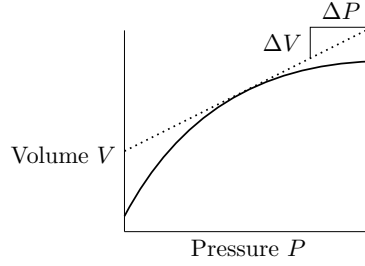
Figure 2.6: Illustration of the dependence of compliance on values of P. The solid curve represents the physiological relationship while the dotted line has slope C. Reproduced after [54].

risk [27]. Indeed it has been shown [54] that the relationship

$$c_0 = \sqrt{\frac{A_c}{\rho \cdot C_A}} \tag{2.4}$$

holds where A_c denotes the cross-sectional area, ρ denotes blood density and C_A is area compliance. There are several methods to obtain wave velocity for a given arterial system. The most direct method is to measure the time it takes the foot of the wave to travel over a known distance. Other methods use equation (2.4) or changes in flow and area [54]. By equation (2.3) pulse wave velocity can be linked to characteristic impedance.

Resistance [54]. Blood flow and pressure drop in a uniform tube of radius r and length L can be linked using Poiseuille's law

$$Q = \frac{\Delta P \cdot \pi \cdot r^4}{8 \cdot \eta \cdot L} \tag{2.5}$$

where η denotes the (assumed to be constant) viscosity of blood. Inserting $R = 8\eta L/\pi r^2$ into equation (2.5) yields

$$\frac{\Delta P}{Q} = R,$$

which is in accordance with Ohm's law of electricity that links voltage drop and current via resistance. Thus, R is called *resistance* of the vessel P and Q are referring to. Using the dimensions of different vessel types it can be seen that the main resistance of the arterial tree is found in the small arteries and arterioles. It is often named *peripheral resistance*. As for impedance calculation of peripheral resistance only makes sense for linear and time-invariant systems.

Inertance [54]. Consider Newton's law,

$$F = m \cdot \frac{dv}{dt},$$

where F is force, m is mass and v is the velocity of blood. For a vessel with given length L and cross-sectional area A_c the net force is given by $F = \Delta P \cdot A_c$ and mass is given by

$\rho \cdot L \cdot A_c$. The rate of change of velocity, dv/dt, can be expressed in terms of volume flow by $(1/A_c) \cdot dQ/dt$. Combining these identities with Newton's law yields

$$\Delta P \cdot A_c = \rho \cdot L \cdot \frac{dQ}{dt}$$

which simplifies to

$$\Delta P = I \cdot \frac{dQ}{dt}$$

by defining *inertance* $I = \rho \cdot L/A_c$.

2.2.3   Mathematical Models of the Cardiovascular System

Many different models have been developed to describe the flow of blood in the cardiovascular system both in time and frequency domain [39], accounting for different properties. This section will only mention a few types of models in the time domain to give an idea of the diversity in models.

Fluid Dynamics [13].   One large class of models often referred to as *distributed models* [54] uses fluid dynamics to describe blood flow. Due to the properties of blood effects of viscosity can only be neglected if the vessel to be modeled is large enough. Since in this thesis we are only interested in the behavior of blood flow in the aorta we will focus on this case. Flow can be described by the *Navier-Stokes* equations, partial differential equations linking blood flow velocity, not to be confused with wave velocity [54], and pressure in a three-dimensional domain. Usually in this class of models only segments of the arterial system are considered, resulting in a need for boundary conditions not only at the vessel wall but also at the *inlet* and the *outlet* boundary. To further improve the model fluid dynamics can be linked with continuum dynamics, taking into account displacements of the vessel wall. Unfortunately these full three-dimensional models are very complex due to the large number of vessels in the system and their different length scales.

For this reason simplifications of the 3D models have been developed. One major simplification is to reduce the number of dimensions in space to one by integrating over the cross-sectional area of the vessel, thus avoiding the explicit modeling of arterial wall mechanics [12]. Even though the information these models provide lacks the precision of the three-dimensional ones they are able to describe the propagation of pressure waves in arteries. In particular they enable us to study the global circulation instead of only artery segments.

Another possibility is the assumption of two dimensions such that radial variation of blood flow and pressure in an axisymmetric tube can be represented [39].

Windkessel Models [52].   An entirely different approach is taken by *Windkessel models* that make use of the analogy between the cardiovascular system and an electric circuit. They are zero-dimensional, *lumped parameter* models meaning they contain no spatial in-

formation. Spatially distributed phenomena as well as the wave-like nature of pulse waves are ignored. The first so-called two-element Windkessel model was introduced by Otto Frank [14] already in 1899 and describes hemodynamics with respect to compliance and resistance, linking aortic pressure and flow by Ohm's law. Because significant differences were found between measured pressure and the one modeled by the two-element Windkessel during systole, a third element was added: characteristic impedance of the aorta. This three-element Windkessel links the original two-element Windkessel to wave phenomena due to the relationship represented in (2.3). It has been found, however, that the three-element Windkessel only produces realistic aortic pressure and flow if the parameters are chosen in a way that does not reflect the properties of the arterial system [43]. A solution to this problem is the introduction of a fourth element, total inertance of the arterial system [7]. Because this inertance is difficult to estimate, however, often the three-element Windkessel is used. Windkessel models serve a variety of purposes, from offering boundary conditions for other models to the determination of parameters.

Tube Models [54]. Because distributed models are very complex and the easier Windkessel models ignore the wave-like behavior of blood pressure and flow, a new class of models has been proposed. In *single tube models* the entire arterial system is modeled as a single tube that represents the aorta combined with a model of the peripheral vascular beds, often a Windkessel model. This type of model can be refined by including the tapering of the aorta. Wave reflections are accounted for in single tube models with the simplifying assumption that they all originate in the same reflection site. Often [10, 54] the aortic bifurcation is mentioned as the principal bifurcation site. Instead of a single tube an *asymmetric T-tube* can be used where reflections from the upper (head and arms) and lower body parts are distinguished.

Unlike distributed and Windkessel models the term *tube model* does not refer to a particular mathematical method. The characterizing property of tube models is the geometry. In this thesis a single tube as well as an asymmetric T-tube model will be realized with difference equations.

2.2.4 Mathematical Assessment of Pulse Wave Reflection

The models discussed in the previous section help increase understanding of the cardiovascular system. Often, however, it is desired to interpret pulse wave data obtained from measurements in patients with respect to wave reflection. In this section we will present some methods to do that.

Wave Separation Analysis. It has been mentioned above that both flow and pressure can be split up in their forward and backward component. Since it is not possible to measure the components separately, it was necessary to develop a method to calculate them from measured flow and pressure values. The method presented here [20, 53] makes use of the analogy of arteries and transmission line theory and includes both characteristic

15

impedance Z_0 and input impedance Z of the aorta. First of all consider once again

$$P = P^f + P^b \qquad \text{and} \qquad Q = Q^f + Q^b. \tag{2.6}$$

Forward and backward pressure are linked by

$$P^b = \Gamma \cdot P^f \tag{2.7}$$

where the reflection coefficient Γ is defined as

$$\Gamma = \frac{Z - Z_0}{Z + Z_0}. \tag{2.8}$$

Combining equations (2.6)-(2.8) with the definition of input impedance,

$$Z = \frac{P}{Q},$$

yields

$$P^{f/b} = \frac{1}{2}(P \pm Z_0 \cdot Q) \qquad \text{and} \qquad Q^{f/b} = \frac{1}{2}\left(Q \pm \frac{P}{Z_0}\right).$$

Together with an appropriate approximation of Z_0 such as equation (2.3) this is a simple and fast method for quantifying wave reflection and its influence of pressure and flow. Since its development wave separation analysis has been used in a variety of clinical studies, confirming that wave reflections play a major role in cardiovascular dynamics [27]. An illustration of a pressure curve separated in its forward and its backward component can be found in figure 2.7.
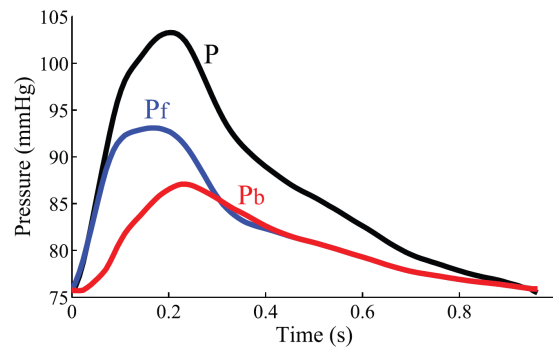
Figure 2.7: Separation of a pressure wave into its forward (blue) and backward (red) component. Modified from [36].

Augmentation Index. Another way of quantifying pulse wave reflection is the *augmentation index* (AI), defined as

$$AI = \frac{AP}{PP}$$

where AP indicates the late systolic boost in the aortic pressure wave [27] and PP is the pulse pressure. The late systolic boost is the height of the peak above the shoulder of the wave where the shoulder is defined as the first concavity on the upstroke of the wave [16]. Several methods are available for the determination of AP [27]. The definition of the AI is illustrated in figure 2.8.
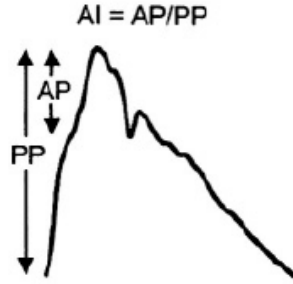
Figure 2.8: Augmentation Index (AI) is defined as the ratio of AP and PP, from [56].

The advantage of using the AI instead of pulse wave separation lies in the fact that only the measurement of pressure is required. Unfortunately, however, augmentation index does not only depend on the magnitude of wave reflection but also on the time delay between original and reflected wave, limiting its usefulness for estimating the magnitude of reflections [54].

Wave Intensity Analysis [34]. Instead of decomposing waves in the frequency domain using Fourier analysis it is possible to decompose waves into a sequence of small *wavefronts*. They are best described by the change of properties during a sampling period Δt, such as

$$dP = P(t + \Delta t) - P(t).$$

The starting point of *wave intensity analysis* are the one-dimensional Euler equations describing flow in an elastic tube with respect to pressure P and flow velocity U. Using the methods of characteristics one can derive the *water hammer equations*

$$dP^{f/b} = \pm \rho \cdot c_0 \cdot dU^{f/b}$$

with blood density ρ and pulse wave velocity c_0 and, with their help, separate pressure and velocity into their forward and backward component. Wave intensity is defined by $dI_w = dP \cdot dU$ and measures the flux of energy per unit area carried by the wave.

Wave intensity analysis provides information about several aspects of the arterial mechanics. At the moment, however, it is mostly a research tool and not yet widely used for clinical applications.

17

Difference Equation Model Using One Reflection Site

In our first model we imagine the arterial system to be a single uniform tube with the heart on one end, hereafter referred to as (*aortic*) *valve* or *heart*, and an elastic boundary on the other, herafter referred to as (*distal*) *reflection site*, see figure 3.1. Different authors [23, 27, 59] have already showed this idea to be reasonable by comparing experimental results with those computed using the model. The single tube model has already been used to model repeated reflections in the arterial system [4] but with an approach different from ours.

We are interested in describing the time curve of blood pressure P in a fixed site in the ascending aorta, close to the aortic valve, hereafter referred to as *measuring site*. This *aortic root* is of particular interest because it allows to assess the interaction of reflections in the vascular system and the heart [8]. The distance between measuring site and distal reflection site will be named *effective length* in this thesis. Usually this refers to the length of the tube and is connected with the term *effective reflection site* [25], a terminology expressing the reduction of multiple reflection effects to one. Justification for our usage, however, will be given in sections 3.2 and 3.4.
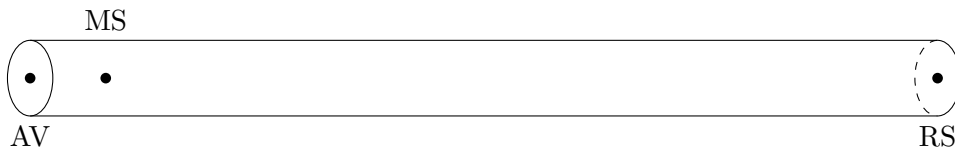
Figure 3.1: Tube model of the arterial system as presented above. AV - aortic valve, MS - measuring site, RS - distal reflection site.

The tube models developed so far have at least one spatial dimension [59] and take into

account the elastic properties of the tube wall. Our model, however, will be dimensionless, only depending on time. All spatial and elasticity information will therefore be integrated in various constants and parameters, as explained below.

Several parameters and variables are needed to describe the reflections arising on both ends of the tube. They can be grouped as follows:

Technical parameters:

- ◆ Time will be described by the discrete variable $k \in \mathbb{N}$ where the length of a time step $k \to k + 1$ is given by the *step size* τ. Accordingly, we are looking for the discrete function $(P_k)_{k \in \mathbb{N}}$ and all the upcoming time-dependent parameters will be given in the same form.

Properties of the arterial system:

- ◆ The reflection coefficient at the distal reflection site, arising from a resistance [25] that represents the properties of the arterial bed [27] and the damping of the wave by the fluid (blood) [27], will be denoted by R_D. It was first argued [45] and later verified by experiments by Taylor [46] that to some extent an electric transmission line can be used as an analogue of a fluid-filled elastic pipe. Thus, the reflection coefficient is given [20] by

$$\Gamma = \frac{Z - Z_0}{Z + Z_0} = |\Gamma| e^{i\phi} \quad \in \mathbb{C},$$

  where Z_0 denotes the characteristic impedance, see equation (2.2), of the tube and Z the input impedance, see equation (2.1). The complex number Γ can not be used for our model because it requires separation of the given wave in its harmonics using Fourier transformation. In our model, however, we will consider the wave in the time domain and thus need a reflection coefficient that does not depend on frequency. The ratio of the amplitudes of forward and reflected wave, derived by classical wave separation, can be used as a real valued approximation [54], i.e.

$$\Gamma \approx R_D = \frac{P^b}{P^f} \quad \in \mathbb{R}.$$

  In some papers [51] this real number is called *reflection magnitude* and denoted by RM. Amplitudes are always positive, and due to the aforementioned damping effects the amplitude of the reflected wave will always be less than the original one [27], yielding $0 \leqslant R_D < 1$.

  The choice of R_D is coupled with the position of the distal reflection site, i.e. *effective length* of the tube [9, 37, 51].

- ◆ The number of time steps it takes a pressure impulse to travel from the measuring site to the distal reflection site and back will be denoted by the time constant $t_b \in \mathbb{N}$.

It includes information on both the distance between measuring site and reflection site and PWV. It has been shown [51] that the time of return of the reflected wave is also affected by the phase shift that occurs in the complex description of reflection. Due to our simplification of the reflection coefficient, this *time delay* must be included in the time constant t_b. As mentioned above, the choice of the distal reflection site and with it the choice of t_b is coupled with the choice of the reflection coefficient.

According to prior studies [38] wave propagation in the arterial system is fast enough to ensure that the return time is much shorter than the duration of one cardiac cycle. In fact, we will see in section 3.5 that the return time is even significantly shorter than systole duration.

- Analogously to t_b, the number of time steps it takes a pressure impulse to travel from the measuring site to the aortic valve will be denoted by $t_f \in \mathbb{N}$. This time constant is computed from distance between measuring site and aortic valve and PWV. Again, the time constant should include the time delay produced by complex reflection. Seeing that the measuring site is very close to the valve we can demand $t_f \ll t_b$.

Properties of the heart:

- The reflection coefficient at the aortic valve will be denoted by R^{av} where, with the same arguments as above, $0 \leqslant R^{av} < 1$. Since reflection intensity depends on the state of the valve (open or closed or somewhere in between), R^{av} is ideally chosen to be time dependent, i.e. $R^{av} = (R^{av}_k)_{k \in \mathbb{N}}$ [49]. Other choices, such as the limit cases $R^{av} \equiv 1$, i.e. treating the heart as a total reflector and $R^{av} \equiv 0$, i.e. treating the heart as a total absorber, are possible as well [49].

- While the distal reflection site is a closed end that only produces reflections, the heart also operates as a driving force for pressure dynamics. During systole, when the valve is open, blood is pumped into the system, increasing the pressure. This phenomenon is represented by the (discrete) function $(P^{in}_k)_{k \in \mathbb{N}}$. Unfortunately knowledge about this systolic input is limited [45], so one goal of this thesis is to find a good estimation

To formulate the equations we now split the total pressure P_k into its forward and backward component P^f_k and P^b_k, i.e. $P_k = P^f_k + P^b_k$, see section 2.1.2.

Using everything defined above we can find the equations

Model 1

$$P^f_k = P^{in}_k + P^b_{k-2t_f} R^{av}_{k-t_f}, \qquad\qquad k \in \mathbb{N}_{>2t_f}, \qquad (3.1\text{a})$$

$$P^b_k = P^f_{k-t_b} R_D, \qquad\qquad k \in \mathbb{N}_{>t_b}. \qquad (3.1\text{b})$$

Figure 3.2 illustrates the idea behind equation (3.1a). For equation (3.1b) the situation is practically the same, only in the opposite direction.
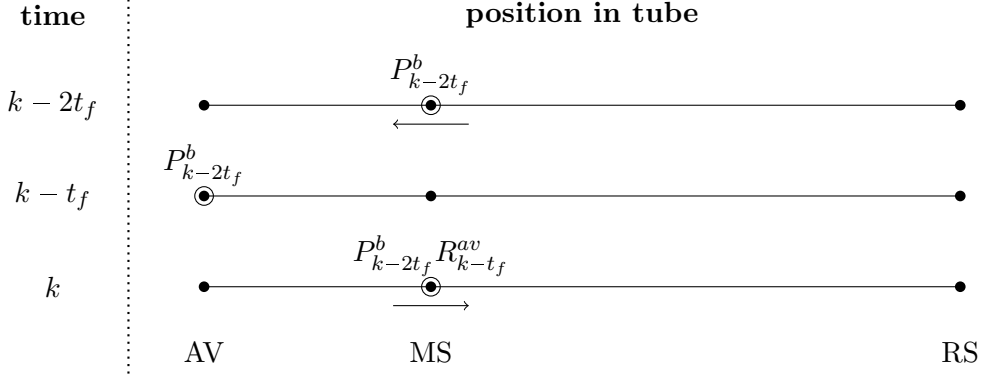
Figure 3.2: Backward pressure is reflected at the time-dependent aortic valve as described in equation (3.1a).

It can be seen in model 1 that for $R_D = 0$ there holds $P_k^b = 0$ and thus $P_k = P_k^f = P_k^{in}$ which makes the idea of a difference equation model redundant. For this reason from now on we will assume $0 < R_D < 1$.

3.1 Difference Equation Solutions

Inserting (3.1a) into (3.1b) and vice versa yields the two independent linear equations

$$P_k^f = P_k^{in} + P_{k-2t_f-t_b}^f R_D R_{k-t_f}^{av}, \qquad k \in \mathbb{N}_{>2t_f+t_b}, \qquad (3.2a)$$

$$P_k^b = P_{k-t_b}^{in} R_D + P_{k-2t_f-t_b}^b R_D R_{k-t_b-t_f}^{av}, \qquad k \in \mathbb{N}_{>2t_f+t_b}. \qquad (3.2b)$$

Obviously both equations are of order N where $N = 2t_f + t_b$. Since they only define a recurrence relation for $k > N$, we need to prescribe initial values $P_k^f = \bar{P}_k$ and $P_k^b = \hat{P}_k$, $k = 1, \ldots, N$. Then we know from standard literature [1, 11] that the initial value problems

$$\begin{cases} P_k^f = P_k^{in} + P_{k-2t_f-t_b}^f R_D R_{k-t_f}^{av}, & k \in \mathbb{N}_{>N}, \\ P_k^f = \bar{P}_k, & k = 1, \ldots, N \end{cases}$$

and

$$\begin{cases} P_k^b = P_{k-t_b}^{in} R_D + P_{k-2t_f-t_b}^b R_D R_{k-t_b-t_f}^{av}, & k \in \mathbb{N}_{>N}, \\ P_k^b = \hat{P}_k, & k = 1 \ldots, N, \end{cases}$$

defined by equations (3.2a) and (3.2b) and initial conditions, have unique solutions. Deriving these solutions with traditional methods is tedious since it requires rewriting each equation into a system of equations of first order, solving the homogeneous equation and applying the variation of constants formula [1]. Fortunately, a solution theory was developed by Mallik [21] for exactly this type of equation. The procedure is very technical

and only provided here for completeness. Following it is not necessary to understand the fundamental aspects of the model.

Let us first consider equation (3.2a). Again, define $N = 2t_f + t_b$ and transform the equation to

$$P^f_{k+N} = P^{in}_{k+N} + P^f_k R_D R^{av}_{k+N-t_f}, \qquad k \in \mathbb{N}.$$

In his paper Mallik proves that for equations of the type

$$y_{k+N} = \sum_{j=1}^{N} a_{k,j} y_{k+N-j} + x_{k+N}, \qquad k \in \mathbb{N},$$

with the initial values $y_1, \ldots, y_N$ and prescribed values x_k the explicit form of the unique solution is given by

$$y_{k+N} = \sum_{j=1}^{N} d_{k,j} y_{N+1-j} + \sum_{j=2-k}^{0} d_{k,j} x_{N+1-j} + x_{k+N}, \qquad k \in \mathbb{N}, \tag{3.3}$$

with the coefficients

$$d_{k,j} = \sum_{r=1}^{k+j-1} \sum_{\substack{(l_1,\ldots,l_r) \\ 1 \leqslant l_1,\ldots,l_r \leqslant N \\ l_r \geqslant j \\ l_1+l_2+\ldots+l_r=k+j-1}} \left(\prod_{m=1}^{r} a_{k+l_m-\sum_{n=1}^{m-1} l_n, l_m} \right) \tag{3.4}$$

for $j = 2 - k, \ldots, N$ and $k \in \mathbb{N}$. In the case of equation (3.2a) we have

$$a_{k,j} = \begin{cases} R_D R^{av}_{k+N-t_f}, & j = N, \\ 0, & \text{else,} \end{cases} \qquad \text{for } k \in \mathbb{N}.$$

Inserting this in equation (3.4) we see that all summands vanish except for those with $l_m = N$ for all $m = 1, \ldots, r$, hence $\sum_{m=1}^{r} l_m = r \cdot N$. Since the choice of l_m demands $\sum_{m=1}^{r} l_m = k + j - 1$ this can only be the case for $k + j - 1 = r \cdot N \Leftrightarrow j = r \cdot N + 1 - k$ for some $r \in \mathbb{N}$. Applying these considerations to (3.4) yields

$$d_{k,j} = \begin{cases} \prod_{m=1}^{\frac{k+j-1}{N}} R_D R^{av}_{k-(m-2)N-t_f}, & \exists r \in \mathbb{N} : \frac{k+j-1}{N} = r, \\ 0, & \text{else.} \end{cases} \tag{3.5}$$

for $j = 2 - k, \ldots, N$ and $k \in \mathbb{N}$. In our case the initial values are chosen as $P^f_k = P^{in}_k$, $k = 1, \ldots, N$. By inserting this and equation (3.5) into (3.3) we obtain

$$P^f_{k+N} = \sum_{\substack{2-k \leqslant j \leqslant N \\ \exists r \in \mathbb{N}: j=r \cdot N+1-k}} P^{in}_{N+1-j} \prod_{m=1}^{\frac{k+j-1}{N}} R_D R^{av}_{k-(m-2)N-t_f} + P^{in}_{k+N}, \qquad k \in \mathbb{N}$$

and, by substituting $r = \frac{k+j-1}{N}$,

$$P_{k+N}^f = \sum_{r=1}^{\lfloor \frac{k-1+N}{N} \rfloor} P_{k+N-r \cdot N}^{in} \prod_{m=1}^{r} R_D R_{k-(m-2)N-t_f}^{av} + P_{k+N}^{in}, \qquad k \in \mathbb{N}.$$

After inserting the definition of N and shifting the index by N we get

$$P_k^f = P_k^{in} + \sum_{j=1}^{\lfloor \frac{k-1}{2t_f+t_b} \rfloor} P_{k-j(2t_f+t_b)}^{in} R_D^j \prod_{m=1}^{j} R_{k-(m-1)(2t_f+t_b)-t_f}^{av} \tag{3.6}$$

for $k \in \mathbb{N}_{>2t_f+t_b}$. Applying exactly the same procedure with the initial values $P_k^b = 0$, $k = 1, \ldots, t_b$ and $P_k^b = R_D P_{k-t_b}^{in}$, $k = t_b + 1, \ldots, N$ to equation (3.2b) yields

$$P_k^b = P_{k-t_b}^{in} R_D + \sum_{j=1}^{\lfloor \frac{k-t_b-1}{2t_f+t_b} \rfloor} P_{k-j(2t_f+t_b)-t_b}^{in} R_D^{j+1} \prod_{m=1}^{j} R_{k-(m-1)(2t_f+t_b)-t_f-t_b}^{av} \tag{3.7}$$

for $k \in \mathbb{N}_{>2t_f+t_b}$. Summing up equations (3.6) and (3.7) yields the explicit formula

$$\begin{aligned}
P_k = P_k^{in} + P_{k-t_b}^{in} R_D &+ \sum_{j=1}^{\lfloor \frac{k-1}{2t_f+t_b} \rfloor} P_{k-j(2t_f+t_b)}^{in} R_D^j \prod_{m=1}^{j} R_{k-(m-1)(2t_f+t_b)-t_f}^{av} \\
&+ \sum_{j=1}^{\lfloor \frac{k-t_b-1}{2t_f+t_b} \rfloor} P_{k-j(2t_f+t_b)-t_b}^{in} R_D^{j+1} \prod_{m=1}^{j} R_{k-(m-1)(2t_f+t_b)-t_f-t_b}^{av}
\end{aligned} \tag{3.8}$$

for $k \in \mathbb{N}_{>2t_f+t_b}$.

3.2 Plausibility of the Model

Before we start analyzing how the change of parameters influences the outcome of the model it is important to verify if it makes any sense at all, i.e. if it produces curves that correspond to reality. In order to do this we plot the modeled pressure and compare it with a measured one. The measured curve that is used here and in sections 3.4, 4.2 and 4.4 is taken from a data set that was collected and used in a study by Weber et al. [50].

We choose P^{in} as a half sine during systole and zero during diastole, see figure 3.3.

The reflection coefficient of the heart, R^{av} is chosen as the step function $R^{av} = \mathbb{1}_{diastole}$[1]. Both these choices are taken from a paper by Wang and Parker [49] where they gave

---

[1] Both P^{in} and R^{av} are discrete functions. For reasons of practicability we will refer to them as continuous functions here and in the following. $R^{av} = \mathbb{1}_{diastole}$ means that it assumes the value one for all discrete points in time during diastole and zero for all the other discrete points in time.
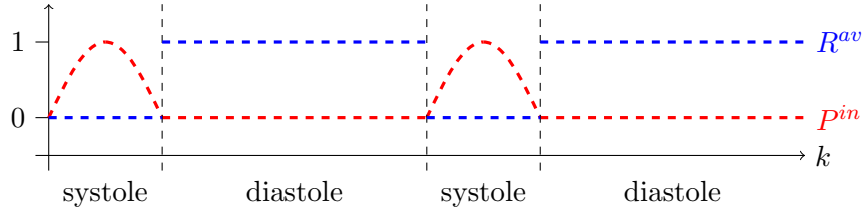
Figure 3.3: Choice of P^{in} as half sine during systole and zero during diastole and $R^{av} = \mathbb{1}_{diastole}$, as used in figure 3.4.

good results. For the choice of P^{in} further arguments have been found [12]. Because the authors were only interested in wave forms, not in absolute values, the choice of amplitude is arbitrary.

For implementation it is necessary to shift the input function, i.e. $P^{in}_k \to P^{in}_{k+t_f}$ by t_f steps: Because it takes the pressure wave t_f time steps to arrive at the measuring site, systole and diastole are shifted by the same number of steps compared to the aortic valve.
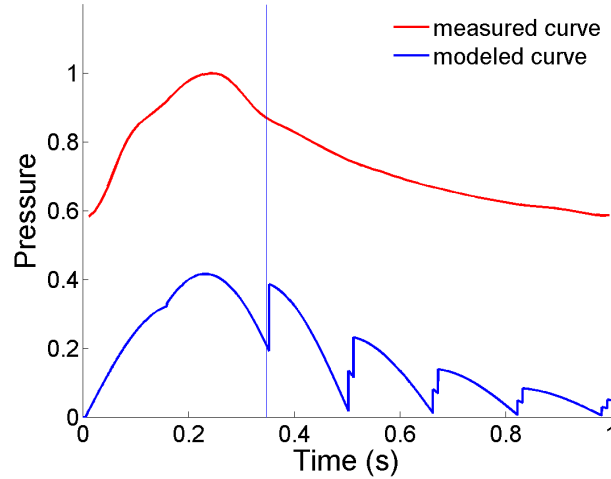
Figure 3.4: Comparison of measured and modeled curve, normalized to the same pulse pressure. Choice of parameters (see section 3.5): $s = 0.348$, $d = 0.652$, $t_{b,ms} = 150ms$, $t_{f,ms} = 5ms$, $R_D = 0.6$, $\tau = 0.0001$.

In figure 3.4 we see that even though the modeled curve shows more spikes and is generally less smooth, the main characteristics of a blood pressure curve are represented. We have a (relatively) fast systolic upstroke, a notch at the end of systole (indicated by the vertical blue line) and a slow diastolic decay.

The presence of distinct spikes in the modeled curve can be explained with the simplification of assuming only one distal reflection site. Why they look the way they do will be analyzed later, see section 3.7.3.

Since the arbitrary choice of the value 1 for the maximum of the input function P^{in} leads to values very different from the measured curve that assumes values between 80 and

140 mmHg, the two curves in figure 3.4 were normalized to have the same pulse pressure. Absolute values should not be given too much weight here since we do not know the correct scaling yet. See section 3.10 for more information on the correct scaling of the modeled curves.

In the following sections we will analyze properties of model 1 and the influence of the parameters. Wherever we already have information about the real arterial system, comparison can help further underline the plausibility of the model.

3.3 Periodicity and Properties

Considering once again equation (3.8), one might wonder if P_k is increasing infinitely in k. After all, the number of summands seems to be growing almost linearly with k. In reality, however, blood pressure obviously does not increase infinitely over time. It oscillates between *diastolic* (DBP) and *systolic* (SBP) blood pressure, see section 2.1.2.

3.3.1 Stability and Boundedness of Solutions

To prove that the modeled curve displays the same behavior, we will use stability theory for linear difference equation systems, see appendix A.1. Therefore we need to transform equations (3.1a) and (3.1b) to equivalent systems of difference equations of order one. Consider the equation

$$x_k = x_{k-N} R_D + P_k^{in}, \qquad k \in \mathbb{N}_{>N} \tag{3.9}$$

that is equivalent to (3.1a) with $R^{av} \equiv 1$ and $N = t_b + 2t_f$. By defining

$$u_k := (x_{k+1}, \ldots, x_{k+N})^T \qquad \text{and} \qquad b_k := (0, \ldots, 0, P_{k+N}^{in})^T$$

equation (3.9) can be transformed to the equivalent system

$$u_{k+1} = Au_k + b_{k+1}, \qquad k \in \mathbb{N}_0 \tag{3.10}$$

where

$$A = \begin{pmatrix} 0 & 1 & 0 & \ldots & \ldots & 0 \\ \vdots & 0 & 1 & \ddots & & \vdots \\ \vdots & \vdots & \ddots & \ddots & \ddots & \vdots \\ \vdots & \vdots & & \ddots & \ddots & 0 \\ 0 & \vdots & & & \ddots & 1 \\ R_D & 0 & \ldots & \ldots & \ldots & 0 \end{pmatrix} \in \mathbb{R}^{N \times N}$$

is nonsingular. First of all we will prove properties of the system matrix A.

Claim 3.3.1 *The powers of the matrix A are given by the following formulas.*

1. *There holds*

$$A^r = \left(\begin{array}{c|c} 0 & I_{N-r} \\ \hline R_D I_r & 0 \end{array} \right) \tag{3.11}$$

   for $r = 0, \ldots, N - 1$.

2. *There holds $A^{mN} = R_D^m I_N$ for $m \in \mathbb{N}$.*

Proof.

1. Proof by mathematical induction. Due to the definition of A the induction base is obviously fulfilled. The inductive step follows from the induction hypothesis by multiplication with A.

2. Proof by mathematical induction. Consider formula (3.11) for $r = N - 1$. Multiplication by A proves the induction base. There holds

$$A^{mN} = A^N A^{(m-1)N} = R_D I_N R_D^{m-1} I_N = R_D^m I_N$$

   which proves the inductive step.

$\qquad \square$

Claim 3.3.2 *For any matrix norm $\| \cdot \|$ there exists $c > 0$ such that*

$$\|A^k\| \leqslant c \cdot R_D^{\left\lfloor \frac{k}{N} \right\rfloor}$$

for $k \in \mathbb{N}_0$.

Proof. It is known [15] that all matrix norms in $\mathbb{R}^{N \times N}$ are equivalent. For our purposes we will choose the maximum absolute column sum of the matrix,

$$\|A\|_1 = \max_{1 \leqslant j \leqslant N} \sum_{i=1}^{N} |a_{ij}|.$$

For all $k \in \mathbb{N}$ there exist $m \in \mathbb{N}$, $r = 0, \ldots, N - 1$ such that $k = mN + r$ and $\left\lfloor \frac{k}{N} \right\rfloor = m$. By claim 3.3.1 it follows

$$\|A^k\|_1 = \|A^{mN+r}\|_1 = \|A^{mN} A^r\|_1 = \|R_D^m A^r\|_1 = R_D^m \|A^r\|_1 = R_D^m.$$

Because of the aforementioned equivalence of matrix norms for any generic matrix norm

$\|\cdot\|$ there exists $c > 0$ such that $\|B\| \leqslant c \cdot \|B\|_1$ for any matrix $B \in \mathbb{R}^{N \times N}$ and thus

$$\|A^k\| \leqslant c \cdot \|A^k\|_1 = c \cdot R_D^{\lfloor \frac{k}{N} \rfloor}.$$

$\square$

Next we will prove a claim for the homogeneous system.

Claim 3.3.3 *For any vector norm $\|\cdot\|$ there holds*

$$\lim_{k \to \infty} \|u_k\| = 0$$

for all solutions u_k of the homogeneous system

$$u_{k+1} = Au_k, \qquad k \in \mathbb{N}_0. \tag{3.12}$$

Proof. According to theorem A.1.2 the general solution of (3.12) can be written as

$$u_k = A^k u_0, \qquad k \in \mathbb{N}_0$$

where $u_0 \in \mathbb{R}^N$ is the initial condition.

Let $\|\cdot\|_{Op}$ denote the matrix operator norm induced by the vector norm $\|\cdot\|$. It follows

$$\|u_k\| \leqslant \|A^k\|_{Op} \|u_0\|, \qquad k \in \mathbb{N}_0$$

and, using claim 3.3.2,
$$\|u_k\| \leqslant c \cdot R_D^{\lfloor \frac{k}{N} \rfloor} \|u_0\|, \qquad k \in \mathbb{N}_0$$

for some $c > 0$ and $k \in \mathbb{N}_0$. Because $\|u_0\|$ is bounded and $0 < R_D < 1$, we obtain

$$\lim_{k \to \infty} \|u_k\| \leqslant \lim_{k \to \infty} c \cdot R_D^{\lfloor \frac{k}{N} \rfloor} \|u_0\| = 0.$$

$\square$

Claim 3.3.3 can be used to asses stability of the original system 3.10.

Claim 3.3.4 *All solutions of system* (3.10) *are globally asymptotically stable.*

Proof. From claim 3.3.3 and theorem A.1.12 it follows that the trivial solution of the homogeneous system (3.12) is globally asymptotically stable. Applying theorem A.1.13 proves the statement. $\square$

Even more than in stability we are interested in the boundedness of solutions. Again, we

can use the result from claim 3.3.3.

Claim 3.3.5 *All solutions of system* (3.10) *are bounded.*

Proof.   From claim 3.3.3 and theorem A.1.12 it follows that there exists $c \in \mathbb{R}^+$ such that

$$\|U_k\| \leqslant c, \qquad k \in \mathbb{N}_0$$

where U_k denotes the principal fundamental matrix of (3.12).

According to theorem A.1.9 the solution of (3.10) with initial condition u_0 is given by

$$u_k = U_k u_0 + \sum_{j=1}^{k} A^{k-j} b_{j-1}, \qquad k \in \mathbb{N}_0$$

which yields the estimate

$$\|u_k\| \leqslant \|U_k\| \|u_0\| + \sum_{j=1}^{\infty} \|A^{k-j}\| \|b_{j-1}\|, \qquad k \in \mathbb{N}_0.$$

We now use that $\|b_{j-1}\| \leqslant b_0$, $\forall j \in \mathbb{N}$ for some $b_0 \in \mathbb{R}$ and claim 3.3.2, obtaining

$$\|u_k\| \leqslant \|U_k\| \|u_0\| + \sum_{j=1}^{N-1} b_0 + \sum_{j=N}^{2N-1} R_D b_0 + \ldots \quad = \|U_k\| \|u_0\| + (N-1)b_0 \sum_{j=0}^{\infty} R_D^j, \qquad k \in \mathbb{N}_0$$

and thus, due to $0 < R_D < 1$,

$$\|u_k\| \leqslant c \|u_0\| + (N-1)b_0 \frac{1}{1 - R_D}, \qquad k \in \mathbb{N}_0. \tag{3.13}$$

Hence, $\max_{k \in \mathbb{N}_0} \|u_k\| < \infty$ for constant $0 < R_D < 1$. $\square$

Claim 3.3.5 can be extended to equation (3.9) and further to (3.1a).

Claim 3.3.6 *All solutions* $\left(P_k^f\right)_{k \in \mathbb{N}}$ *of equation* (3.1a) *are bounded.*

Proof.   Because solutions for (3.9) can be found by

$$x_k = (u_{k+1-N})_N, \qquad k \in \mathbb{N}_{>N}. \tag{3.14}$$

boundedness follows from

$$|x_k| = |(u_{k+1-N})_N| \leqslant \|u_{k+1-N}\|, \qquad k \in \mathbb{N}_{>N}$$

By theorem A.1.14 and claim 3.3.5 we know that $(0 \leqslant) P_k^f \leqslant x_k$ for $k \in \mathbb{N}_{>N}$ where P_k^f is the solution of (3.1a) with the same initial condition. $\square$

Exactly the same analysis can be done for equation (3.1b) to prove that every solution $(P_k^b)_{k \in \mathbb{N}}$ is bounded. Obviously this implies the boundedness of $(P_k)_{k \in \mathbb{N}}$.

3.3.2 Number of Relevant Summands in the Explicit Solution

Since we already know that $(P_k)_{k \in \mathbb{N}}$ is bounded, we also know that the sums in (3.8) converge for $k \to \infty$ and thus the summands converge to zero. To find the maximum number of "relevant" summands we first make the estimation

$$P_k \leqslant 1 + R_D + \sum_{j=1}^{\left\lfloor \frac{k-1}{2t_f+t_b} \right\rfloor} R_D^j + \sum_{j=1}^{\left\lfloor \frac{k-t_b-1}{2t_f+t_b} \right\rfloor} R_D^{j+1}, \qquad k \in \mathbb{N}_{>N}$$

for all $k \in \mathbb{N}_{>2t_f+t_b}$, assuming $P_k^{in} = R_k^{av} \equiv 1$. This is an upper bound for any solution where $\max_{k \in \mathbb{N}} P_k^{in} = 1$ and $\max_{k \in \mathbb{N}} R_k^{av} = 1$. The sums still converge for $k \to \infty$ because they can be majorised by the geometric series. Next define some tolerance level $\delta > 0$. The idea is that the contribution of a summand less than δ is negligible. A similar idea was pursued to determine the number of relevant reflected waves by Berger et al. [4], though they used a relative instead of an absolute tolerance. We have

$$R_D^j < \delta \Leftrightarrow j \ln R_D < \ln \delta \Leftrightarrow j > \frac{\ln \delta}{\ln R_D},$$

so we know we can neglect all summands with $j \geqslant \left\lceil \frac{\ln \delta}{\ln R_D} \right\rceil =: m^*(R_D)$ if we choose a sufficiently small $\delta > 0$. The value $m^*(R_D)$ is monotonously increasing in R_D which agrees with previous results [4] and intuition. We obtain the approximation

$$P_k \approx \tilde{P}_k = P_k^{in} + P_{k-t_b}^{in} R_D + \sum_{j=1}^{m^*(R_D)} P_{k-j(2t_f+t_b)}^{in} R_D^j \prod_{m=1}^{j} R_{k-(m-1)(2t_f+t_b)-t_f}^{av}$$

$$+ \sum_{j=1}^{m^*(R_D)} P_{k-j(2t_f+t_b)-t_b}^{in} R_D^{j+1} \prod_{m=1}^{j} R_{k-(m-1)(2t_f+t_b)-t_f-t_b}^{av}$$

for $k > k_0$ with

$$k_0 = m^*(R_D)(2t_f + t_b) + t_b.$$

Thus, $\tilde{P}_k$ has the same number of summands for all $k > k_0$. The error $P_k - \tilde{P}_k$ can be expressed by

$$P_k - \tilde{P}_k = \sum_{j=m^*(R_D)+1}^{\left\lfloor \frac{k-1}{2t_f+t_b} \right\rfloor} P_{k-j(2t_f+t_b)}^{in} R_D^j \prod_{m=1}^{j} R_{k-(m-1)(2t_f+t_b)-t_f}^{av}$$

$$+ \sum_{j=m^*(R_D)+1}^{\left\lfloor \frac{k-t_b-1}{2t_f+t_b} \right\rfloor} P_{k-j(2t_f+t_b)-t_b}^{in} R_D^{j+1} \prod_{m=1}^{j} R_{k-(m-1)(2t_f+t_b)-t_f-t_b}^{av}$$

for $k > k_0$.

An upper bound is given by

$$P_k - \tilde{P}_k \leqslant \sum_{j=m^*(R_D)+1}^{\infty} R_D^j + \sum_{j=m^*(R_D)+1}^{\infty} R_D^{j+1} = (1 + R_D) \sum_{j=m^*(R_D)+1}^{\infty} R_D^j$$

for $k > k_0$. Using the geometric sum formula and inserting the definition of $m^*(R_D)$ yields

$$P_k - \tilde{P}_k \leqslant \frac{1 + R_D}{1 - R_D} R_D^{\frac{\ln \delta}{\ln R_D}} = \frac{1 + R_D}{1 - R_D} \delta, \qquad k > k_0. \tag{3.15}$$

To illustrate this section let $\delta = 0.00005$. Table 3.1 provides different values of R_D and their respective $m^*(R_D)$. An upper bound of the error $P_k - \tilde{P}_k$ according to (3.15) is also given.

$\mathbf{R_D}$	$\mathbf{m^*(R_D)}$	error
0.1	5	$< 7 \cdot 10^{-4}$
0.3	9	$< 1 \cdot 10^{-3}$
0.5	15	$< 2 \cdot 10^{-3}$
0.7	28	$< 9 \cdot 10^{-3}$
0.9	94	$< 1 \cdot 10^{-2}$

Table 3.1: Different values of R_D, their respective $m^*(R_D)$ and upper bounds for the error $P_k - \tilde{P}_k$.

Table 3.1 clearly shows that for large values of R_D a large number of summands is required. Still, the error is considerably larger than for small values of R_D. The importance of the number of relevant numbers mainly lies in determining the setting time of the model as will be seen in the following section.

It must be noted that due to the simplification $P_k^{in} \equiv R_k^{av} \equiv 1$ the values obtained in this section are much larger than in the realistic versions of the model.

3.3.3 Periodicity of Solutions

Next we want to show that P_k, the sum of products of periodic functions, is periodic again. In reality blood pressure curves are approximately periodic. The period length equals the sum of the duration of systole and diastole, i.e. the duration of one cardiac cycle, and is indirectly proportional to the heart rate. Let K be the period of P^{in} and R^{av} (i.e. discrete length of systole plus discrete length of diastole, $P_{k+K}^{in} = P_k^{in}$ and $R_{k+K}^{av} = R_k^{av}$)

31

and consider the difference $P_{k+K} - P_k$ for $k \in \mathbb{N}_{>N}$:

$$P_{k+K} - P_k = (P_{k+K}^{in} - P_k^{in}) + R_D(P_{k+K-t_b}^{in} - P_{k-t_b}^{in})$$

$$+ \sum_{j=1}^{\left\lfloor \frac{k-1}{2t_f+t_b} \right\rfloor} R_D^j \left(P_{k+K-j(2t_f+t_b)}^{in} \prod_{m=1}^{j} R_{k+K-(m-1)(2t_f+t_b)-t_f}^{av} \right.$$

$$\left. - P_{k-j(2t_f+t_b)}^{in} \prod_{m=1}^{j} R_{k-t_f-(m-1)(2t_f+t_b)}^{av} \right)$$

$$+ \sum_{j=\left\lfloor \frac{k-1}{2t_f+t_b} \right\rfloor+1}^{\left\lfloor \frac{k+K-1}{2t_f+t_b} \right\rfloor} R_D^j P_{k+K-j(2t_f+t_b)}^{in} \prod_{m=1}^{j} R_{k+K-(m-1)(2t_f+t_b)-t_f}^{av}$$

$$+ \sum_{j=1}^{\left\lfloor \frac{k-t_b-1}{2t_f+t_b} \right\rfloor} R_D^{j+1} \left(P_{k+K-j(2t_f+t_b)-t_b}^{in} \prod_{m=1}^{j} R_{k+K-(m-1)(2t_f+t_b)-t_f-t_b}^{av} \right.$$

$$\left. - P_{k-j(2t_f+t_b)-t_b}^{in} \prod_{m=1}^{j} R_{k-(m-1)(2t_f+t_b)-t_f-t_b}^{av} \right)$$

$$+ \sum_{j=\left\lfloor \frac{k-t_b-1}{2t_f+t_b} \right\rfloor+1}^{\left\lfloor \frac{k+K-t_b-1}{2t_f+t_b} \right\rfloor} R_D^{j+1} P_{k+K-j(2t_f+t_b)-t_b}^{in} \prod_{m=1}^{j} R_{k+K-(m-1)(2t_f+t_b)-t_f-t_b}^{av}.$$

Due to the periodicity of P^{in} and R^{av} all but two terms cancel out, yielding

$$P_{k+K} - P_k = \sum_{j=\left\lfloor \frac{k-1}{2t_f+t_b} \right\rfloor+1}^{\left\lfloor \frac{k+K-1}{2t_f+t_b} \right\rfloor} R_D^j P_{k+K-j(2t_f+t_b)}^{in} \prod_{m=1}^{j} R_{k+K-(m-1)(2t_f+t_b)-t_f}^{av}$$

$$+ \sum_{j=\left\lfloor \frac{k-t_b-1}{2t_f+t_b} \right\rfloor+1}^{\left\lfloor \frac{k+K-t_b-1}{2t_f+t_b} \right\rfloor} R_D^{j+1} P_{k+K-j(2t_f+t_b)-t_b}^{in} \prod_{m=1}^{j} R_{k+K-(m-1)(2t_f+t_b)-t_f-t_b}^{av}.$$

Using the tolerance level defined above the summands can be neglected if $j \geqslant m^*(R_D)$, i.e.

$$\frac{k-t_b-1}{2t_f+t_b} \geqslant m^*(R_D) \Leftrightarrow k \geqslant (2t_f+t_b)m^*(R_D) + t_b + 1.$$

This tells us that after a setting time of $(2t_f + t_b)m^*(R_D) + t_b + 1$ time steps P_k can be considered periodic with the same period as P^{in}, R^{av}. There holds $\lim_{k\to\infty} (P_{k+K} - P_k) = 0$ because the number of summands remains the same while their absolute value decreases with increasing k.

3.4 Shifting the Measuring Site towards the Heart

The solution for the general equations (3.2a) and (3.2b) is a rather unwieldy formula. In the upcoming sections we will set $t_f = 0$ to facilitate further calculations, a choice that agrees with our idea of describing pressure in the aortic root. Are we allowed to do that, though? After all, setting $t_f = 0$ merges the measuring site with the aortic valve, a site of reflection. Pressure might behave entirely different in this place. Still, arguments can be found why this choice is reasonable under certain conditions.

First consider formula (3.7) with the input function

$$P_k^{in} = \begin{cases} 1, & k = 1, \\ 0, & \text{else.} \end{cases}$$

For $t_f > 0$ forward pressure is nontrivial if either $k = 1$ or there exists $j = 1, \ldots, \left\lfloor \frac{k-1}{2t_f + t_b} \right\rfloor$ such that $k - j(t_f + t_b) = 1$ which is equivalent to

$$\frac{k-1}{2t_f + t_b} \in \mathbb{N}. \tag{3.16}$$

Backward pressure is nontrivial if either $k = t_b + 1$ or there exists $j = 1, \ldots, \left\lfloor \frac{k - t_b - 1}{2t_f + t_b} \right\rfloor$ such that $k - j(2t_f + t_b) - t_b = 1$ which is equivalent to

$$\frac{k - t_b - 1}{2t_f + t_b} \in \mathbb{N}. \tag{3.17}$$

Equations (3.16) and (3.17) cannot both be satisfied for the same $k \in \mathbb{N}_{>2t_f + t_b}$, hence there holds

$$P_k^f > 0 \Rightarrow P_k^b = 0 \qquad \text{and} \qquad P_k^b > 0 \Rightarrow P_k^f = 0,$$

a connection that complies with the intuitive idea that a single impulse moves within the system but remains a single impulse.

If $t_f = 0$, however, equations (3.16) and (3.17) simplify to

$$\frac{k-1}{t_b} \in \mathbb{N} \qquad \text{and} \qquad \frac{k - t_b - 1}{t_b} \in \mathbb{N}$$

two equivalent conditions. This implies that the single impulse is present twice at certain points in time. Setting $t_f = 0$ is therefore not reasonable in this case.

Now consider the input function

$$P_k^{in} = \begin{cases} 1, & k = 1, \ldots, k_{max} \\ 0, & \text{else} \end{cases} \tag{3.18}$$

33

where $k_{max} > 2t_f + t_b$ for a given $t_f > 0$. Since return times are significantly shorter than systole duration (see section 3.5) and we will assume $P^{in} > 0$ during systole throughout the thesis, this assumption makes sense.

Forward pressure is nontrivial if there exists $j \in \left\{0, \dots, \left\lfloor \frac{k-1}{2t_f+t_b} \right\rfloor \right\}$ such that $k - j(2t_f + t_b) \in \{1, \dots, k_{max}\}$ or, equivalently,

$$\frac{k - k_{max}}{2t_f + t_b} \leqslant j \leqslant \frac{k - 1}{2t_f + t_b}$$

and $j \in \mathbb{N}_0$. Due to our choice of k_{max} such a $j \in \mathbb{N}_0$ can be found for any $k \in \mathbb{N}$, hence at any point in time a forward impulse is present.[2] By applying exactly the same idea to backward pressure we conclude that at any point in time $k \in \mathbb{N}_{>t_b}$ a backward impulse is present.

For $t_f = 0$ and $k_{max} > t_b$ we obtain the same result. Having a forward and a backward running impulse at the same time is no longer a contradiction because from the beginning more than one impulse is present.

Instead of the step function (3.18) any other function can be used as input, as long as $P_k^{in} > 0$ for $k = 1, \dots, k_{max}$ and $k_{max} > t_b$. Assigning $t_f = 0$ will not change the output significantly. Evidence for this phenomenon with an input that is a half sine during systole and vanishes during diastole can be found by comparing figures 3.4 and 3.5.
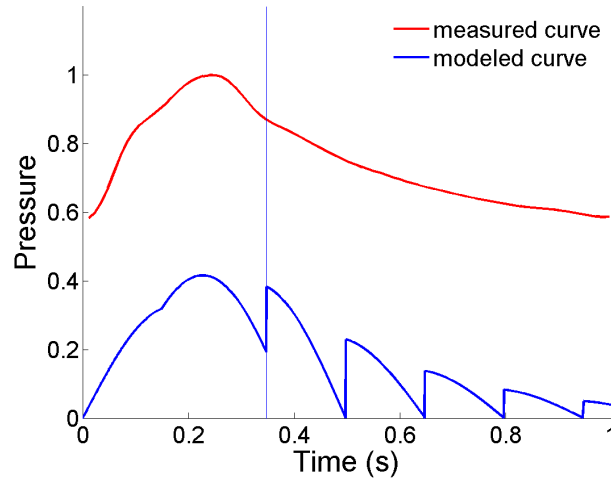
Figure 3.5: Comparison of measured and modeled curve, normalized to the same pulse pressure. Choice of parameters (see section 3.5): $s = 0.348$, $d = 0.652$, $t_{b,ms} = 150ms$, $t_{f,ms} = 0ms$, $R_D = 0.6$, $\tau = 0.0001$.

---

[2]In theory. In practice, forward pressure (and backward) can vanish due to high powers of R_D converging to zero.

Inserting $t_f = 0$ into equation (3.8) yields

$$
\begin{aligned}
P_k = P_k^{in} + P_{k-t_b}^{in} R_D &+ \sum_{j=1}^{\left\lfloor \frac{k-1}{t_b} \right\rfloor} P_{k-jt_b}^{in} R_D^j \prod_{m=1}^{j} R_{k-(m-1)t_b}^{av} \\
&+ \sum_{j=1}^{\left\lfloor \frac{k-t_b-1}{t_b} \right\rfloor} P_{k-(j+1)t_b}^{in} R_D^{j+1} \prod_{m=1}^{j} R_{k-mt_b}^{av},
\end{aligned}
\qquad k \in \mathbb{N}_{>t_b},
$$

which further simplifies to

$$
P_k = P_k^{in} + \sum_{j=1}^{\left\lfloor \frac{k-1}{t_b} \right\rfloor} P_{k-jt_b}^{in} R_D^j (R_k^{av} + 1) \prod_{m=1}^{j-1} R_{k-mt_b}^{av}, \qquad k \in \mathbb{N}_{>t_b}, \tag{3.19}
$$

a handy formula that will be used from now on.

3.5   Implementation and Parameter Values

In order to ensure comprehensibility of the following numerical analysis we will now give an overview of implementation details and used parameter ranges.

The MATLAB code to generate the blood pressure curve, a function called `GenerateCurve-Separated`, is given in algorithm 3.5.1.

Algorithm 3.5.1

```
1   function [Pf, Pb, P] = GenerateCurveSeparated (s, d, J, tau, RD, tbms, tfms)

2   tb = floor (tbms * 0.001 / tau);

3   tf = floor (tfms * 0.001 / tau);

4   [Pin, Rav] = GeneratePinRav (s, d, J, tau, tf);

5   Pf = Pin;

6   Pb = [zeros(1,tb), Pin(1:2*tf) .* RD, zeros(1,length(Pin)-2*tf-tb)];

7   for k = 2 * tf + tb + 1 :  length(Pin)

8       Pb(k) = Pin(k-tb)*RD + Pb(k-2*tf-tb)*Rav(k-tf-tb)*RD;

9       Pf(k) = Pin(k) + Pf(k-2*tf-tb)*Rav(k-tf)*RD;

10  end

11  P = Pf + Pb;

12  end
```

The input parameters are as follows:

- Duration of systole and diastole in seconds are given by `s` and `d`, respectively. Transformation to a finite number of time points (k_s and k_d, respectively, see definition 3.8.1) is done within the function `GeneratePinRav` that will be explained in algorithm 3.5.2. Typical values are $s = 0.3$ and $d = 0.7$ [13]. Variation of systole and diastole duration will be performed around these base values.

- The number of cardiac cycles to be generated is given by a power of 2 with the exponent `J`. Again, this will become clear in algorithm 3.5.2. Choosing $J > 0$ is only necessary if $m^*(R_D) > k_s + k_d$.

- To be able to modify precision and computation time and for some applications it will be necessary to have the possibility to adjust the step size. The size of a time step in seconds is given by `tau`, accordingly the number of time points per second is $1/\tau$.

- The reflection coefficient at the distal reflection site is given by `RD`. Different numbers were computed with different methods by various authors. Latham et al. [19] computed local reflection coefficients from regional cross-sectional areas and regional foot-to-foot pulse wave velocities. The results differ according to the measuring site. In the aorta at the level of the renal arterial branches they found a reflection coefficient of $R_D = 0.43$. Even though the model used slightly differs from the one discussed here and local reflection coefficients differ from the global effective one, the value can be used for orientation because the renal arterial branches are often considered a main reflection site, see section 2.2.3. Other authors [37] computed the global reflection coefficient by P_b/P_f, obtaining $R_D = 0.45 \pm 0.08$ (mean $\pm$ SD). Computing the reflection coefficient by P_b/P_f in a model of the arterial system [51] yielded $R_D = 0.5$ or $R_D = 0.43$, depending on the choice of PWV / effective length.

- Both the return time from the distal reflection site and the travel time to and from the heart are given in milliseconds by `tbms` and `tfms`, respectively. They are transformed to finite numbers of time points in lines `2` and `3` of the code, yielding the parameters t_b and t_f that have been used in the previous sections. To find typical values for $t_{b,ms}$ and $t_{f,ms}$ we need values for PWV and effective length.

  Both as well as travel time directly were determined by Murgo et al. [25]. PWV was measured as foot-to-foot velocity with a value of $6.68 \pm 0.32 m/s$ (mean $\pm$ SEM). The travel time of the wave from the heart to the reflection site and back was defined as the time from the beginning of the systolic upstroke to the beginning of the secondary peak, yielding a value of $149 \pm 7ms$ (mean $\pm$ SEM). Effective length was calculated using PWV and the frequency at which the first minimum of the impedance modulus occurs.

Segers et al. [37] found PWV to be $4.86 \pm 1.1 m/s$ (mean $\pm$ SD), using time and distance traveled by the propagating flow front at four locations. Travel time, defined as before, was determined as $165 \pm 33 ms$ (mean $\pm$ SD) and effective length calculated as $38.7 \pm 6 cm$ (mean $\pm$ SD), using the two previously found parameters.

Westerhof et al. [51] determined all values using mathematical models. Effective length was given as $41 cm$. Travel time was calculated to be $100 ms$ with a resulting PWV of $8.2 m/s$.

The following algorithm presents how `Pin` and `Rav` are generated. In this case P^{in} was chosen to be a sine curve during systole, R^{av} is a step function. To choose different functions, the algorithm can easily be adjusted accordingly.

Algorithm 3.5.2

```
1    function [Pin, Rav] = GeneratePinRav (s, d, J, tau, tf)

2    Pin = [sin(pi*(0:1/floor(s/tau):1)), zeros(1,ceil(d/tau))];

3    Rav = [zeros(1,floor(s/tau)), ones(1,ceil(d/tau))];

4    Pin = [zeros(1,tf), Pin];

5    Pin = Pin(1:length(Rav));

6    for j = 1:J

7        Pin = [Pin, Pin];

8        Rav = [Rav, Rav];

9    end

10   end
```

The main work of the algorithm is done in lines `2` and `3`. Transformation of the values `s` and `d` into numbers of time points is achieved via `floor(s/tau)` and `ceil(d/tau)`, respectively. In lines `4` and `5` the input function `Pin` is translated by `tf` time steps to account for the fact that in the measuring site systole and diastole are shifted by `tf` time steps. Finally, lines `6` to `9` demonstrate how the parameter `J` determines the number of cardiac cycles produced.

3.5.1 Influence of the Input Function

First we want to know how the choice of the input function P^{in} influences the shape of the resulting curve. In particular we want to compare the sine curve we assumed in section 3.2 and will use in all the numerical analysis in the following sections with the step function that will be used in sections 3.8 and 3.9, hoping to justify that simplification that facilitates mathematical analysis. The expectation is that a smoother P^{in} leads to

a smoother curve. Also, the sine function is more realistic than the step function since it takes the opening and closing periods of the valve into account, hence we expect a more realistic curve. A sine function has been used as input previously [12, 49]. Furthermore absolute values should be higher if the step function is used due to the fact that, using the same amplitude, its values are larger or equal to those of the sine function at every point in time.

(a) P^{in} is a sine during systole

(b) P^{in} is constant during systole
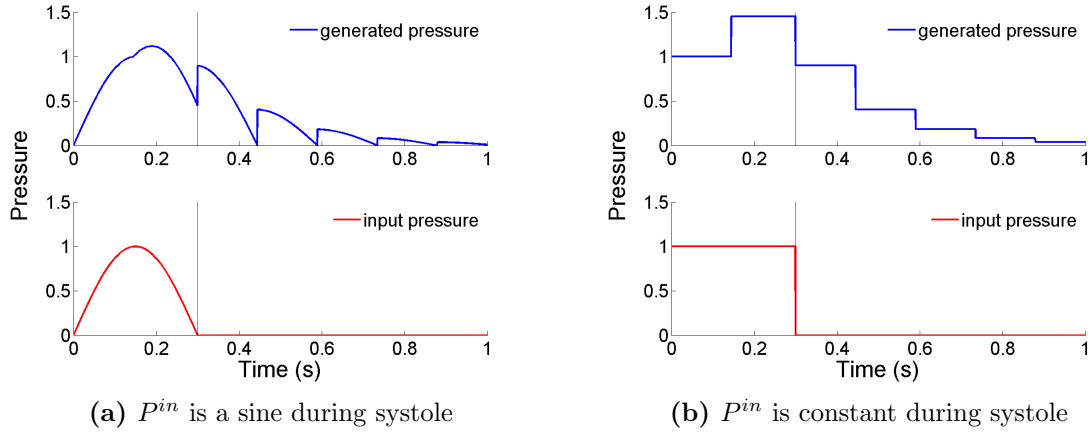
Figure 3.6: Comparison of different shapes of P^{in}. Choice of parameters: $s = 0.3$, $d = 0.7$, $R_D = 0.45$, $t_{b,ms} = 145ms$, $\tau = 0.0001$. Second cardiac cycle.

Figure 3.6 compares the two different choices of P^{in} where all other parameters are held the same. Parameters were chosen according to section 3.5, with R^{av} being a step function. The figures immediately confirm both our expectations. In its major characteristics, however, the shape is very similar in both figures, with a steep ascent in systole and a slower descent during diastole. End of systole is marked by vertical lines. Altogether using the step function instead of the sine function in sections 3.8 and 3.9 seems to be justified.

3.5.2 Influence of Aortic Valve Reflection

Next we will compare different shapes for R^{av} that will be used in sections 3.7, 3.8 and 3.9 for both mathematical and numerical analysis. Mainly, we expect the curves to be smoother if R^{av} is constant. Also, absolute values should be higher or lower, respectively, if we choose an upper or lower bound for the step function R^{av}. Intuitively, choosing R^{av} as a step function should also give the most realistic curve since reflection properties of the valve are expected to be different for an open / closed valve.

The comparison of different choices of R^{av} is shown in Figure 3.7 and again, the end of systole is marked by vertical lines. Parameters were chosen according to section 3.5, with a sine function for P^{in}. Indeed, the curve is smoother where R^{av} is chosen to be constant with less distinct spikes. An explanation for the shape of the spikes in figure 3.7 (a) can be found in section 3.7.3.

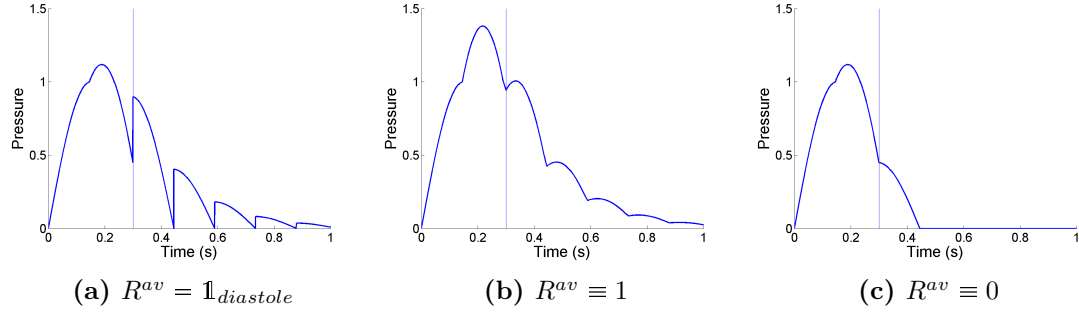**(a)** $R^{av} = \mathbb{1}_{diastole}$ **(b)** $R^{av} \equiv 1$ **(c)** $R^{av} \equiv 0$

Figure 3.7: Comparison of different shapes of R^{av}. Choice of parameters: $s = 0.3$, $d = 0.7$, $R_D = 0.45$, $t_{b,ms} = 145ms$, $\tau = 0.0001$. First cardiac cycle.

The difference in absolute values is not very large but detectable. However, the curve looks most realistic for the choice $R^{av} \equiv 1$, motivating further investigation of that case in section 3.8. Again, the main characteristics of the curves remain the same in all three cases.

3.6 Variation of Cardiovascular System Parameters

3.6.1 Potential Problems

During the following sections we will analyze the influence of different parameters and their underlying physiological equivalents (if applicable) on systolic, diastolic and pulse pressure separately. In reality, however, most of these system parameters are coupled in some way or the other. For example, connections between body height and heart rate [41] as well as connections between body height and reflection coefficient [37] have been found.

This means that the variation of only one of them, with all the others held constant, is very unrealistic. While for some parameters reasonable ideas can still be developed and actually coincide with findings in literature, results should be handled with care.

3.6.2 Reflection Coefficient

Even though we know that the choice of the reflection coefficient R_D is strongly connected with the choice of effective length (see page 19) it can be linked to the arterial system impedance when considering a fixed distance. Hence [27], absolute values are expected to rise with R_D.

Because R_D is the same for all time points, both in systole and diastole, the value should not be responsible for shape or smoothness of the curve. Rather than the number of spikes their prominence is expected to grow with increasing R_D.

Furthermore, according to section 3.3.3, setting time until the produced curves are periodic should rise with R_D.

3.6.3 Systole and Diastole Duration

Diastole and systole duration are connected strongly with the heart rate. We thus need to distinguish two cases:

Variable Heart Rate. We keep one of the two parameters fixed and vary the other. This implies a change of heart rate and is physiologically interesting, since changes of heart rate occur all the time in the human body.

Literature research shows that so far no clear influence of systole or diastole duration on blood pressure has been determined. Wilkinson et al. [57] found that DBP increased significantly with increasing heart rate while SBP did not (which implies a decrease in PP). They even detected a decrease in SBP and PP and an increase in DBP with increasing heart rate, particularly for a heart rate between 65 and 80 bpm [58]. Unfortunately change in heart rate usually means a change in both diastole and systole duration which is why complicates direct application of these results.

Our expectations are therefore only based on intuition. Since an increase in systole duration increases the time span during which blood is ejected by the heart we expect it to positively influence absolute blood pressure values. Similarly (and with the same argumentation) we expect an increase in diastole length to negatively influence blood pressure.

Constant Heart Rate. Let us consider, however, the change of systole and diastole duration while we keep their sum fixed. Physiologically this means looking at different values of systole and diastole duration with a constant heart rate. As before we expect systolic and diastolic pressure to be directly correlated with systole duration which in this case is equivalent to being indirectly correlated with diastole duration.

As for shape, predictions are harder to make in both cases. Again, information is only available for the influence of heart rate instead of the separate variation of systole and diastole duration. Furthermore, both P^{in} and R^{av} depend on systole and diastole duration.

3.6.4 Return Time

Due to its definition (see page 19) variation in t_b can mean both variation in PWV and/or variation in effective length.

PWV is known to be an indicator of arterial stiffness [27], positively influencing PP and SBP [5]. We therefore expect t_b to have the inverse effect, i.e. decreasing pressure with increasing t_b.

It is known (again, see page 19) that the choice of effective length is strongly connected with

the choice of R_D. Still, if we keep R_D constant, variation of effective length does represent variation of the length of the arterial system. The fact that a negative relationship between body height and SBP / PP has been found [18] raises the expectation of a negative relationship between t_b and SBP / PP.

Both these theories indicate that there will be a negative relationship between t_b and absolute pressure values in general.

3.6.5 Step Size

Time step size τ is a purely technical parameter that determines how precise computations are. It does not represent any physiological phenomenon and only occurs in connection with the implementation of the algorithm. Variation of τ should not fundamentally affect shape and magnitude of the model curve, only its precision, i.e. the smoothness.

3.7 Time-Dependent Reflection at the Heart

We have already had a first look at the shape of our curves in sections 3.2 and 3.4 and seen that it is possible to choose the parameters in a way that the resulting curve displays the major characteristics of a physiological blood pressure curve. In this section we want to study how the variation of parameters influences absolute values and shape of the curve when the input function P^{in} and the reflection coefficient at the aortic valve R^{av} are chosen as in section 3.2.

Since it is hard to quantify the shape of a curve, especially a discrete one, we will have to do this analysis numerically, even graphically, by comparing plots. Because we have more than one parameter to analyze and in order to compare plots we can only change one at a time, comparing plots cannot prove general concepts. Still, it can give a hint if our theories are reasonable.

3.7.1 Influence of the Reflection Coefficient

To assess the influence of R_D on the model outcome we compute and plot the curves for different values of R_D, while all other parameters are held constant.

The ideas from section 3.6.2 are partly confirmed by figures 3.8 (a) -(e). While systolic pressure and the prominence of spikes do increase with R_D, diastolic pressure remains very close to zero independent of the reflection coefficient. Also the setting time turns out not to be influenced by R_D, mostly due to the fact that the curves are already periodic from the second cycle on for all considered values of R_D.

Further, we see that the model gives physiological curves only if R_D is "sufficiently small". The threshold, however, depends on the choice of other parameters. Choosing, for example,

(a) $R_D = 0.1$ (b) $R_D = 0.3$ (c) $R_D = 0.5$

(d) $R_D = 0.7$ (e) $R_D = 0.9$
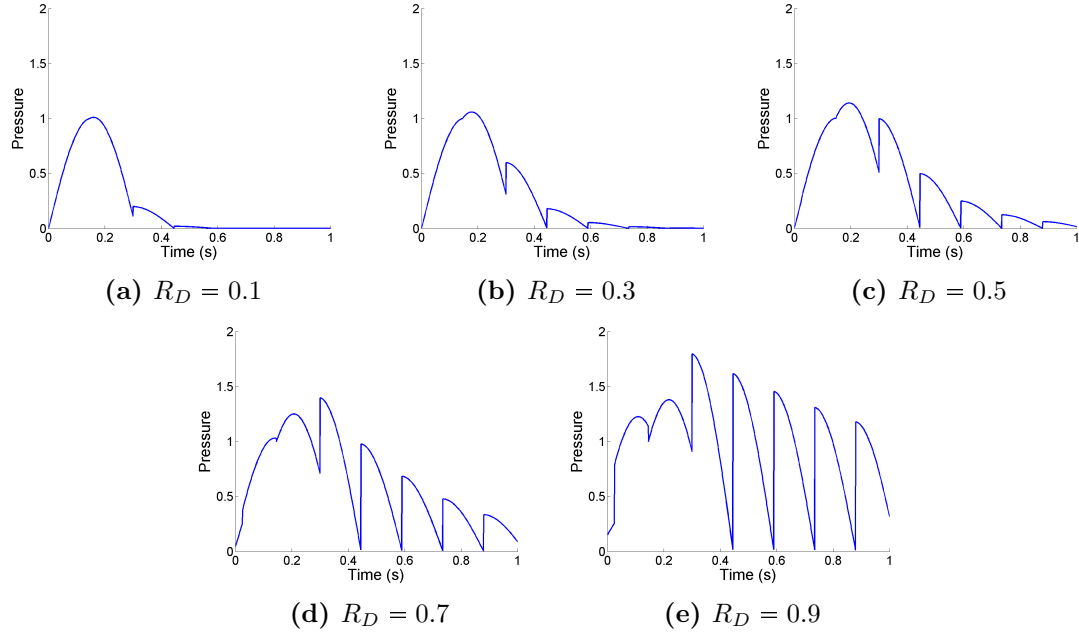
Figure 3.8: Different values of R_D and their influence on curve shape. Second cardiac cycle. Choice of parameters: $s = 0.3$, $d = 0.7$, $t_{b,ms} = 145ms$, $\tau = 0.0001$.

a higher value of t_b results in unrealistic shapes already at lower values of R_D. In particular, for the specific parameter values used a reflection coefficient of $R_D = 0.5$ looks reasonable, agreeing with the values from literature, see section 3.5.

3.7.2   Influence of Systole and Diastole Duration

To asses the impact systole and diastole duration have on absolute values and shape of the pressure curve we compute and plot the curves for different values. We confine ourselves to the case of a variable heart rate, i.e. systole and diastole duration are varied independently.

In figure 3.9 blood pressure curves are plotted for five different values of systole length, with all the other parameters held constant. Systole length ranges from 0.1 seconds to the length of diastole, in this case 0.9 seconds. End of systole is marked by a vertical line in the respective color. We see that systolic blood pressure increases with systole length, a result consistent with the prediction in section 3.6.2. Because diastolic pressure remains zero regardless of systole length, also pulse pressure increases. Interestingly, the prominence of all secondary spikes, that is, spikes that occur during diastole, decreases with increasing $k_s^{t_b}$ while their width remains (almost) the same. The reason for this can be found in section 3.7.3. Both for too low and too high values of $k_s^{t_b}$ the curve does not resemble a measured one any more. The thresholds, though, will depend on the choice of the other parameters again.
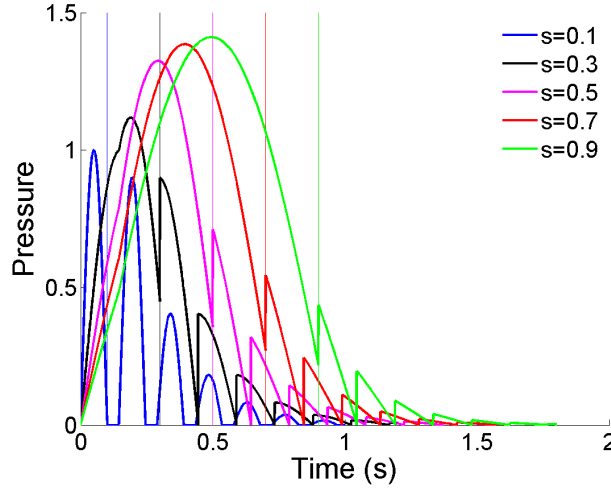
Figure 3.9: Shape of the blood pressure curve for five different values for $k_s^{t_b}$. First cardiac cycle. End of systole is marked by a vertical line in the respective color. Choice of parameters: $d = 0.9$, $t_{b,ms} = 145$, $R_D = 0.45$, $\tau = 0.0001$.

In figure 3.10, however, we see that diastole length does not have a significant impact on the shape of the curve. Blood pressure curves are plotted for four different values of diastole length (ranging from systole length 0.3 seconds to 0.9 seconds).
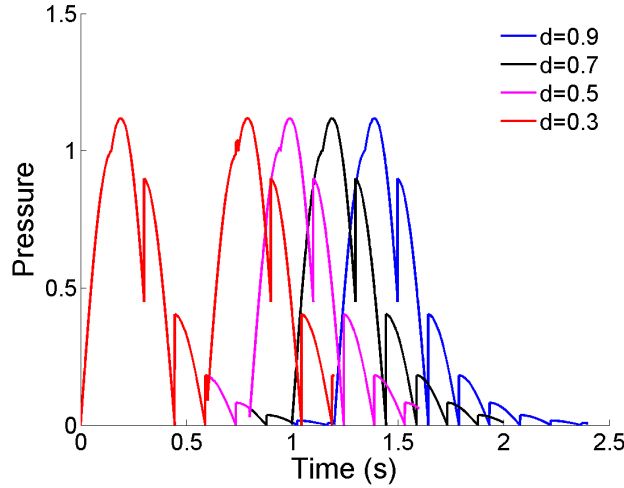
Figure 3.10: Shape of the blood pressure curve for four different values for $k_d^{t_b}$. First two cardiac cycles. Choice of parameters: $s = 0.3$, $t_{b,ms} = 145$, $R_D = 0.45$, $\tau = 0.0001$.

Because during the first cardiac cycle all four curves look identical and time shift only occurs after diastole two cycles were plotted. We see that shape as well as absolute values are almost constant. Again, an explanation for this behavior can be found using the results from section 3.7.3: The shape of the curve mainly depends on the shape of the input function. A longer diastole will thus mainly produce more spikes and only slightly change their shape.

Another interesting observation can be made in figure 3.10, mainly for $d = 0.5$ and $d = 0.7$. At the end of diastole, right at the beginning of systole, pressure decreases significantly before it starts rising due to systolic input. The same phenomenon has been observed before [33, Figure 2] and can be explained as follows: When the aortic valve opens the reflection coefficient at the heart becomes zero. Forward pressure is reduced by the amount of reflections that therefore disappear while the contribution of the input function still is small.

3.7.3 Influence of Return Time

In section 3.6.4 we predicted a negative relationship between t_b and systolic as well as pulse pressure. Numerical analysis confirms these predictions, see figure 3.11. In accordance with previous results [38] $t_{b,ms}$ is chosen to be much shorter than systole duration. Diastolic pressure remains zero regardless of the choice of $t_{b,ms}$.

(a) $t_{b,ms} = 70ms$ **(b)** $t_{b,ms} = 95ms$ **(c)** $t_{b,ms} = 120ms$

(d) $t_{b,ms} = 145ms$ **(e)** $t_{b,ms} = 170ms$ **(f)** $t_{b,ms} = 195ms$
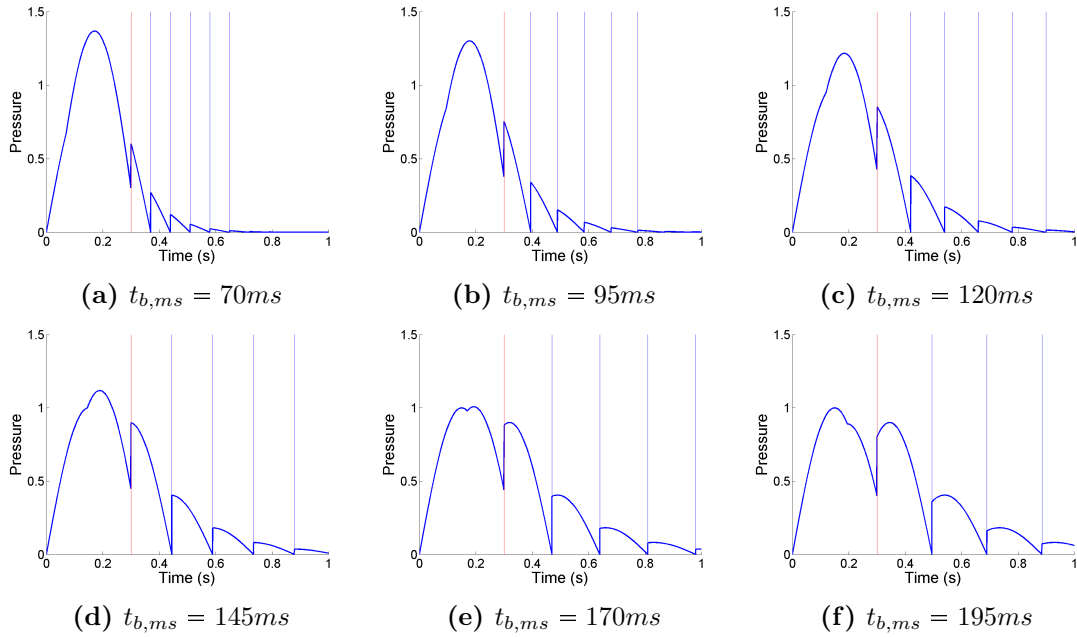
Figure 3.11: Different values of t_b and their influence on curve shape. First cardiac cycle. End of systole is marked by a red vertical line. Return times after the end of systole are marked by blue vertical lines. Choice of parameters: $s = 0.3$, $d = 0.7$, $R_D = 0.45$, $\tau = 0.0001$.

Furthermore we observe that all the secondary spikes (spikes occurring during diastole) become wider, smoother and more prominent with increasing value of t_b. Indeed, the width of each secondary spike equals the return time as can be told by the position of the blue vertical lines indicating the first, second, third,... time of return after the beginning of diastole.

The question is raised whether this phenomenon can be observed for arbitrary parameter values or is due to the specific choice of parameters. An answer to this question together

with a technical explanation for the phenomena can be found in the basic formula (3.19): According to figures 3.11 (a) -(f) all the secondary spikes happen during diastole. During diastole the sum in formula (3.19) only has one nontrivial summand

$$P^{in}_{k-j_0 t_b} R^{j_0}_D (R^{av}_k + 1) \prod_{m=1}^{j_0-1} R^{av}_{k-mt_b}$$

for some $j_0 \in \mathbb{N}$ due to the choice of R^{av}. This can be seen as follows: For $j < j_0$ we obtain $P^{in}_{k-jt_b} = 0$ (still in diastole), with the choice $j > j_0$ there exists $1 \leqslant m < j$ such that $R^{av}_{k-mt_b} = 0$ (already in systole). This means the spikes are the part of the input function between t_b steps prior to the end of systole and the end of systole, multiplied by increasing powers of R_D. The larger t_b the longer is the used part of the input function, hence the spikes look smoother.

Another question is what happens to reflections during systole. The bump that can be observed t_b time steps after the beginning of systole indicates the return of the first reflection. Also in systole formula (3.19) can only have one nontrivial summand

$$P^{in}_{k-j_0 t_b} R^{j_0}_D (R^{av}_k + 1) \prod_{m=1}^{j_0-1} R^{av}_{k-mt_b} = P^{in}_{k-j_0 t_b} R^{j_0}_D \prod_{m=1}^{j_0-1} R^{av}_{k-mt_b}$$

for some $j_0 \in \mathbb{N}$. There holds

$$j_0 \begin{cases} = 1 & \text{if } k \text{ is more than } t_b \text{ time steps after the beginning of systole,} \\ > 1 & \text{else.} \end{cases}$$

This can be seen as follows: In the first case for $j > 1$ there exists $1 \leqslant m < j$ such that $R^{av}_{k-mt_b} = 0$. In the second case for $j < j_0$ there holds $P^{in}_{k-jt_b} = 0$, for $j > j_0$ there exists $1 \leqslant m < j$ such that $R^{av}_{k-mt_b} = 0$. The second case, however, is only relevant for relatively large values of R_D, such that $j_0 \leqslant m^*(R_D)$. If applicable reflections from the first (second, third,...) cardiac cycle influence the systolic spike of the second (third, fourth,...) one, causing a jump a multiple of t_b time steps after the end of the previous systole. The bump that can be observed t_b time steps after the beginning of systole becomes a distinct incision, see figure 3.12. Parameters were chosen such that systole or diastole length are not multiples of $t_{b,ms}$ and that the aforementioned incision is visible.

Because both P^{in}_k and $P^{in}_{k-t_b}$ do not make jumps there are no further bumps during systole. At the end of systole the summands are doubled since R^{av}_k switches from 0 to 1, causing the first visible spike.

Next, we want to study the case where $t_{b,ms}$ is larger than systole length, see figure 3.13.

The shape of the curve is less realistic if $t_{b,ms}$ is chosen larger than systole duration. It is clearly visible that during one cardiac cycle each segment of length t_b is a copy of the previous one multiplied by some constant, which can be verified by formula (3.19).
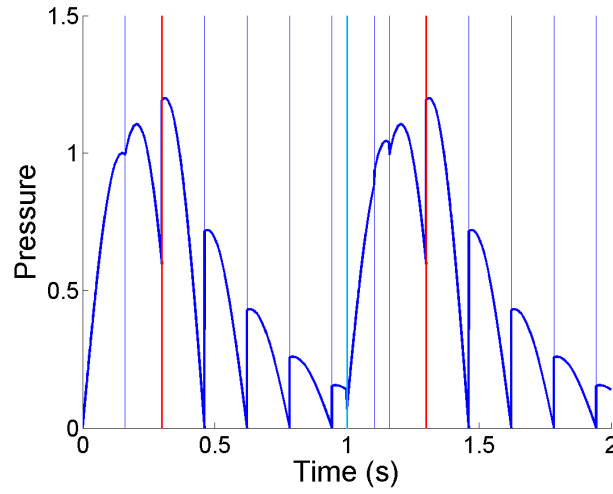
Figure 3.12: Plot of blood pressure curve with $t_{b,ms} = 161ms$. First two cardiac cycles. End of systole is marked by a red, beginning by a cyan vertical line. Return times are marked by blue vertical lines. Choice of parameters: $s = 0.3$, $d = 0.7$, $R_D = 0.6$, $\tau = 0.0001$.
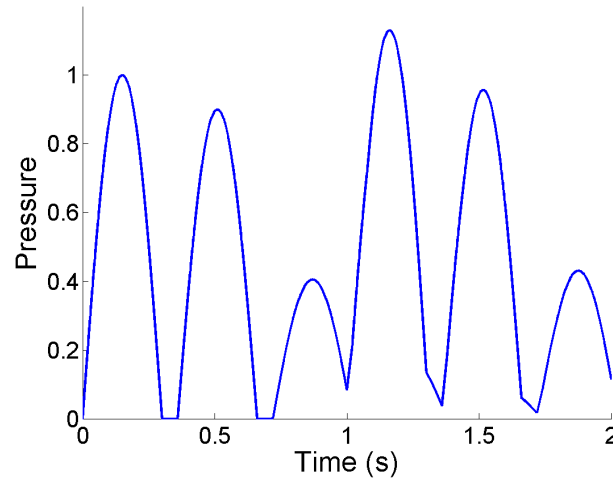
Figure 3.13: Plot of blood pressure curve with $t_{b,ms} = 360ms$. First two cardiac cycles. Choice of parameters: $s = 0.3$, $d = 0.7$, $R_D = 0.45$, $\tau = 0.0001$.

In the second cardiac cycle interference with waves from the previous cycle are responsible for the difference in shape.

3.7.4 Influence of Step Size

In figure 3.14 six different values for τ are used to compute and plot curves in order to asses the influence of the step size τ.
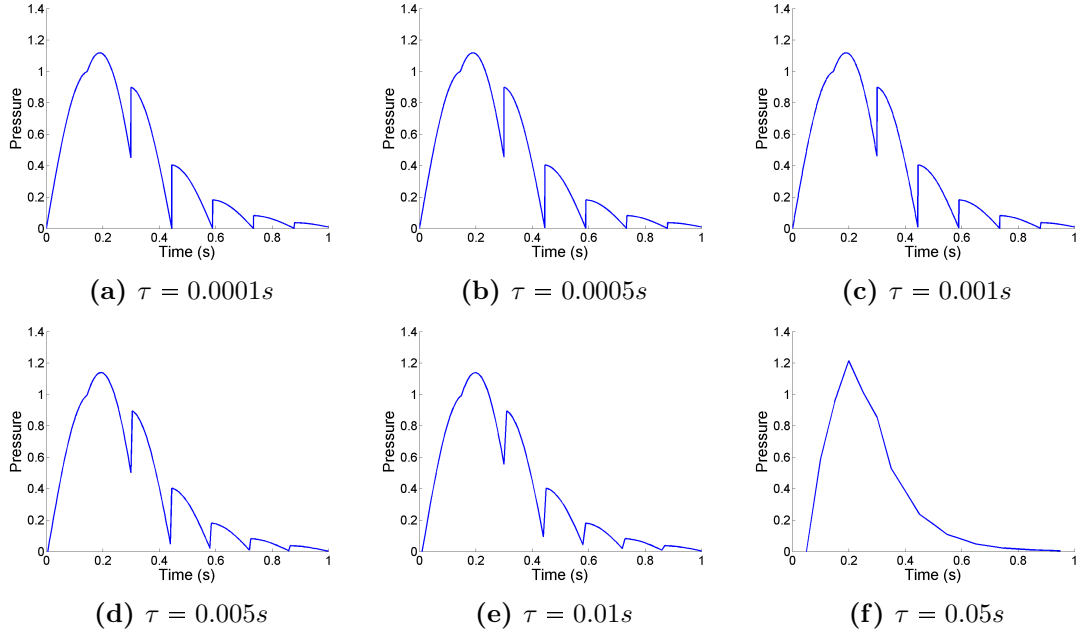
Figure 3.14: Different values of τ and their influence on curve shape. First cardiac cycle. End of systole is marked by a vertical line. Choice of parameters: $s = 0.3$, $d = 0.7$, $t_{b,ms} = 145$, $R_D = 0.45$.

We can see that indeed the curves remain practically unchanged for $\tau = 0.0001s$ to $\tau = 0.01s$. The curve computed using $\tau = 0.05s$, however, does not show any of the characteristic spikes of the model, indicating that this time step size is too large. In algorithm 3.5.1 we could see that τ was needed to compute the time parameters t_b and t_f using the `floor` function. An increase of τ leads to a possible increase of the error caused by this function and thus a lower value of t_b.

3.8 The Heart as Total Reflector

Since in section 3.5.2 we could see that modeling the heart as a total reflector, i.e. $R^{av} \equiv 1$, gives fairly reasonable results, we want to further investigate that case. We will see that using a step function instead of a sine for the input function P^{in} enables us to analyze the model not only numerically but also (to some extent) mathematically. In particular, we will be able to find formulas for systolic, diastolic and pulse pressure.

First of all, let P^{in} be the step function $P^{in} = \mathbb{1}_{systole}$. Obviously prescribing a very simple input function influences the behavior of the blood pressure curve but we have seen previously (see section 3.5.1) that the main characteristics of the curves are preserved.

Now equation (3.19) simplifies to

$$
\begin{aligned}
P_k &= P_k^{in} + 2 \sum_{j=1}^{\left\lfloor \frac{k-1}{t_b} \right\rfloor} R_D^j P_{k-jt_b}^{in} \\
&= \mathbb{1}_{systole}(k) + 2 \sum_{j=1}^{\left\lfloor \frac{k-1}{t_b} \right\rfloor} R_D^j \mathbb{1}_{systole}(k - jt_b),
\end{aligned}
\qquad k \in \mathbb{N}_{>t_b}. \qquad (3.20)
$$

Next, we will develop formulas for both SBP and DBP and thus also for PP.

3.8.1 Systolic, Diastolic and Pulse Pressure

Let $k \in \mathbb{N}$, $k \geqslant t_b \left(m^*(R_D) + 1 \right) + 1$ be given. The goal is to find a formula for P_k, depending on the temporal position of k within the cardiac cycle, using the notation introduced in the following definition.

Definition 3.8.1 *The number of time points in systole will be denoted by k_s, the number of time points in diastole by k_d. Further, we set*

$$
k_s^{t_b} := \left\lceil \frac{k_s}{t_b} \right\rceil \qquad and \qquad k_d^{t_b} := \left\lceil \frac{k_d}{t_b} \right\rceil.
$$

To understand the analysis that will be conducted regarding the influence of parameters on SBP and DBP in sections 3.8.3 - 3.8.5 it is not necessary to follow the very technical arguments in this section. They are only provided for reasons of completeness.

In formula (3.20) the number R_D^j only adds to P_k if $k - jt_b$ is a point in systole. In the following we will need to know for how many consecutive values of j this is true. Likewise we will need the number of consecutive values of j such that $k - jt_b$ is in diastole. Using the notation from definition 3.8.1 one recognizes that the number is either $k_s^{t_b}$ or $k_s^{t_b} - 1$ for systole and $k_d^{t_b}$ or $k_d^{t_b} - 1$ for diastole if the starting point is one that can be reached within t_b time steps from the previous diastole or systole, respectively. Figure 3.15 illustrates this for $k_s = 5$, $k_d = 10$ and $t_b = 3$, i.e. $k_s^{t_b} = 2$ and $k_d^{t_b} = 4$.

Now imagine repeatedly taking t_b time steps, passing through several cardiac cycles. Determining exactly how many points of each systole and diastole are reached will be tedious work and impossible to do without knowledge of k_s, k_d and t_b. Instead we will call these numbers n_s and n_d respectively, with $n_s \in \{k_s^{t_b} - 1, k_s^{t_b}\}$ and $n_d \in \{k_d^{t_b} - 1, k_d^{t_b}\}$ and ignore the fact that we do not know which of the two values n_s and n_d really attain. Specifying n_s and n_d will later lead to our first estimation.

The assumption of k being in systole gives k_s possibilities of what P_k might look like.

(a) Systole: Depending on the starting point one ($k_s^{t_b} - 1$, blue dot) or two ($k_s^{t_b}$, red and black dots) points are reached by going back t_b steps.

(b) Diastole: Depending on the starting point three ($k_s^{t_b} - 1$, blue and red dots) or four ($k_s^{t_b}$, black dots) points are reached by repeatedly going back t_b steps.
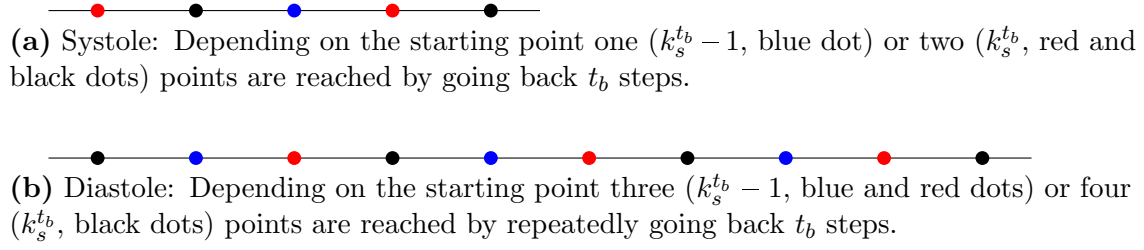
Figure 3.15: Illustration of the number of consecutive values j such that $k - jt_b$ is in systole or diastole, respectively.

◆ If k is the last time point in systole, the first $n_s - 1$ time points reached by $k - jt_b$ with $j \geqslant 1$ are still in systole, meaning that R_D^j will be added to P_k. The next n_d are in diastole (nothing gets added to P_k), followed by n_s time points in systole. This pattern will be continued while $k - jt_b \geqslant 1$. Instead of a verbal description, a mathematical expression for these considerations can be obtained by adaptation of formula (3.20), yielding

$$
\begin{aligned}
P_k = 1 + 2 \sum_{i=1}^{n_s-1} R_D^i + 2 \sum_{i=1}^{n_s} R_D^{n_s+n_d+i-1} + 2 \sum_{i=1}^{n_s} R_D^{2(n_s+n_d)+i-1} \\
+ \ldots \\
+ 2 \sum_{i=1}^{n_s} R_D^{(l-1)(n_s+n_d)+i-1} + 2 \sum_{i=1}^{i_{max}} R_D^{l(n_s+n_d)+i-1}
\end{aligned}
\tag{3.21}
$$

where $\ldots$ indicates that the sums continue in the same manner until

$$
k - t_b\Big(l\,(n_s + n_d) + i_{max} \Big) \leqslant 0
$$

for some $1 \leqslant i_{max} < n_s$ and $l \in \mathbb{N}$, see equation (3.20). In order to simplify the following calculations we assume to have infinitely many sums. This can be justified by the fact that there holds $k \geqslant t_b\,(m^*(R_D) + 1) + 1$ and thus

$$
t_b\Big(l\,(n_s + n_d) + i_{max} \Big) \geqslant t_b\,(m^*(R_D) + 1) + 1
\tag{3.22}
$$

which makes all the additional sums negligibly small, see section 3.8.2.

By adding the negligibly small summands to obtain an infinite number of sums formula (3.21) now simplifies to

$$
P_k \approx 1 + 2 \sum_{i=1}^{n_s-1} R_D^i + 2 \sum_{j=1}^{\infty} R_D^{j(n_s+n_d)} \sum_{i=1}^{n_s} R_D^{i-1}
$$

which is transformed to

$$P_k \approx 1 + 2\left(\frac{1 - R_D^{n_s}}{1 - R_D} - 1\right) + 2\frac{1 - R_D^{n_s}}{1 - R_D}\left(\frac{1}{1 - R_D^{n_s+n_d}} - 1\right)$$

using the geometric sum formula. Rearranging further yields

$$P_k \approx 1 + 2\frac{R_D - R_D^{n_s}}{1 - R^D} + 2\frac{1 - R_D^{n_s}}{1 - R_D}\frac{R_D^{n_s+n_d}}{1 - R_D^{n_s+n_d}}.$$

- ◆ Now assume k to be such that only the first $n_s - 2$ points reached by $k - jt_b$ with $j \geqslant 1$ are in systole. Everything else is shifted by one. Carrying out the same estimations and transformations as above finally yields

$$P_k \approx 1 + 2\frac{R_D - R_D^{n_s-1}}{1 - R_D} + 2\frac{1 - R_D^{n_s}}{1 - R_D}\frac{1}{R_D}\frac{R_D^{n_s+n_d}}{1 - R_D^{n_s+n_d}}$$

- ◆ ...

Going through the same process as above for all the possible temporal positions for k within systole finally leads to the general formula

$$P^{syst}(l, n_s, n_d) := 1 + \frac{2R_D}{1 - R_D} + 2R_D^{-l}\left(R_D^{n_s+n_d}\frac{1 - R_D^{n_s}}{1 - R_D}\frac{1}{1 - R_D^{n_s+n_d}} - \frac{R_D^{n_s}}{1 - R_D}\right) \quad (3.23)$$

for some $l = 0, \ldots, n_s - 1$ indicating at what temporal position within systole k is.

Unfortunately formula (3.23) still depends on the particular values of n_s and n_d as well as on the exact temporal position of k within systole. Since we are interested in finding maximum and minimum values, though, we do not need this general form. Rather, we want to choose l (and later also n_s and n_d) such that the expression given by (3.23) is maximized / minimized.

Claim 3.8.2   *The expression $P^{syst}(l, n_s, n_d)$ given by (3.23) is decreasing monotonously in l.*

Proof.   In consequence of $0 < R_D < 1$ the term $2R_D^{-l}$ is increasing monotonously in l and thus all we need to check is the sign of $\left(\ldots\right)$ in (3.23).

Consider

$$R_D^{n_s+n_d}\frac{1 - R_D^{n_s}}{1 - R_D}\frac{1}{1 - R_D^{n_s+n_d}} - \frac{R_D^{n_s}}{1 - R_D} < 0$$

$$\Leftrightarrow \quad R_D^{n_d}\frac{1 - R_D^{n_s}}{1 - R_D}\frac{1}{1 - R_D^{n_s+n_d}} - \frac{1}{1 - R_D} < 0$$

$$\Leftrightarrow \quad R_D^{n_d}(1 - R_D^{n_s}) - 1 + R_D^{n_s+n_d} < 0$$

$$\Leftrightarrow \quad R_D^{n_d} - 1 < 0.$$

The last inequality is true because $0 < R_D < 1$. $\qquad\square$

Now assume k to be in diastole. Again, we have to find the formula for k_d different possible temporal positions.

The same procedure as above yields

$$P^{diast}(l, n_s, n_d) := 2R_D^{d-l} \sum_{i=1}^{n_s-1} R_D^{i-1} \sum_{j=0}^{\infty} R_D^{j(n_s+n_d)} = 2\frac{1 - R_D^{n_s}}{1 - R_D} R_D^{n_d-l} \frac{1}{1 - R_D^{n_s+n_d}} \quad (3.24)$$

for some $l = 0, \dots, n_d - 1$ indicating at which temporal position in diastole l lies.

Claim 3.8.3 *The expression $P^{diast}(l, n_s, n_d)$ given by (3.24) is monotonously increasing in l.*

Proof.   Can be seen directly due to $0 < R_D < 1$. $\qquad\square$

Choice of n_s, n_d.   As mentioned above, $n_s \in \left\{k_s^{t_b} - 1, k_s^{t_b}\right\}$, $n_d \in \left\{k_d^{t_b} - 1, k_d^{t_b}\right\}$ and it is at best very tedious to determine exactly which of the two values to choose. For this reason at this point we need to make estimations. The idea is to maximize / minimize formulas (3.23) and (3.24) with respect to n_s and n_d to find upper estimates for SBP and lower estimates for DBP.

Claim 3.8.4 *Formulas (3.23) and (3.24) depend on n_s and n_d as follows:*

1. *$P^{syst}(l, n_s, n_d)$ is monotonously increasing in n_s and decreasing in n_d.*

2. *$P^{diast}(l, n_s, n_d)$ is monotonously increasing in n_s and decreasing in n_d.*

Proof.

1. We need to calculate the derivatives with respect to n_s and n_d respectively.

   ◆ There holds

   $$\frac{\mathrm{d}}{\mathrm{d}n_s} P^{syst}(l, n_s, n_d) = R_D^{-l} \frac{2(R_D^{n_d} - 1)}{1 - R_D} \frac{R_D^{n_s} \ln R_D}{(1 - R_D^{n_s+n_d})^2}.$$

   Due to $0 < R_D < 1$ it follows that $R_D^{n_s} - 1 < 0$ and $\ln R_D < 0$, while all other factors are positive. Altogether this yields $\frac{d}{dn_s} P^{syst}(l, n_s, n_d) > 0$ for all l, n_s, n_d.

   ◆ There holds

   $$\frac{\mathrm{d}}{\mathrm{d}n_d} P^{syst}(l, n_s, n_d) = R_D^{-l} \frac{2R_D^{n_s}}{1 - R_D} \ln R_D \frac{R_D^{n_d}(1 - R_D^{n_s})}{(1 - R_D^{n_s+n_d})^2} < 0 \qquad \forall l, n_d, n_s$$

with similar arguments as above.

2. Again, we calculate the derivatives with respect to n_s and n_d.

   ◆ There holds

$$\frac{\mathrm{d}}{\mathrm{d}n_s}P^{diast}(l,n_s,n_d) = \frac{2R_D^{n_d-l}}{1-R_D}\ln R_D\,\frac{R_D^{n_s}(R_D^{n_d}-1)}{(1-R_D^{n_s+n_d})^2} > 0 \qquad \forall l,n_d,n_s,$$

   where again the main argument is $0 < R_D < 1$.

   ◆ There holds

$$\frac{\mathrm{d}}{\mathrm{d}n_d}P^{diast}(l,n_s,n_d) = \frac{2(1-R_D^{n_s})}{1-R_D}\,\frac{R_D^{n_d-l}\ln R_D}{(1-R_D^{n_s+n_d})^2} < 0 \qquad \forall l,n_d,n_s,$$

   with similar arguments as above.

   $\square$

Actual form of diastolic, systolic and pulse pressure.   To find out the actual (estimated) representations for SBP and DBP we will maximize / minimize P^{syst} and P^{diast} with respect to l, n_s and n_d and compare the results.

Claim 3.8.5 *The minimum of the curve after a setting time of $m^*(R_D)$ time steps, diastolic pressure, is approximately given by*

$$DBP = \min_{k \geqslant m^*(R_D)} P_k \approx 2\frac{1-R_D^{k_s^{t_b}-1}}{1-R_D}R_D^{k_d^{t_b}}\,\frac{1}{1-R_D^{k_s^{t_b}+k_d^{t_b}-1}}$$

for any positive integer values of $k_s^{t_b}$ and $k_d^{t_b}$.

Proof.   There holds

$$\min_{l,n_s,nd} P^{diast} = 2\frac{1-R_D^{k_s^{t_b}-1}}{1-R_D}R_D^{k_d^{t_b}}\,\frac{1}{1-R_D^{k_s^{t_b}+k_d^{t_b}-1}}. \tag{3.25}$$

and

$$\min_{l,n_s,n_d} P^{syst} = 1 + \frac{2R_D}{1-R_D} + R_D^{2-k_s^{t_b}}\left(2R_D^{k_s^{t_b}+k_d^{t_b}-1}\frac{1-R_D^{k_s^{t_b}-1}}{1-R_D}\,\frac{1}{1-R_D^{k_s^{t_b}+k_d^{t_b}-1}} - 2\frac{R_D^{k_s^{t_b}-1}}{1-R_D}\right).$$

To prove the claim we need to show that $\min\limits_{l,n_s,n_d} P^{diast} \leqslant \min\limits_{l,n_s,n_d} P^{syst}$ for all $0 < R_D < 1$ or, equivalently, $\min\limits_{l,n_s,n_d} P^{diast} - \min\limits_{l,n_s,n_d} P^{syst} \leqslant 0$. Multiplying the difference with the (positive) common denominator gives (after simplification)

$$\min_{l,n_s,n_d} P^{diast} - \min_{l,n_s,n_d} P^{syst} \leqslant 0 \Leftrightarrow (1-R_D)\left(2R_D^{k_d^{t_b}} - R_D^{k_s^{t_b}+k_d^{t_b}-1} - 1\right) \leqslant 0.$$

This can be further simplified by dividing by $1 - R_D$ which is positive, yielding

$$\min_{l,n_s,n_d} P^{diast} - \min_{l,n_s,n_d} P^{syst} \leqslant 0 \Leftrightarrow 2R_D^{k_d^{t_b}} - R_D^{k_s^{t_b} + k_d^{t_b} - 1} - 1 \leqslant 0. \tag{3.26}$$

Now consider

$$\frac{d}{dR_D} 2R_D^{k_d^{t_b}} - R_D^{k_s^{t_b} + k_d^{t_b} - 1} - 1 = 2k_d^{t_b} R_D^{k_d^{t_b} - 1} - (k_s^{t_b} + k_d^{t_b} - 1)R_D^{k_s^{t_b} + k_d^{t_b} - 2} > 0$$

which is equivalent to

$$R_D < \left(\frac{2k_d^{t_b}}{k_s^{t_b} + k_d^{t_b} - 1} \right)^{\frac{1}{k_s^{t_b} - 1}}.$$

Since physiologically realistic values must meet $k_s^{t_b} < k_d^{t_b}$ and thus

$$1 < \left(\frac{2k_d^{t_b}}{k_s^{t_b} + k_d^{t_b} - 1} \right)^{\frac{1}{k_s^{t_b} - 1}},$$

this condition is always fulfilled and the expression in (3.26) is monotonously increasing in R_D. Hence, it is sufficient to prove the inequality for the limiting case $R_D \to 1$. We have

$$\left(2R_D^{k_d^{t_b}} - R_D^{k_s^{t_b} + k_d^{t_b} - 1} - 1 \right)\bigg|_{R_D = 1} = 0,$$

proving our claim. $\qquad\qquad\qquad\qquad\qquad\qquad\qquad\qquad\qquad\qquad\qquad$ $\square$

Unfortunately, no similar claim can be proved for systolic blood pressure. An explicit approximate formula for SBP can only be found if the values k_s, k_d and t_b are known, as the following computations show.

There holds

$$\max_{l,n_s,n_d} P^{syst} = 1 + \frac{2R_D}{1 - R_D} + 2\left(R_D^{k_s^{t_b} + k_d^{t_b} - 1} \frac{1 - R_D^{k_s^{t_b}}}{1 - R_D} \frac{1}{1 - R_D^{k_s^{t_b} + k_d^{t_b} - 1}} - \frac{R_D^{k_s^{t_b}}}{1 - R_D} \right) \tag{3.27}$$

and

$$\max_{l,n_s,n_d} P^{diast} = 2\frac{1 - R_D^{k_s^{t_b}}}{1 - R_D} R_D \frac{1}{1 - R_D^{k_s^{t_b} + k_d^{t_b} - 1}}. \tag{3.28}$$

We want to know where $\max\limits_{l,n_s,n_d} P^{syst} \gtrless \max\limits_{l,n_s,n_d} P^{diast}$ or, equivalently,

$$\max_{l,n_s,n_d} P^{syst} - \max_{l,n_s,n_d} P^{diast} \gtrless 0$$

holds. Multiplying the difference with the (positive) common denominator gives (after

simplification)

$$\max_{l,n_s,n_d} P^{syst} - \max_{l,n_s,n_d} P^{diast} \gtreqqless 0 \quad \Leftrightarrow \quad (1 - R_D)\left(1 + R_D^{k_s^{t_b} + k_d^{t_b} - 1} - 2R_D^{k_s^{t_b}}\right) \gtreqqless 0.$$

This can be further simplified by dividing by $1 - R_D$ which is positive, yielding

$$\max_{l,n_s,n_d} P^{syst} - \max_{l,n_s,n_d} P^{diast} \gtreqqless 0 \quad \Leftrightarrow \quad \left(1 + R_D^{k_s^{t_b} + k_d^{t_b} - 1} - 2R_D^{k_s^{t_b}}\right) \gtreqqless 0.$$

Unfortunately the polynomial on the left hand side can have a root $0 < R_D^* < 1$, depending on the values of $k_s^{t_b}$ and $k_d^{t_b}$. Consider, for example, $k_s^{t_b} = 3$ and $k_d^{t_b} = 6$, yielding the root $R_D^* \approx 0.9$. Thus, the maximum is given by (3.27) for $0 < R_D \leqslant R_D^*$ and by (3.28) for $R_D^* < R_D \leqslant 1$. A more general expression for R_D^* that does not need inserting values for $k_s^{t_b}$ and $k_d^{t_b}$ cannot be found analytically.

Once we know systolic and diastolic pressure it is possible to compute pulse pressure, the difference of those two values.

Claim 3.8.6 *Pulse pressure PP can be approximated by*

$$PP \approx \frac{1}{(1 - R_D)\left(1 - R_D^{k_s^{t_b} + k_d^{t_b} - 1}\right)}\left[1 + R_D - 2R_D^{k_s^{t_b}} - 2R_D^{k_d^{t_b}} + 3R_D^{k_s^{t_b} + k_d^{t_b} - 1} - R_D^{k_s^{t_b} + k_d^{t_b}}\right]$$

for $0 < R_D \leqslant R_D^*$ and

$$PP \approx \frac{2}{(1 - R_D)\left(1 - R_D^{k_s^{t_b} + k_d^{t_b} - 1}\right)}\left[R_D - R_D^{k_s^{t_b} + 1} - R_D^{k_d^{t_b}} + R_D^{k_s^{t_b} + k_d^{t_b} - 1}\right]$$

for $R_D^* < R_D \leqslant 1$.

Proof. Use systolic and diastolic pressure as calculated in claim 3.8.5 and equations (3.27) and (3.28) and take the difference. $\qquad\square$

3.8.2 Error Analysis

There are two causes for errors in above estimations:

♦ Using the geometric series formula for a finite sum causes the error

$$err := \left|\sum_{j=1}^{l-1} R_D^{j(n_s + n_d)}\sum_{i=1}^{n_s} R_D^{i-1} + \sum_{i=1}^{i_{max}} R_D^{l(n_s + n_d) + i - 1} - \sum_{j=1}^{\infty} R_D^{j(n_s + n_d)}\sum_{i=1}^{n_s} R_D^{i-1}\right|$$

$$= \left|\sum_{j=l}^{\infty} R_D^{j(n_s + n_d)}\sum_{i=1}^{n_s} R_D^{i-1} - \sum_{i=1}^{i_{max}} R_D^{l(n_s + n_d) + i - 1}\right|.$$

This can be simplified to

$$err = \frac{R_D^{l(n_s+n_d)}}{1 - R_D^{n_s+n_d}} \frac{1 - R_D^{n_s}}{1 - R_D} - R_D^{l(n_s+n_d)} \frac{1 - R_D^{i_{max}}}{1 - R_D}$$

and further to

$$err = \frac{R_D^{l(n_s+n_d)}}{(1 - R_D^{n_s+n_d})(1 - R_D)} \left(1 - R_D^{n_s} - 1 + R_D^{i_{max}} + R_D^{n_s+n_d}(1 - R_D^{i_{max}})\right)$$

$$\leqslant \frac{R_D^{l(n_s+n_d)}}{(1 - R_D^{n_s+n_d})(1 - R_D)} \left(R_D^{i_{max}} + R_D^{n_s+n_d}\right).$$

Because of $i_{max} < n_s < n_s + n_d$ we obtain

$$err \leqslant 2\frac{R_D^{l(n_s+n_d)+i_{max}}}{(1 - R_D^{n_s+n_d})(1 - R_D)}$$

and can use the fact that $l(n_s + n_d) + i_{max} \geqslant m^*(R_D) + 1 + \frac{1}{t_b}$, see (3.22), and therefore $R_D^{l(n_s+n_d)+i_{max}} \leqslant \delta$. We finally obtain the upper bound

$$err \leqslant \frac{2\delta}{(1 - R_D^{n_s+n_d})(1 - R_D)}.$$

For $R_D \to 1$ this upper bound increases monotonously to infinity but so do SBP, DBP and PP, see section 3.8.3. Furthermore, we have seen in section 3.7.1 that the model does not yield realistic solutions for high values of R_D. For sufficiently low values of R_D the upper bound is a small number.

◆ The second source of error is the overestimation of systolic pressure and underestimation of diastolic pressure due to our choices of n_s and n_d. We can find upper bounds for the errors (in SBP and DBP, respectively and for n_s, n_d separately) by taking the differences between upper and lower estimates.

Consider, for example, the error caused by the choice of n_s in the P^{syst} formula. Take the difference

$$P^{syst}(l = 0, n_s = k_s^{t_b}, n_d) - P^{syst}(l = 0, n_s = k_s^{t_b} - 1, n_d)$$

as an upper bound for the error, yielding

$$err \leqslant 2\frac{R_D^{k_s^{t_b}}(1 - R_D^{n_d})}{(1 - R_D^{k_s^{t_b}+n_d})(1 - R_D^{k_s^{t_b}+n_d-1})}.$$

As before the upper bound increases to infinity for $R_D \to 1$ but due to the same reasons as before this does not pose a significant problem. Differentiation with respect to $k_s^{t_b}$ reveals that the upper bound is monotonously decreasing in $k_s^{t_b}$. Similarly, the

upper bound for the error caused by the choice of n_d is monotonously decreasing in $k_d^{t_b}$. The same analysis can be done for the errors in the P^{diast} formula.

However, the actual errors are not monotonous in either t_b, k_s or k_d because they depend on the residuals $\left\lceil \frac{k_s}{t_b} \right\rceil - \frac{k_s}{t_b}$ and $\left\lceil \frac{k_d}{t_b} \right\rceil - \frac{k_d}{t_b}$.

Combining both sources of error we see that systolic pressure will always be overestimated by our formulas. For diastolic pressure the absolute error depends on if and how the positive error from the geometric series compensates the underestimation due to the choice of n_s and n_d.

3.8.3 Influecne of the Reflection Coefficient

If we go back to the beginning of this section, we can see directly that both systolic and diastolic blood pressure are monotonously increasing in R_D because they are sums of increasing values, matching our predictions from section 3.6.2. Obviously there holds

$$\lim_{R_D \to 0} DBP(R_D, k_s^{t_b}, k_d^{t_b}) = 0, \quad \lim_{R_D \to 0} SBP(R_D, k_s^{t_b}, k_d^{t_b}) = 1$$

and

$$\lim_{R_D \to 1} DBP(R_D, k_s^{t_b}, k_d^{t_b}) = \lim_{R_D \to 1} SBP(R_D, k_s^{t_b}, k_d^{t_b}) = \infty.$$

Considering the derivatives of SBP and DBP with respect to R_D we find that also the derivatives are monotonously increasing and

$$\lim_{R_D \to 0} \frac{\mathrm{d}}{\mathrm{d}R_D} DBP(R_D, k_s^{t_b}, k_d^{t_b}) = 0, \quad \lim_{R_D \to 0} \frac{\mathrm{d}}{\mathrm{d}R_D} SBP(R_D, k_s^{t_b}, k_d^{t_b}) = 1$$

and

$$\lim_{R_D \to 1} \frac{\mathrm{d}}{\mathrm{d}R_D} DBP(R_D, k_s^{t_b}, k_d^{t_b}) = \lim_{R_D \to 1} \frac{\mathrm{d}}{\mathrm{d}R_D} SBP(R_D, k_s^{t_b}, k_d^{t_b}) = \infty.$$

Thus, we have convex functions with respect to R_D with a steep ascent towards $R_D = 1$.

Claim 3.8.7 *Pulse pressure has the limits*

$$\lim_{R_D \to 0} PP(R_D, k_s^{t_b}, k_d^{t_b}) = 1 \quad and \quad \lim_{R_D \to 1} PP(R_D, k_s^{t_b}, k_d^{t_b}) = \infty.$$

Proof. The limit $\lim_{R_D \to 0} PP(R_D, k_s^{t_b}, k_d^{t_b}) = 1$ is obvious considering the limits of SBP and DBP. For the second one we use the formulas in claim 3.8.6 and L'Hôpital's rule. $\square$

Unfortunately we are not able to prove monotony as easily as we did with SBP and DBP.

In figure 3.16 it can be seen that even though some simplifying estimations were made in finding above formulas, they give reasonable values compared to those produced by
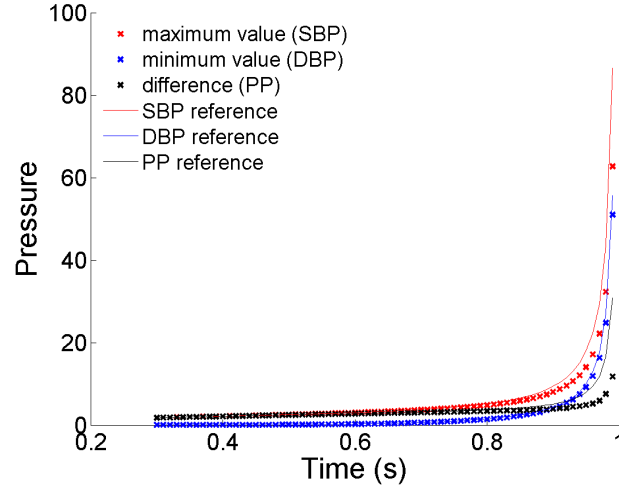
Figure 3.16: Systolic and diastolic pressure computed by the model compared to our reference values, depending on R_D, with fixed values of $k_s^{t_b}$ and $k_d^{t_b}$. First 128 cardiac cycles. Choice of parameters: $s = 0.3$, $d = 0.7$, $t_{b,ms} = 145$, $\tau = 0.0001$. 2^7 cardiac cycles. SBP, DBP and PP are generated using algorithm 3.5.1. The reference values are computed using formulas (3.27) and (3.28), claim 3.8.5 and claim 3.8.6.

the actual model with a step function as input P^{in}. We can also see that pulse pressure is increasing monotonously in R_D as well, even though we were not able to prove this analytically. However, it increases slower than systolic and diastolic pressure. The increase in SBP, DBP and PP can also be observed in figure 3.17.

(a) $R_D = 0.1$ **(b)** $R_D = 0.3$ **(c)** $R_D = 0.5$

(d) $R_D = 0.7$ **(e)** $R_D = 0.9$
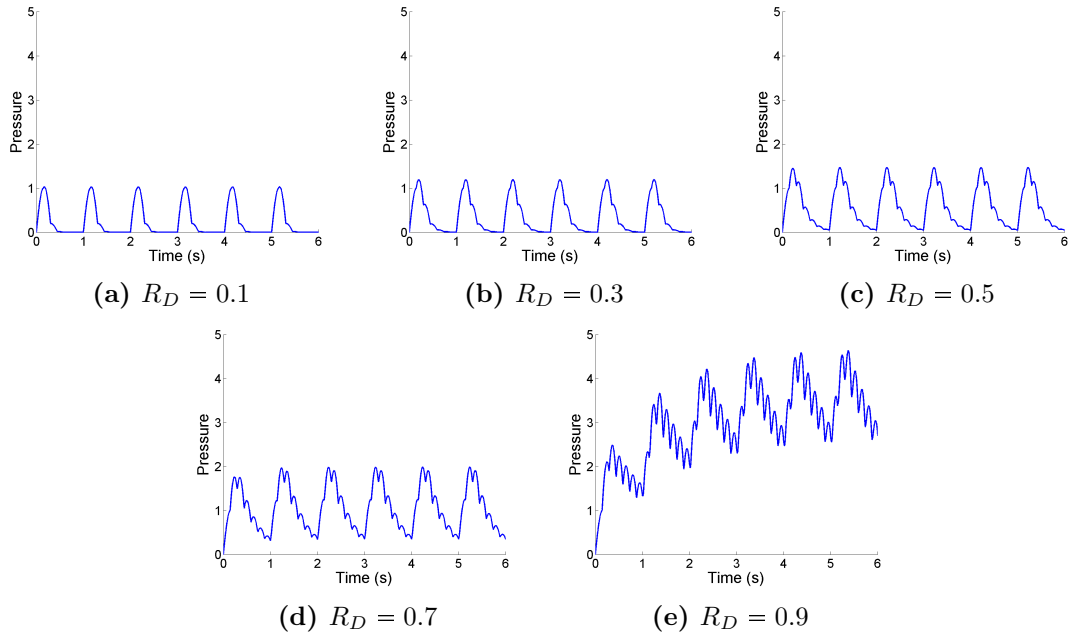
Figure 3.17: Different values of R_D and their influence on curve shape. First six cardiac cycles. Choice of parameters: $s = 0.3$, $d = 0.7$, $t_{b,ms} = 145ms$, $\tau = 0.0001$.

As for shape, we can make two observations. First of all, setting time does increase with

R_D, see figure 3.17 even though it remains low even for large values of R_D. For the second observation it is necessary to zoom into figure 3.17 and have a closer look at the last cardiac cycle, see figure 3.18.

(a) $R_D = 0.1$ (b) $R_D = 0.3$ (c) $R_D = 0.5$

(d) $R_D = 0.7$ (e) $R_D = 0.9$
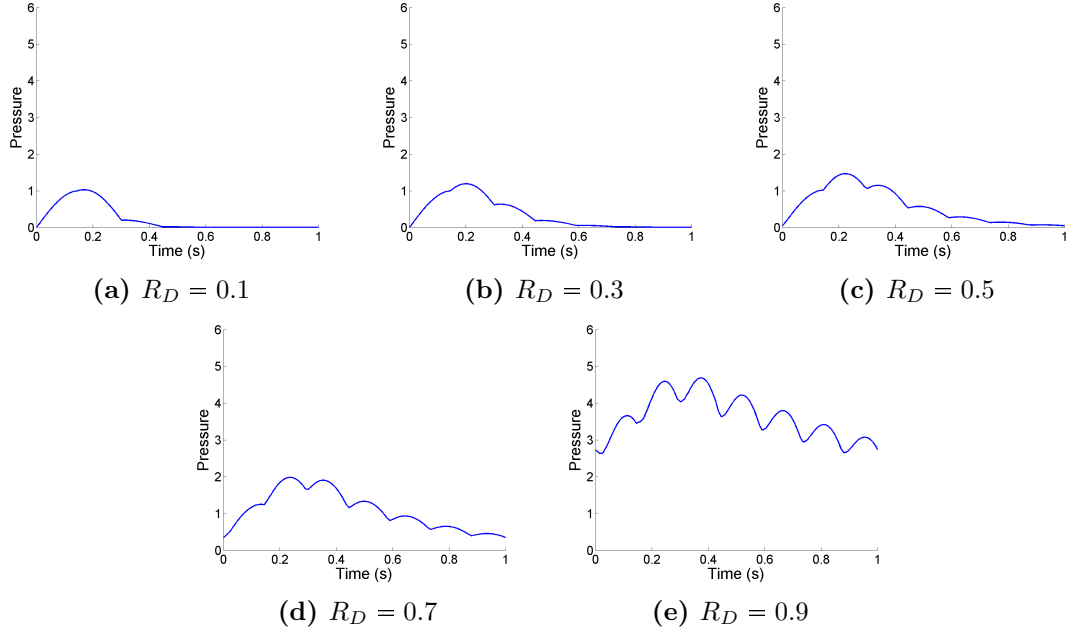
Figure 3.18: Different values of R_D and their influence on curve shape. Sixth cardiac cycle. Choice of parameters: $s = 0.3$, $d = 0.7$, $t_{b,ms} = 145ms$, $\tau = 0.0001$.

It seems that not only the spikes' prominence but also their number increases with increasing R_D, contradicting our ideas in section 3.6.2. However, further zooming in reveals that the same spikes that are clearly visible in figure 3.18 (e) are also present in figures 3.18 (a) -(d), only less prominent.

3.8.4 Influence of Systole and Diastole Duration

In the formulas describing SBP, DBP and PP the duration of systole and diastole are not used directly, but in the form of the parameters $k_d^{t_b}$ and $k_s^{t_b}$. According to definition 3.8.1 these are (almost) directly proportional to k_d and k_s which are directly related to the durations via the step size τ. Thus, we will do the following calculations with $k_s^{t_b}$ and $k_d^{t_b}$, respectively.

We find that indeed, the theories from section 3.6.3 are (at least for SBP and DBP) confirmed for both variable and constant heart rate, see the following claims.

First consider the case of variable heart rate, i.e. $k_d^{t_b}$ and $k_s^{t_b}$ are varied independently of each other.

Claim 3.8.8 *Keeping $k_d^{t_b}$ fixed, diastolic and systolic pressure are monotonously increasing in $k_s^{t_b}$. They are monotonously decreasing in $k_d^{t_b}$ if we keep $k_s^{t_b}$ fixed.*

Proof. See claim 3.8.4. For systolic pressure the distinction between $0 < R_D \leqslant R_D^*$ and $R_D^* < R_D \leqslant 1$ has to be made. Fortunately the claim is true for both forms of SBP. $\square$

Unfortunately it is not as easy to prove a similar claim as claim 3.8.8 for pulse pressure: Distinguishing between $0 < R_D \leqslant R_D^*$ and $R_D^* < R_D \leqslant 1$ gives different results for the two cases. Because R_D^* depends on $k_s^{t_b}$ and $k_d^{t_b}$ again, this leads to circular reasoning.

Next we consider the heart rate to be constant which implies that variation of one of the parameters $k_s^{t_b}$ and $k_d^{t_b}$ results in variation of the other too.

Claim 3.8.9 *Keeping the heart rate fixed, i.e. $k_s^{t_b} + k_d^{t_b} = c$ for some $c \in \mathbb{N}$, systolic and diastolic pressure are monotonously increasing in k_s and monotonously decreasing in k_d.*

Proof. Setting $k_d^{t_b} = c - k_s^{t_b}$ simplifies the formula from claim 3.8.5 to

$$P^{diast} = \frac{2R_D^c}{(1 - R_D)(1 - R_D^{c-1})}\left(R_D^{-k_s^{t_b}} - R_D^{-1}\right),$$

which obviously is monotonously increasing in k_s. Analogously the monotony in $k_d^{t_b}$ can be seen directly by setting $k_s^{t_b} = c - k_d^{t_b}$.

The same observations can be made for the systolic pressure but as in the proof of claim 3.8.8 separate formulas have to be used for $R_D \leqslant R_D^*$ and $R_D > R_D^*$. Again, the argument works because the claim is true for both forms of SP. $\square$

A similar result can be proved for pulse pressure too because (almost) the same result can be obtained for $0 < R_D \leqslant R_D^*$ and $R_D^* < R_D \leqslant 1$.

Claim 3.8.10 *Keeping the heart rate fixed, i.e. $k_s^{t_b} + k_d^{t_b} = c$ for some $c \in \mathbb{N}$, pulse pressure is increasing in $k_s^{t_b}$ and decreasing in $k_d^{t_b}$ under the "physiological condition" $k_s^{t_b} < k_d^{t_b}$.*

Proof. Plugging $k_d^{t_b} = c - k_s^{t_b}$ into the formulas in claim 3.8.6 yields

$$PP = \begin{cases} \frac{1}{(1-R_D)(1-R_D^{c-1})}\left[1 + R_D - 2R_D^{k_s^{t_b}} - 2R_D^{c-k_s^{t_b}} + 3R_D^{c-1} - R_D^c\right], & 0 \leqslant R_D \leqslant R_D^*, \\ \frac{2}{(1-R_D)(1-R_D^{c-1})}\left[R_D - R_D^{k_s^{t_b}+1} - R_D^{c-k_s^{t_b}} + R_D^{c-1}\right], & R_D^* < R_D \leqslant 1. \end{cases}$$

Differentiation shows

$$\frac{\mathrm{d}}{\mathrm{d}k_s^{t_b}}PP \geqslant 0 \quad \Leftrightarrow \quad R_D^{c-k_s^{t_b}} \leqslant R_D^{k_s^{t_b}+1} \quad \Leftrightarrow \quad k_s^{t_b} \leqslant \frac{c-1}{2} \quad \Leftrightarrow \quad k_s^{t_b} \leqslant k_d^{t_b} - 1$$

for $0 < R_D \leqslant R_D^*$ and

$$\frac{\mathrm{d}}{\mathrm{d}k_s^{t_b}}PP \geqslant 0 \quad \Leftrightarrow \quad R_D^{c-k_s^{t_b}} \leqslant R_D^{k_s^{t_b}} \quad \Leftrightarrow \quad k_s^{t_b} \leqslant \frac{c}{2} \quad \Leftrightarrow \quad k_s^{t_b} \leqslant k_d^{t_b}$$

for $R_D^* < R_D \leqslant 1$ which proves the claim. The proof for $\frac{\mathrm{d}}{\mathrm{d}k_d^{t_b}}PP$ is analogous. $\qquad\square$

These theoretical (and simplified) results, at least for variable heart rate, are confirmed by figures 3.19 (a) and (b). As for shape, we see that the influence of systole and diastole duration is the same as in section 3.7.2. Similar results can be obtained in the case of constant heart rate.

(a) Variation of systole duration with a diastole duration of $d = 0.9$. First cardiac cycle.

(b) Variation of diastole duration with a systole duration of $s = 0.3$. First two cardiac cycles.
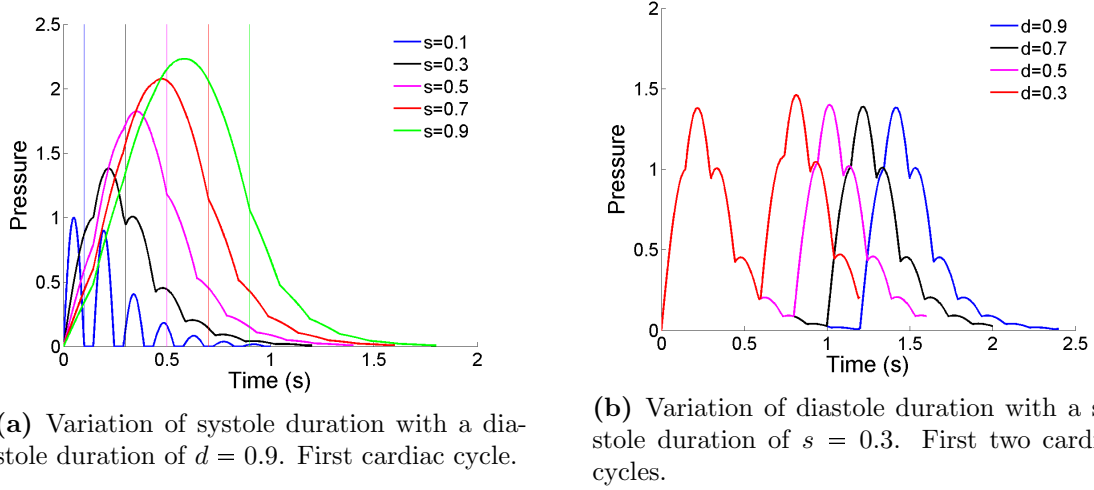
Figure 3.19: Influence of systole and diastole duration on curve shape. In (a) the beginning of systole is marked by a vertical line. Choice of parameters: $t_{b,ms} = 145$, $R_D = 0.45$, $\tau = 0.0001$.

It was already mentioned in section 3.6.3 that Wilkinson et al. showed that central diastolic pressure increased significantly with an increasing heart rate while central systolic pressure decreased significantly [58] or did not change significantly [57]. These phenomena can numerically be observed in our very simple model as well. For an illustration of an increase in DBP and decrease in SBP, at least for certain combinations of parameters, see figure 3.20. It is known [10] that as the heart rate increases, there is a much greater decrease of diastole length than of systole length [6], which in this model means a large decrease in $k_d^{t_b}$ and a smaller one in $k_s^{t_b}$. For this reason diastole duration d was decreased from 0.9 to 0.3 seconds while simultaneously systole duration s was decreased from 0.4 to 0.3 seconds to produce figure 3.20, generating heart rates between ~ 46 and 100 bpm.

However, the relationship between heart rate and SBP is not the same for all parameter combinations. Increasing R_D and or $t_{b,ms}$ to very large values reverses the behavior of SBP, especially for high heart rates. This is due to the fact that systole and diastole duration have opposing impact on SBP while they play together in influencing DBP.

3.8.5 Influence of Return Time

The time constant is related to $k_s^{t_b}$ and $k_d^{t_b}$ via definition 3.8.1. Ignoring the ceiling function they would be inversely proportional. The ceiling function, however, only slows
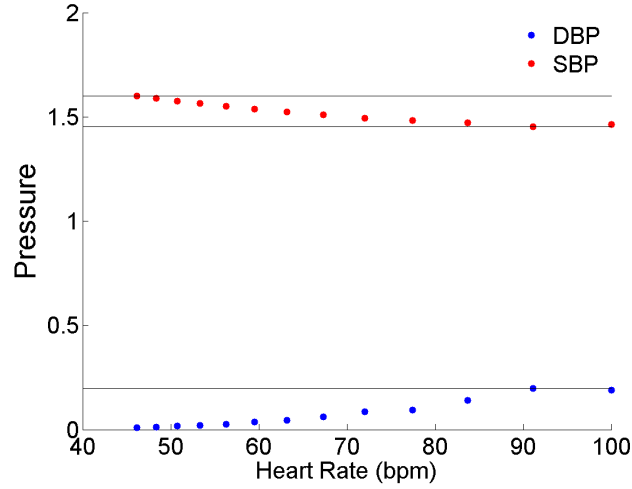
Figure 3.20: Influence of heart rate on SBP and DBP. First 128 cardiac cycles. Choice of parameters: $R_D = 0.45$, $t_{b,ms} = 145$, $\tau = 0.0001$.

down change, since different values of t_b can lead to the same values of $k_s^{t_b}$ or $k_d^{t_b}$ when k_s and k_d, respectively, are held constant.

Unluckily the change of t_b influences $k_s^{t_b}$ and $k_d^{t_b}$ at the same time. These parameters have opposite impact on systolic and diastolic pressure and their impact on pulse pressure cannot be determined analytically. Altogether it is not possible to find an analytic description of the time constants' influence. We thus have to rely on numerical analysis.

(a) $t_{b,ms} = 75ms$ **(b)** $t_{b,ms} = 100ms$ **(c)** $t_{b,ms} = 125ms$

(d) $t_{b,ms} = 150ms$ **(e)** $t_{b,ms} = 175ms$ **(f)** $t_{b,ms} = 200ms$
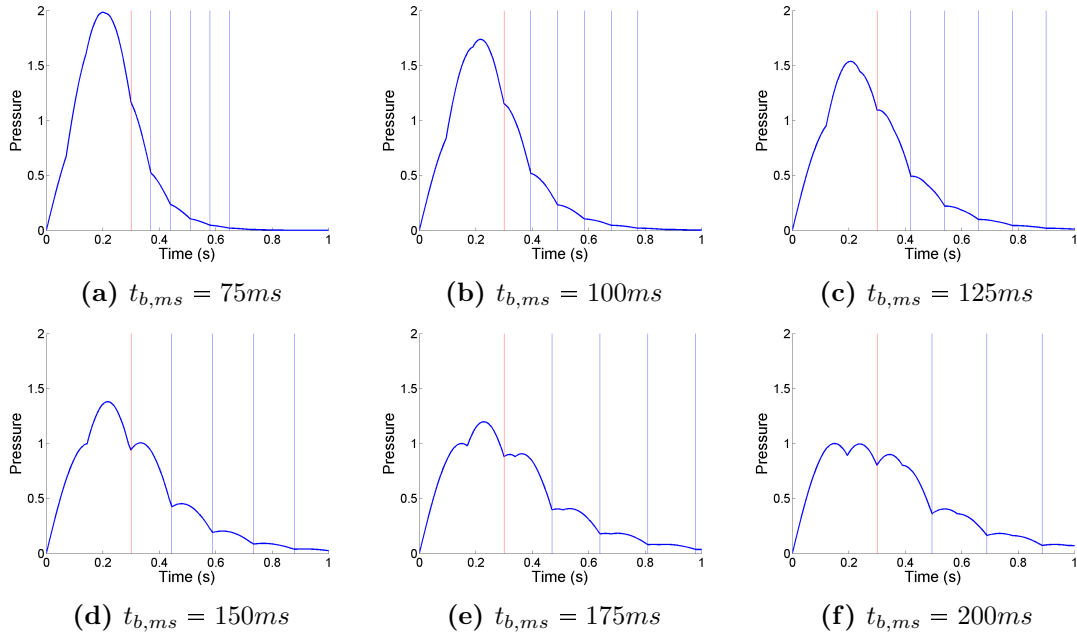
Figure 3.21: Different values of t_b and their influence on curve shape. First cardiac cycle. End of systole is marked by a red vertical line. Return times are marked by blue vertical lines. Choice of parameters: $s = 0.3$, $d = 0.7$, $R_D = 0.45$, $\tau = 0.0001$.

In figure 3.21 several observations can be made. First of all it is confirmed that increasing the return time decreases SBP and increases DBP. More peaks appear and become more prominent relative to the prominence of the entire curve. As opposed to the observation from section 3.7.3 the width of the spikes does not equal $t_{b,ms}$ this time. This is due to the fact that reflections do not die out as quickly and therefore superposition of reflected waves takes place.

3.8.6   Influence of Step Size

The influence of the time step size τ has been discussed and illustrated in section 3.7.4.

3.9   The Heart as Total Absorber

After considering the heart to be both a time-dependent reflector and a total reflector at all times we will now study the case where the heart is a total absorber at all times. Using a general input function P^{in} and setting $R^{av} \equiv 0$ leads to a much easier solution formula,

$$P_k = P_k^{in} + P_{k-t_b}^{in} R_D, \qquad k \in \mathbb{N}_{>t_b}.$$

It can be seen directly that for any choice of P^{in} that equals zero during diastole the lowest possible value is $P_k = 0$, as long as

$$k_d^{t_b} \geqslant 2. \tag{3.29}$$

Therefore DBP remains constant. The highest possible value, i.e. SBP (and with it PP), is influenced by the particular choice of P^{in} and, depending on its shape, also $k_s^{t_b}$. If P^{in} is assumed to be a half sine during systole, the time position of the maxima of the curve changes with R_D, resulting in a more complex relationship between SBP (and with it PP) and R_D, see figure 3.22.

In general, most results from sections 3.7 and 3.8 are also valid in this case and will therefore not be repeated.

3.10   Scaling

One question that is not addressed in any of the previous sections is that of scaling. In physiological blood pressure curves there holds

$$\mathrm{DBP} : \mathrm{PP} \quad \approx \quad 2 : 1,$$
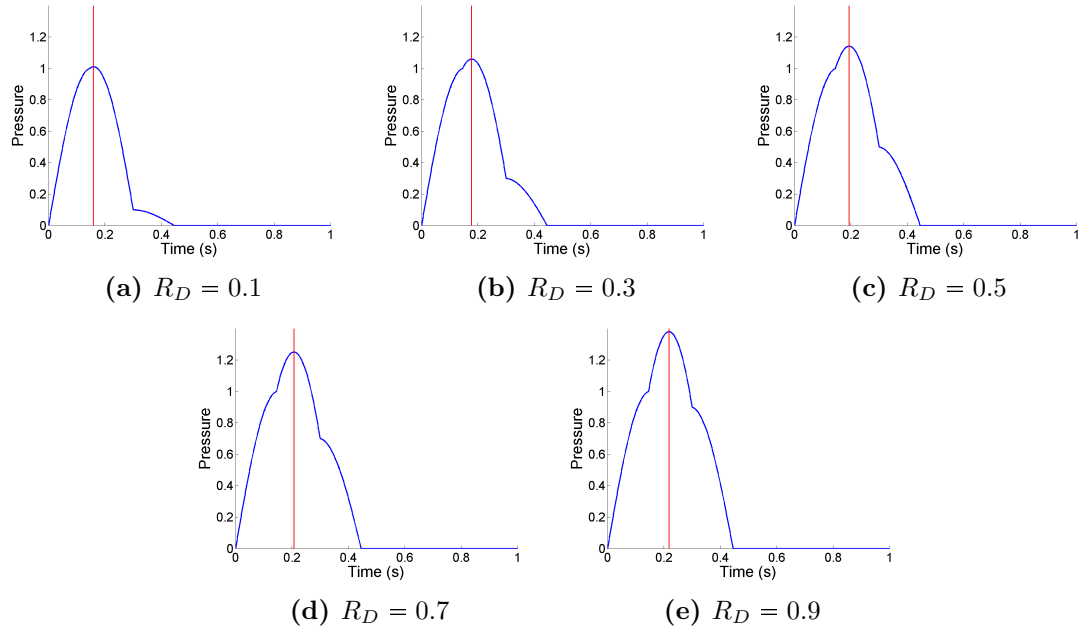
Figure 3.22: Different values of R_D and their influence on curve shape. First cardiac cycle. Position of maximum is indicated by red vertical line. Choice of parameters: $s = 0.3$, $d = 0.7$, $t_{b,ms} = 145ms$, $\tau = 0.0001$.

see section 2.1.2. In order for the model to reflect reality it is therefore desirable to produce curves that fulfill the same condition.

Now consider sections 3.7 and 3.9. Since we have DBP = 0 for all choices of parameters it is impossible to scale the model accordingly such that the desired ratio is obtained. Unfortunately, this is a sign that the model might not be a good representation of reality even though the shape of the curves looks promising.

In section 3.8, however, DBP increases with both R_D and $t_{b,ms}$, see sections 3.8.3 and 3.8.5, enabling us to obtain the desired ratio.

Using the results from figure 3.23 it is possible to associate the values on the ordinate with their respective values in mmHg, i.e.

$$2.8571 \text{ model units} \approx 80 \text{mmHg} \quad \text{and} \quad 4.2857 \text{ model units} \approx 120 \text{mmHg}.$$

This enables us to interpret the magnitude of the input function P^{in} that we were unable to determine earlier: The maximum value of P^{in}, that was chosen to be one in this model, must be equivalent to a magnitude of ~ 28mmHg in reality.

As can be seen in figure 3.23, the necessary parameter combination leads to a diminished quality in shape of the curve. Apparently one must choose between meaningful absolute values and a meaningful curve shape. The shape, however, can be changed further by adding more reflection sitesas will be done in the following chapter.
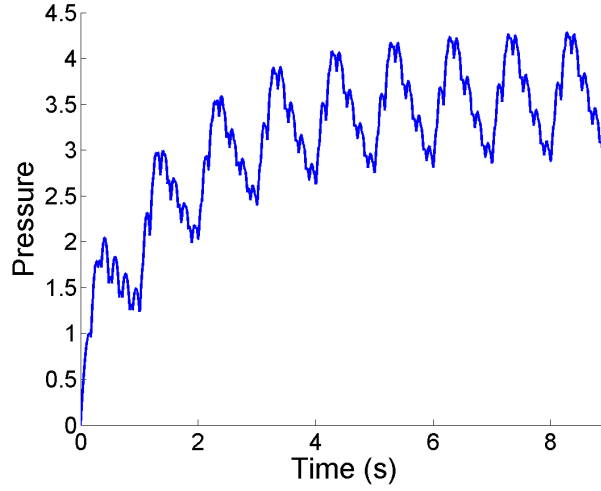
Figure 3.23: Modeled curve that satisfies DBP : PP $\approx$ 2 : 1. First nine cardiac cycles. Choice of parameters: $s = 0.3$, $d = 0.7$, $R_D = 0.9$, $t_{b,ms} = 178$, $\tau = 0.0001$.

3.10.1 Prolonged Diastole

It has been shown before [26] that if the heart stops, blood pressure experiences an approximately exponential decay until a constant value is reached. Studying this case with our model only makes sense for parameter combinations that yield a diastolic pressure that is not equal to zero. To increase comparability of absolute values to measured curves we will only work with the parameters established in this section.
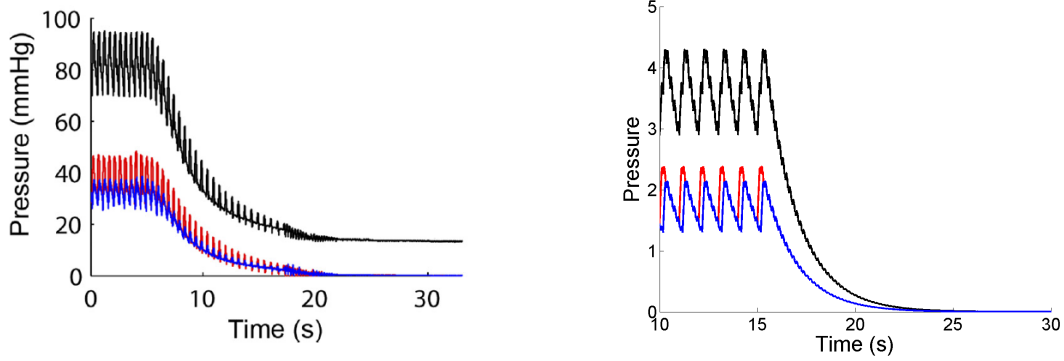
(a) Pulse pressure after heart stops beating. Adapted from [26].

(b) Pulse pressure after heart stops beating. 10th to 25th cardiac cycle. Choice of parameters: $s = 0.3$, $d = 0.7$, $R_D = 0.9$, $t_{b,ms} = 178$, $\tau = 0.0001$.

Figure 3.24: Pulse pressure after heart stops beating, i.e. extreme case of prolonged diastole. Comparison between measured and modeled curve.

In figure 3.24 we compare the results that were (a) obtained by measuring absolute blood pressure and performing a novel approach of wave separation [26] with (b) results from our model. We can see that the overall development in time is very similar in both figures,

with one major difference. In figure (a) measured blood pressure converges to a value distinctly unequal zero while in figure (b) all forward, backward and full blood pressure converge to zero as time progresses. Obviously, in (a) the sum of forward and backward pressure does not yield measured pressure, a fact that the explain authors by the existence of *undisturbed pressure.*

This concept could also be applied to our model in further studies. By adding a constant value to the sum of forward and backward pressure it might become possible to obtain correctly scaled curves with a meaningful shape.

3.11 Conclusion

In this chapter we presented arguments for the simplifying assumption of a single reflection site in the arterial system, proposed model equations (3.1a) and (3.2a) and solved them in section 3.1.

By conducting both mathematical and numerical analysis on several versions of the model we were able to verify that the modeled curves display the characteristic features and properties of physiological blood pressure curves. We can therefore conclude that the approach of modeling blood pressure curves with difference equations is a promising one.

Comparison of different ways to model input pressure from the heart as well as the reflection property of the aortic valve yielded the following: Assuming the heart to be a time-independent absolute reflector gives better results than the more intuitive time-dependent reflection coefficient. It is very well possible that truth lies somewhere in between those two very simple cases, i.e. the reflection coefficient is time-dependent but does not become zero during systole. This question could be addressed in further studies.

However, even though the modeled curves do display characteristic features of blood pressure curves, they are much less smooth, presumably due to the simplifying assumption of a single reflection site. For this reason in the next chapter we will extend the model to include more than one reflection site.

Difference Equation Models Using More Reflection Sites

In the previous chapter we showed that modeling the arterial system as a single tube and describing reflection phenomena with difference equations is a useful approach. However, even though the model curves display all the important features of a central blood pressure curve (see section 3.2) they clearly differ from measured curves, in particular in their smoothness.

While the single tube model has been popular with many researchers, others have found evidence that the ascending aorta "sees" two reflection sites instead of only one, one closer to the heart than the other [30, 40]. In both papers the experiments were conducted with dogs but the underlying principles are the same in humans. The two reflection sites can be interpreted as one in the lower part of the body and one in the upper part [30].

Modeling two reflection sites is often accomplished with an asymmetric *T-tube model* as was proposed by O'Rourke [29]. The shorter arm of the T represents the arteries in head, neck and upper limbs while the longer arm represents descending aorta and the arteries in trunk and lower limbs.

Determination of parameter values is even harder for the T-tube model than the single tube model [4]. This is because parameters in one arm of the tube depend on those of the other arm. We will encounter this difficulty in section 4.3.

However, in the model(s) developed and studied in this chapter instead of a branching tube we will consider a set-up as shown in figure 4.1. The two reflection sites are assumed to be independent from each other, all interactions already being accounted for by the choice of parameter values.

The parameters are the same as were introduced in chapter 3, with only two differences.
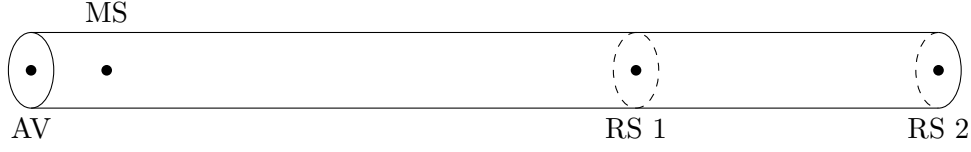
Figure 4.1: Tube model of the arterial system with two reflection sites as presented above. AV - aortic valve, MS - measuring site, RS 1 - first distal reflection site, RS 2 - second distal reflection site.

Instead of one reflection coefficient R_D we now have to distinguish between R_D^1 and R_D^2, the reflection coefficients of the first and second reflection site, respectively. Analogously, we have two time constants t_b^1 and t_b^2. Both are computed using the same PWV but obviously the distances between measuring site and reflection sites as well as the phase shift of the reflected wave may differ. Without loss of generality we may assume $t_b^1 < t_b^2$.

Again, total pressure is split into its forward and backward component, i.e. $P_k = P_k^f + P_k^b$, yielding the difference equation system

---

Model 2

$$P_k^f = P_k^{in} + P_{k-2t_f}^b R_{k-t_f}^{av}, \tag{4.1a}$$

$$P_k^b = P_{k-t_b^1}^f R_D^1 + P_{k-t_b^2}^f R_D^2. \tag{4.1b}$$

By inserting equation (4.1a) into (4.1b) and vice versa we obtain the two independent equations

$$P_k^f = P_k^{in} + P_{k-2t_f-t_b^1}^f R_D^1 R_{k-t_f}^{av} + P_{k-2t_f-t_b^2}^f R_D^2 R_{k-t_f}^{av}, \tag{4.2a}$$

$$P_k^b = P_{k-t_b^1}^{in} R_D^1 + P_{k-2t_f-t_b^1}^b R_D^1 R_{k-t_f-t_b^1}^{av} + P_{k-t_b^2}^{in} R_D^2 + P_{k-2t_f-t_b^2}^b R_D^2 R_{k-t_f-t_b^2}^{av} \tag{4.2b}$$

for $k \in \mathbb{N}_{>2t_f+t_b^2}$ that are both of order $N = 2t_f + t_b^2$.

Again, we know from standard literature [1, 11] that the initial value problems defined by equations (4.2a) and (4.2b) for $k \in \mathbb{N}_{>N}$ and some initial values $\bar{P}_k$ and $\hat{P}_k$ for $k = 1, \ldots, N$, have unique solutions. For the forward pressure the initial condition can be chosen as $P_k^f = P_k^{in}$ for $k = 1, \ldots, N$. For the backward pressure it is

$$P_k^b = \begin{cases} 0, & k = 1, \ldots, t_b^1, \\ R_D^1 P_{k-t_b^1}^{in}, & k = t_b^1 + 1, \ldots, t_b^2, \\ R_D^1 P_{k-t_b^1}^{in} + R_D^2 P_{k-t_b^2}^{in}, & k = t_b^2 + 1, \ldots, N. \end{cases}$$

Finding these solutions is not as straightforward as it was for equations (3.2a) and (3.2b).

Thus, numerical analysis will play an even more important role in this chapter than it did in chapter 3.

4.1 Boundedness of Homogeneous Solution

Stability analysis as in section 3.3.1 turns out to be impossible, even for the homogeneous equations because we fail to prove any convergence of the norm of the system matrix A.

The only statement we are able to show is the boundedness of the solutions of the homogeneous equation

$$x_k = x_{k-N_1} R_D^1 + x_{k-N_2} R_D^2 \tag{4.3}$$

that is equivalent to equations (4.2a) and (4.2b) with $N_1 = 2t_f + t_b^1$ and $N_2 = 2t_f + t_b^2$, respectively, and $R^{av} \equiv 1$, under certain conditions.

Claim 4.1.1 *Every solution* $(x_k)_{k \in \mathbb{N}}$ *of equation* (4.3) *is bounded, i.e. there exists* $c > 0$, *depending on the initial condition such that*

$$|x_k| \leqslant c \qquad \forall k \in \mathbb{N}$$

if $R_D^1 + R_D^2 < 1$.

Proof. The proof is a simple mathematical induction. Let $x_1, \ldots, x_{N_2}$ be the initial condition and define $c = \max_{i=1,\ldots,N_2} |x_i|$, directly implying the induction base for $k = 1, \ldots, N_2$. Now assume $k > N_2$. By (4.3) and the triangle inequality it follows

$$|x_k| \leqslant R_D^1 |x_{k-N_1}| + R_D^2 |x_{k-N_2}|.$$

Inserting the induction hypothesis and the condition $R_D^1 + R_D^2 < 1$ finally yields

$$|x_k| \leqslant (R_D^1 + R_D^2)c \leqslant c,$$

completing the proof. □

The boundedness of the homogeneous solution combined with the fact that the input function vanishes for a large proportion of time points hints that the solutions of (4.1a) and (4.1b) are bounded too but we will have to resort to numerical analysis to confirm this prognosis.

4.2 Comparison to First Model and Measured Curves

In this section we want to compare the curves produced by the new model with those produced by the original model in chapter 3 as well as with measured curves.

Since in chapter 3 treating the heart as a time-independent reflector gave useful results, we will consider both the cases $R^{av} \equiv 1$ and $R^{av} = \mathbb{1}_{diastole}$ in this chapter. The choice of P^{in} will be the same as in chapter 3. Due to our results from section 3.4 we will concentrate on $t_f = 0$ and omit the possibility of $t_f > 0$. The combinations of parameters used to generate the curve in figures 4.2 (a) and (b) were found by trial and error, including information from the previous chapter. They are chosen such that the curves look as similar to the measured curve as possible, therefore different parameter values are used in (a) and (b).
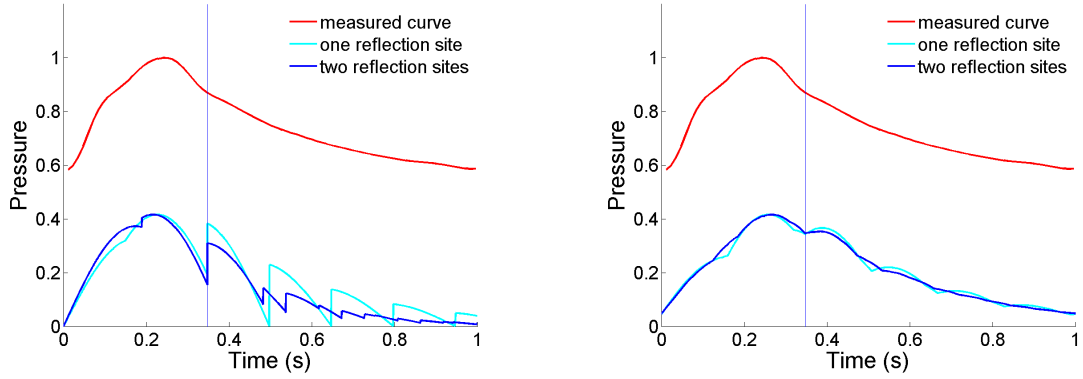
(a) $R^{av} = \mathbb{1}_{diastole}$. Choice of parameters for blue curve: $s = 0.348$, $d = 0.652$, $t^1_{b,ms} = 135$, $t^2_{b,ms} = 190$, $R^1_D = 0.2$, $R^2_D = 0.23$, $\tau = 0.0001$. Choice of parameters for cyan curve as in figure 3.5.

(b) $R^{av} \equiv 1$. Choice of parameters for blue curve: $s = 0.348$, $d = 0.652$, $t^1_{b,ms} = 125$, $t^2_{b,ms} = 185$, $R^1_D = 0.3$, $R^2_D = 0.3$, $\tau = 0.0001$. Choice of parameters for cyan curve: $s = 0.348$, $d = 0.652$. $t_{b,ms} = 160$, $R_D = 0.6$, $\tau = 0.0001$.

Figure 4.2: Comparison of measured curve, a curve modeled with one reflection site and a curve modeled with two reflection sites. Normalization to same pulse pressure. End of systole is marked by a vertical line.

Figure 4.2 (a) compares the second cardiac cycle of each of the models using $R^{av} = \mathbb{1}_{diastole}$ with a measured curve. In figure 4.2 (b) the same comparison is done for $R^{av} \equiv 1$. While the second cardiac cycle differs from the first one, the curve has reached its periodic state after two cycles. Thus, the second cardiac cycle (or any cycle after the first one) is more meaningful for analyzing model properties. The main characteristics of a blood pressure curve are still represented in the new model (blue). Even though the curve is still not as smooth as the measured one, we can see that the spikes have become less prominent, thus better approximating the diastolic decay. In particular, the blood pressure does not decrease to zero after each spike in figure 4.2 (a), presumably a result of the superposition of reflected waves. In figure 4.2 (b) we can observe that, again, choosing $R^{av} \equiv 1$ yields very good results, even smoother than in the previous chapter. Altogether figures 4.2 (a) and (b) justify further analysis of the enhanced model, using both versions of R^{av}, despite its difficulty.

4.3 Numerical Analysis

Unline in chapter 3, the theoretical knowledge of the enhanced model is very limited. In this section we hope to fill the gaps by numerical experiments and interpretation of plotted curves. Considering the increased number of parameters interpreting the plots will be a more delicate task than it was before.

4.3.1 Implementation and Parameter Values

Again, we will give an overview of implementation and parameter ranges before we start varying the parameters. In algorithm 4.3.1 the MATLAB function `GenerateCurveSeparatedTwo` that generates blood pressure curves according to the model is given.

Algorithm 4.3.1

```
1    function [Pf,Pb,P] = GenerateCurveSeparatedTwo (s, d, J, tau, RD1, RD2,
                          tbms1, tbms2, tfms)

2    tb1 = floor(tbms1 * 0.001 / tau);

3    tb2 = floor(tbms2 * 0.001 / tau);

4    tf = floor(tfms * 0.001 / tau);

5    [Pin,Rav]=GeneratePinRav(s, d, J, tau, tf);

6    Pf=Pin;

7    Pb = [zeros(1,tb1), Pin(1:tb2-tb1) .* RD1, Pin(tb2-tb1+1:tb2+2*tf-tb1)
            .* RD1 + Pin(1:2*tf) .* RD2, zeros(1,length(Pin)-2*tf-tb2)];

8    for k = 2*tf + tb2 + 1:length(Pin)

9        Pb(k) = Pin(k-tb1)*RD1 + Pb(k-2*tf-tb1)*RD1*Rav(k-tf-tb1)
                + Pin(k-tb2)*RD2 + Pb(k-2*tf-tb2)*RD2*Rav(k-tf-tb2);

10       Pf(k) = Pin(k) + Pf(k-2*tf-tb1)*RD1*Rav(k-tf)
                        + Pf(k-2*tf-tb2)*RD2*Rav(k-tf);

11   end

12   P = Pf + Pb;

13   end
```

The function `GeneratePinRav` that is used in line 5 is the same that was used in chapter 3 and can be found in algorithm 3.5.2. Also parameters `s`, `d`, `J`, `tau` and `tfms` remain unchanged, meaning that reasonable values can be found in section 3.5.

The only parameters that need to be further specified are the reflection coefficients and return times.

◆ Instead of one distal reflection coefficient there now is one for each of the reflection sites, `RD1` and `RD2`. Unfortunately finding reference values in literature proves to be impossible. The result from section 4.1, though, indicates that the values should be lower than those that were used for R_D in the previous chapter.

◆ The situation is similar for return times. Even though pulse wave velocity does not differ rom that presented in the first model and the same values can be used, now there are two different distances, implying different return times `tbms1` and `tbms2`. Also for these parameters the search for reference values turns out not to be successful.

An alternative to using reference values from literature can be found in figure 4.2(a). The particular combination of parameters in this figure led to a valid blood pressure curve. Thus we will take the used numbers as reference values for further analysis.

4.3.2   Periodicity and Boundedness of Solutions

So far it has not been discussed if the curve generated by the inhomogeneous equations (4.2a) and (4.2b) is periodic or even has an upper bound for $k \to \infty$.

From sections 3.7.3, 3.8.3 and 3.8.4 we know that for the model with one reflection site large values of reflection coefficient and systole duration and low values of diastole duration and return time lead to an increase in pressure. Considering that equations (4.1a) and (4.1b) have the same structure as equations (3.1a) and (3.1b) the behavior should be essentially the same in this model. Details will be addressed in the following sections. In section 3.3 it was also showed that the setting time until the curve is periodic increases with increasing values of reflection coefficient and return time. We can therefore assume this to be true in this model.

Combining the information from the previous two paragraphs motivates the particular choice of parameters in figures 4.3 and 4.4.

In figure 4.3 parameters were chosen appropriately to increase absolute values according to the previous paragraphs. Therefore systole duration is chosen longer and diastole duration is chosen shorter than generally used, return times are low and reflection coefficients high. As was already indicated in section 4.1, the inequality $R_D^1 + R_D^2 < 1$ must hold in order to obtain a bounded solution if $R^{av} \equiv 1$ is used. For a variable function R^{av} it is possible to use higher values. In both figures (a) and (b) it is clearly visible that while the curves do not resemble a measured blood pressure curve they are periodic and bounded for $k \to \infty$.

In figures 4.4 (a) and (b) parameters were chosen appropriately to increase setting time according to the previous paragraphs, i.e. return times and reflection coefficients are high.

(a) $R^{av} = \mathbb{1}_{diastole}$. First four cardiac cycles. Choice of parameters: $s = 0.4$, $d = 0.6$, $t^1_{b,ms} = 50$, $t^2_{b,ms} = 100$, $R^1_D = R^2_D = 0.9$, $\tau = 0.0001$.

(b) $R^{av} \equiv 1$. First 16 cardiac cycles. Choice of parameters: $s = 0.4$, $d = 0.6$, $t^1_{b,ms} = 50$, $t^2_{b,ms} = 100$, $R^1_D = R^2_D = 0.49$, $\tau = 0.0001$.
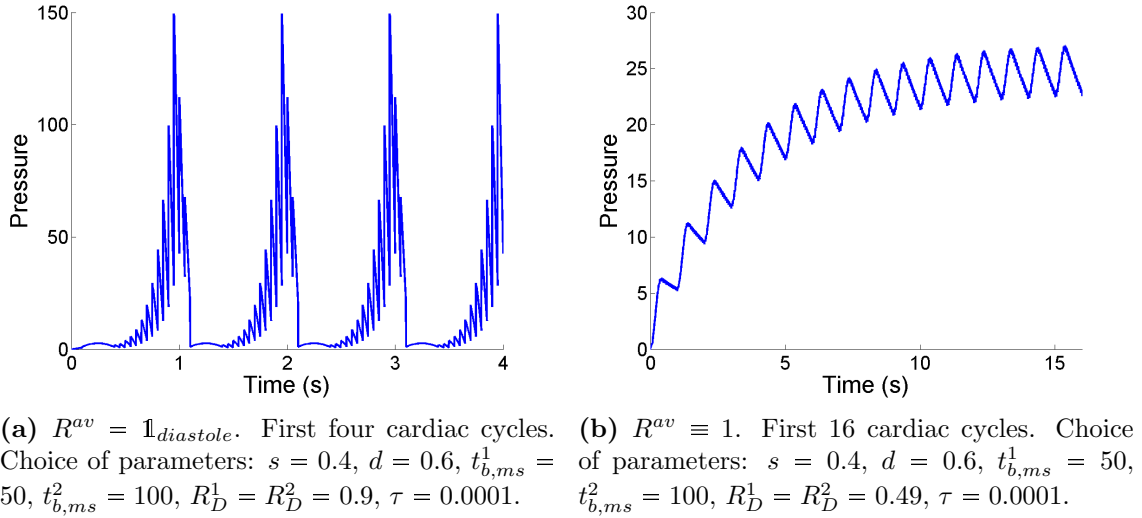
Figure 4.3: Curves with parameter combinations that increase absolute values for both choices of R^{av}.

(a) $R^{av} = \mathbb{1}_{diastole}$. First four cardiac cycles. Choice of parameters: $s = 0.4$, $d = 0.6$, $t^1_{b,ms} = 180$, $t^2_{b,ms} = 210$, $R^1_D = R^2_D = 0.9$, $\tau = 0.0001$.

(b) $R^{av} \equiv 1$. First 32 cardiac cycles. Choice of parameters: $s = 0.4$, $d = 0.6$, $t^1_{b,ms} = 180$, $t^2_{b,ms} = 210$, $R^1_D = R^2_D = 0.49$, $\tau = 0.0001$.
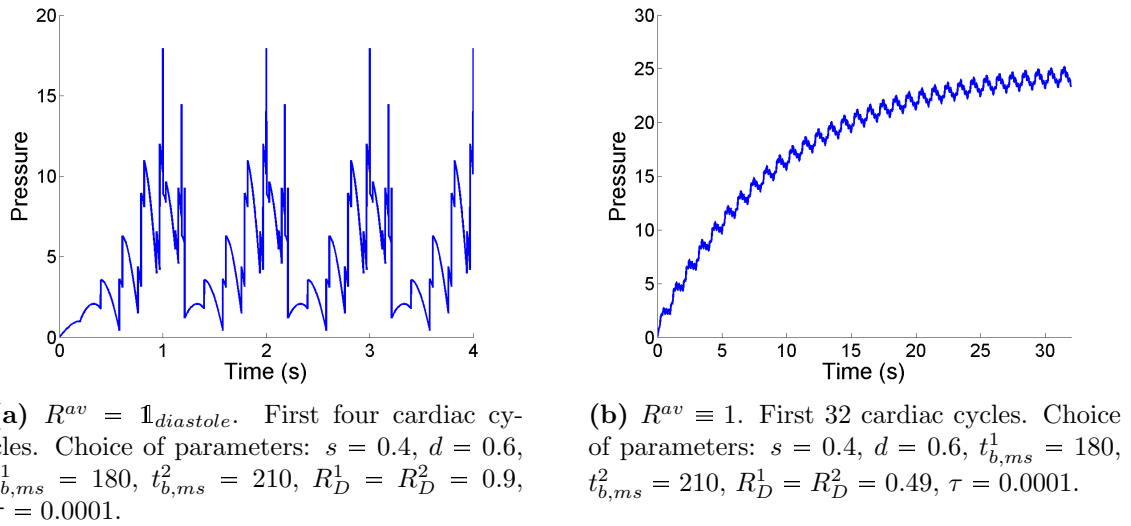
Figure 4.4: Curves with parameter combinations that increase setting time for both choices of R^{av}.

While in the case of $R^{av} = \mathbb{1}_{diastole}$ the curves are periodic from the second cardiac cycle on, a longer setting time is necessary for $R^{av} \equiv 1$.

4.3.3 Influence of the Reflection Coefficients

In principle the results obtained in sections 3.7.1 and 3.8.3 are valid even if the model now includes two reflection sites with their respective reflection coefficients. However, the question is if the influence of both reflection coefficients is the same.

Magnitude.   Before we assess the shape of the modeled curves we will investigate the influence of reflection coefficients on SBP, DBP and PP. The results for $R^{av} = \mathbb{1}_{diastole}$ are displayed in figure 4.5. In (a) the first reflection coefficient R_D^1, referring to the reflection site closer to the heart, is held constant while R_D^2 is varied. In (b) the situation is reversed. Since the figures give only exemplary insight and not general information, parameters were chosen such that the desired effects can be observed distinctly.

(a) $R_D^1 = 0.4$, $0 \leqslant R_D^2 \leqslant 1$ (b) $R_D^2 = 0.4$, $0 \leqslant R_D^1 \leqslant 1$
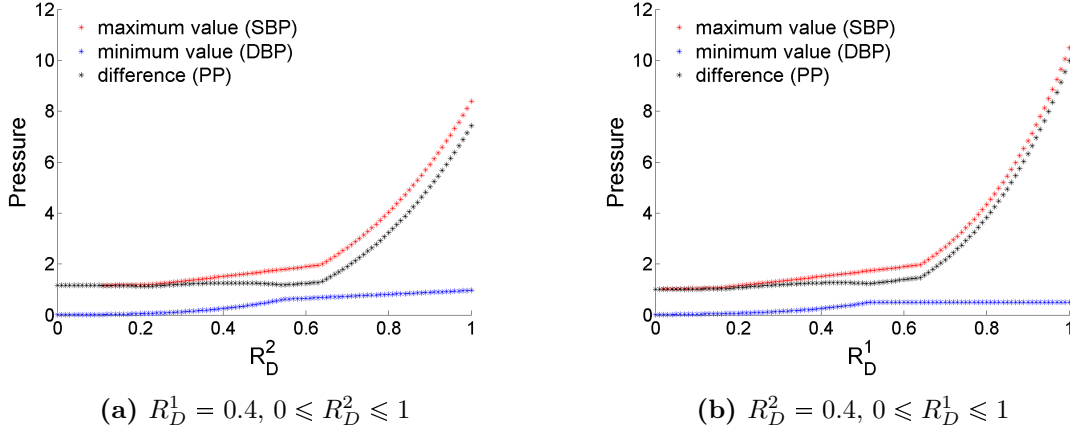
Figure 4.5: Variation of one reflection coefficient while the other is held constant and influence on SBP, DBP and PP. $R^{av} = \mathbb{1}_{diastole}$. Choice of parameters: $s = 0.3$, $d = 0.7$, $t_{b,ms}^1 = 125ms$, $t_{b,ms}^2 = 190ms$, $\tau = 0.0001$

Apart from the fact that SBP, DBP and PP are increasing monotonously in both reflection coefficients which agrees with previous results one major observation can be made: As long as the sum of both reflection coefficients is small, the curves for SBP and DBP are very similar, regardless of which coefficient is held constant and which is varied. Only when the varied parameter tends towards one, increase in SBP is significantly stronger for variation of R_D^1. For DBP, however, increase is significantly stronger for variation of R_D^2, if the coefficient exceeds a certain threshold.

The thresholds for significant differences depend on the choice of the constant coefficient as well as on other parameters. Increasing the difference of the return times and increasing the constant reflection coefficient tend to lower the threshold. Tables that illustrate these tendencies for different parameter values can be found in appendix A.2.

The same analysis can be done for $R^{av} \equiv 1$, see figure 4.6. Again, the curves look very similar as long as the sum $R_D^1 + R_D^2$ is small. When a certain threshold is exceeded, increase in both SBP and DBP is stronger for variation of R_D^1. Again, the threshold depends on the choice of the constant reflection coefficient and on the return times, see tables in appendix A.2.

Shape.   Next the influence of the parameters on the shape of the generated curves will be analyzed. In figure 4.7 the first reflection coefficient R_D^1 is held constant, while R_D^2 is varied.

(a) $R_D^1 = 0.4,\ 0 \leqslant R_D^2 \leqslant 1$

(b) $R_D^2 = 0.4,\ 0 \leqslant R_D^1 \leqslant 1$

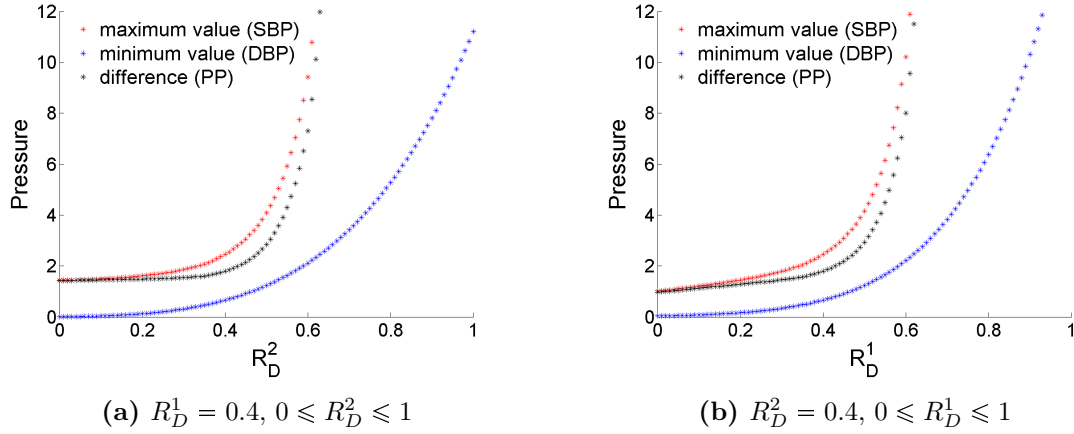**Figure 4.6:** Variation of one reflection coefficient while the other is held constant and influence on SBP, DBP and PP. $R^{av} \equiv 1$. Choice of parameters: $s = 0.3$, $d = 0.7$, $t_{b,ms}^1 = 125ms$, $t_{b,ms}^2 = 190ms$, $\tau = 0.0001$

(a) $R_D^2 = 0.0$

(b) $R_D^2 = 0.1$

(c) $R_D^2 = 0.2$

(d) $R_D^2 = 0.3$

(e) $R_D^2 = 0.4$

(f) $R_D^2 = 0.5$
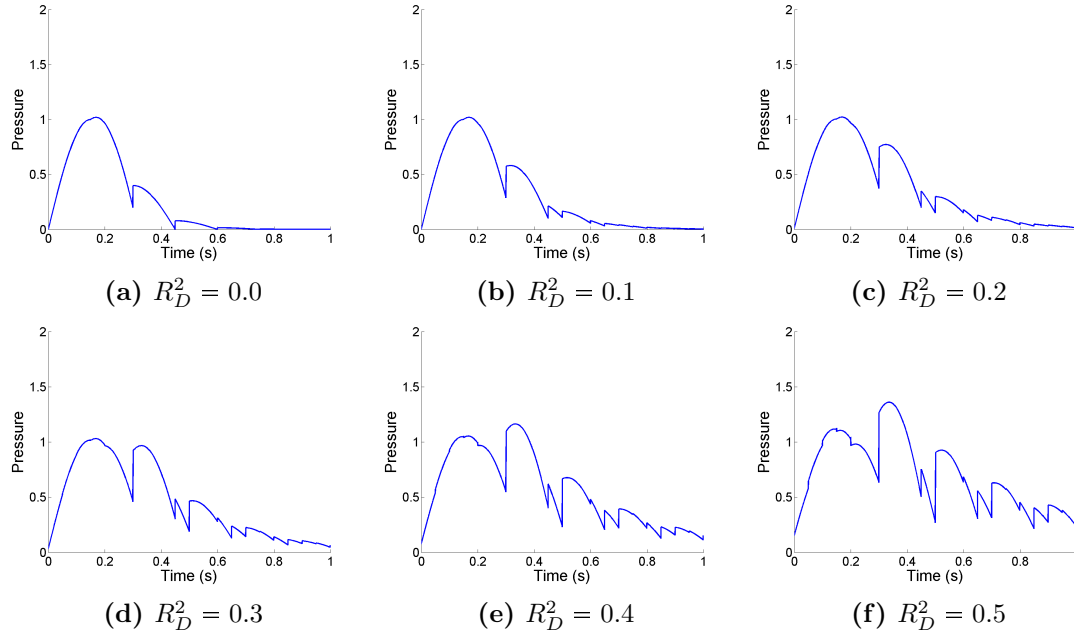
Figure 4.7: Different values of R_D^2 and their influence on curve shape. Second cardiac cycle. $R^{av} = \mathbb{1}_{diastole}$. Choice of parameters: $s = 0.3$, $d = 0.7$, $t_{b,ms}^1 = 150$, $t_{b,ms}^2 = 200$, $R_D^1 = 0.2$, $\tau = 0.0001$.

Several observations can be made:

- It is clearly visible that the number of secondary spikes is larger for $R_D^2 > 0$ than it is for $R_D^2 = 0$. For all values $R_D^2 > 0$, however, the number of secondary spikes remains the same. They only differ in their prominence. This agrees with the results from chapter 3.

- As R_D^2 increases, it becomes harder to distinguish which spikes are produced from which reflection site.

75

- ◆ The curve looks most realistic for $R_D^2 = 0.2$ which could indicate a variety of phenomena. Possibly, the curves will look most realistic for $R_D^1 = R_D^2$. Alternatively, the resemblance between measured and generated curves might depend on the sum $R_D^1 + R_D^2$ instead of the individual values with $R_D^1 + R_D^2 = 0.4$ being a good choice.

(a) $R_D^1 = 0.0$ (b) $R_D^1 = 0.1$ (c) $R_D^1 = 0.2$

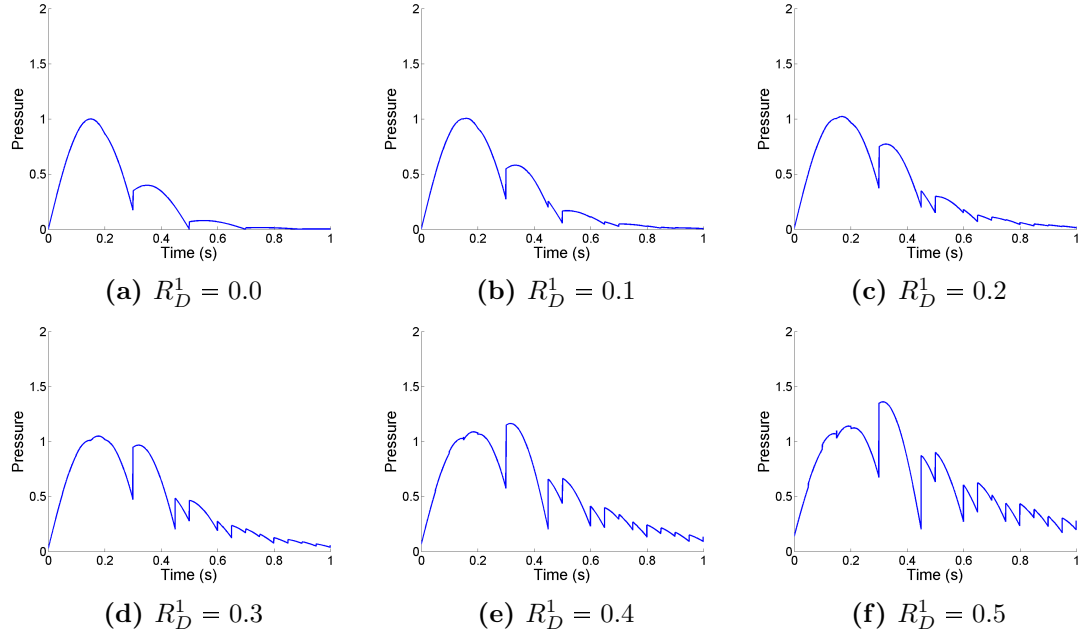(d) $R_D^1 = 0.3$ (e) $R_D^1 = 0.4$ (f) $R_D^1 = 0.5$

Figure 4.8: Different values of R_D^1 and their influence on curve shape. Second cardiac cycle. $R^{av} = \mathbb{1}_{diastole}$. Choice of parameters: $s = 0.3$, $d = 0.7$, $t_{b,ms}^1 = 150$, $t_{b,ms}^2 = 200$, $R_D^2 = 0.2$, $\tau = 0.0001$.

To find out if any of the possible explanations for the third observation is indeed correct, further experiments have to be conducted. Figure 4.8 shows variation of the first reflection coefficient R_D^1 while the second coefficient R_D^2 is held constant. Again, several observations can be made:

- ◆ It is clearly visible that the number of secondary spikes is larger for $R_D^1 > 0$ than it is for $R_D^1 = 0$. For all values $R_D^1 > 0$, however, the number of secondary spikes remains the same. They only differ in their prominence. This agrees with the results from chapter 3.

- ◆ For increasing R_D^1 distinguishing between the influences of the two reflection sites becomes harder.

- ◆ Again, the most realistic shape is obtained for $R_D^1 = 0.2$. This agrees with both explanations suggested above.

After repeating above experiments for different values of the constant reflection coefficient and different return times $t_{b,ms}^1$ and $t_{b,ms}^2$ we can conclude that reasonable curve shapes

can only be obtained if $R_D^1 + R_D^2$ do not exceed some threshold value that itself depends on the return times, a result that agrees with section 3.7.1.

For a constant sum $R_D^1 + R_D^2 = \sigma$ the best[1] results are found around $R_D^1 = R_D^2 = \frac{\sigma}{2}$ This was tested for several values of σ and several return times and is illustrated for $\sigma = 0.4$, $t_{b,ms}^1 = 150ms$ and $t_{b,ms}^2 = 200ms$ in figure 4.9.

(a) $R_D^1 = 0.0$, $R_D^2 = 0.4$ (b) $R_D^1 = 0.1$, $R_D^2 = 0.3$ (c) $R_D^1 = 0.2$, $R_D^2 = 0.2$

(d) $R_D^1 = 0.3$, $R_D^2 = 0.1$ (e) $R_D^1 = 0.4$, $R_D^2 = 0.0$

Figure 4.9: Different values of R_D^1 and R_D^2 such that $R_D^1 + R_D^2 = 0.4$ and their influence on curve shape. Second cardiac cycle. $R^{av} = \mathbb{1}_{diastole}$. Choice of parameters: $s = 0.3$, $d = 0.7$, $\sigma = 0.4$, $t_{b,ms}^1 = 150ms$, $t_{b,ms}^2 = 200ms$, $\tau = 0.0001$.

We conclude that indeed R_D^1 and R_D^2, respectively, have to be chosen smaller than R_D in the model from chapter 3 in order to produce curves that resemble measured ones. This agrees with our assumption from section 4.3.1. Again, no absolute numbers can be found due to a strong interdependence of parameters.

The same analysis can be done for $R^{av} \equiv 1$, see figures 4.10 and 4.11. The results are very similar, up to the fact that very good results are obtained for $R_D^1 = R_D^2 = 0.2$. In general, shape remains reasonable for higher values of both reflection coefficients than before. Again, distinguishing between the effects of the different reflection sites becomes harder when the reflection coefficients increase.

---

[1] The extent to which a curve generated by the model resembles a generic measured one is not quantifiable. Thus, in many cases, it is not possible to state which of a sample of curves is "the best". Still, it is possible to find tendencies, for example in the evenness of secondary spikes.
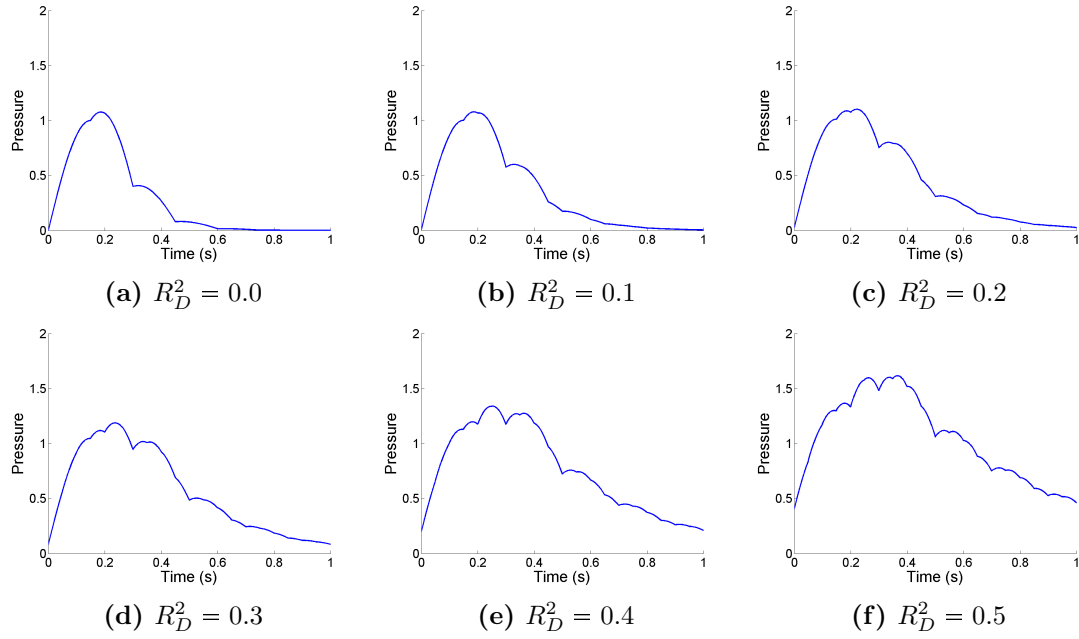
Figure 4.10: Different values of R_D^2 and their influence on curve shape. Second cardiac cycle. $R^{av} \equiv 1$. Choice of parameters: $s = 0.3$, $d = 0.7$, $t_{b,ms}^1 = 150$, $t_{b,ms}^2 = 200$, $R_D^1 = 0.2$, $\tau = 0.0001$.
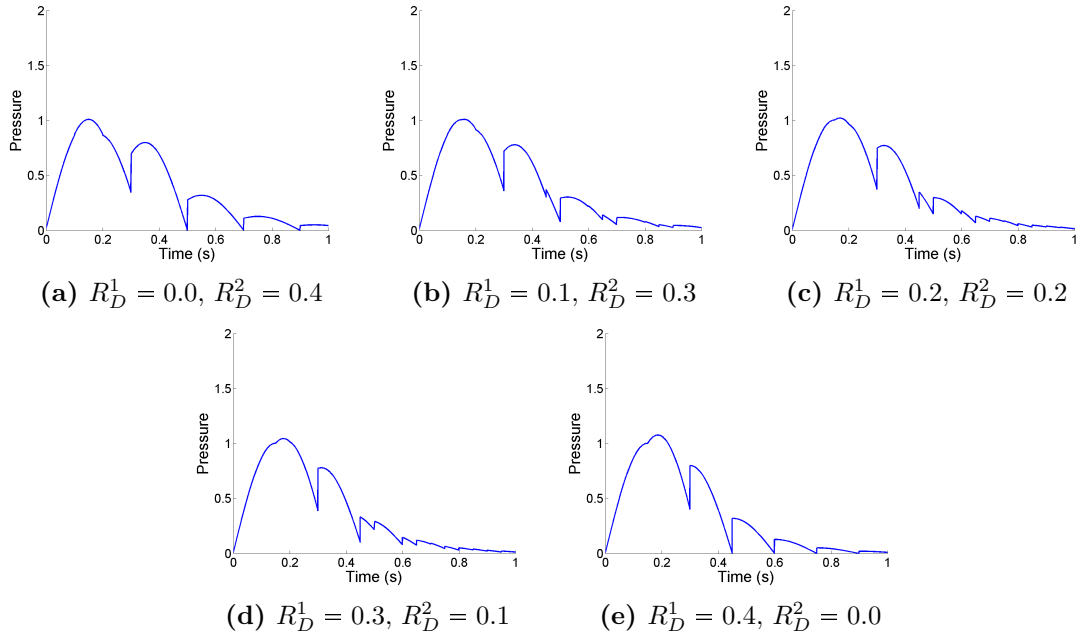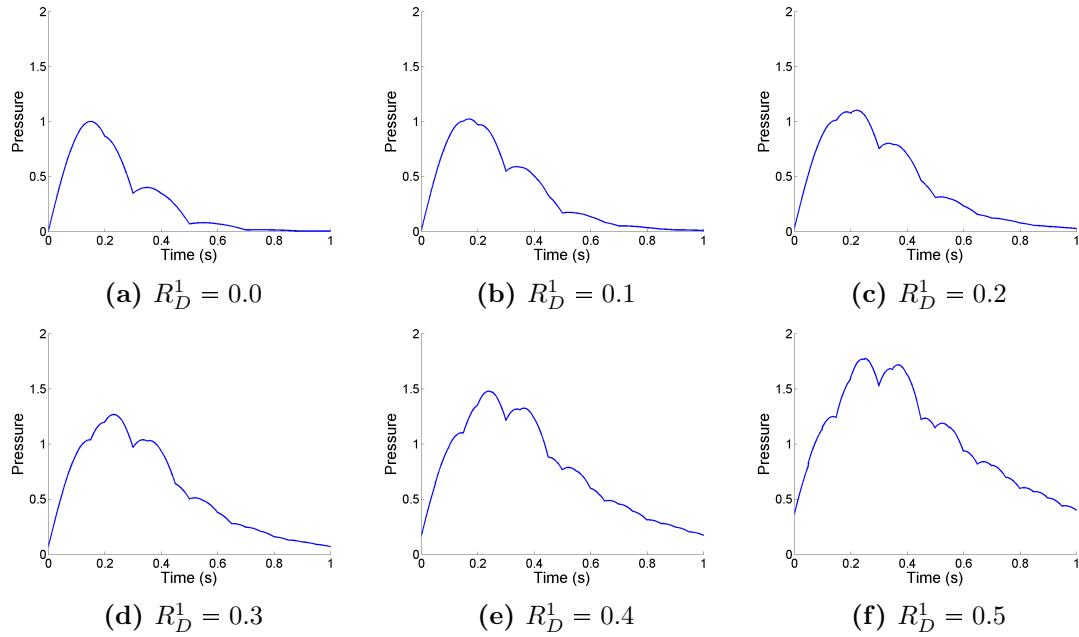

Figure 4.11: Different values of R_D^1 and their influence on curve shape. Second cardiac cycle. $R^{av} \equiv 1$. Choice of parameters: $s = 0.3$, $d = 0.7$, $t_{b,ms}^1 = 150$, $t_{b,ms}^2 = 200$, $R_D^2 = 0.2$, $\tau = 0.0001$.

4.3.4 Influence of Systole and Diastole Duration
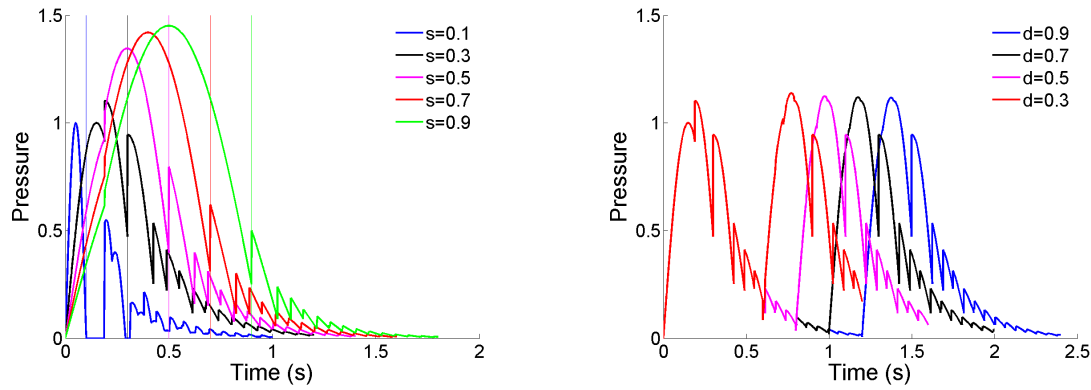
The influence of systole and diastole duration on the curves of this model is the same as was discussed in section 4.3.4. Figure 4.12 (a) shows generated curves for various values of systole duration with all the other parameters held constant. In figure 4.12 (b) generated curves are showed for various values of diastole duration with all the other parameters held constant. Comparison of figure 4.12 with figures 3.9 and 3.10 confirms that the effects of systole and diastole duration are the same in both models. Hence, see section 3.7.2 for further explanation and interpretation.

(a) Variation of systole duration with a diastole duration of $d = 0.9$. First cardiac cycle.

(b) Variation of diastole duration with a systole duration of $s = 0.3$. First two cardiac cycles.

Figure 4.12: Influence of systole and diastole duration. In (a) the beginning of systole is marked by a vertical line. Choice of parameters: $t^1_{b,ms} = 125$, $t^2_{b,ms} = 190$, $R^1_D = 0.3$, $R^2_D = 0.2$, $\tau = 0.0001$.

For $R^{av} \equiv 1$ the effects are generally the same as in figure 3.19 and are therefore not shown again here.

4.3.5 Influence of Return Times

Similar to the reflection coefficients, the general influence of return times on the modeled curves is expected to be the same as in chapter 3. The interesting question is how the influences of t^1_b and t^2_b differ. In this section we will address several aspects. To make sure observed differences are consequences of the choice of return times only, the reflection coefficients were chosen to be the same, $R^1_D = R^2_D$.

First consider figure 4.13. It is visible that so-called *main secondary spikes* are determined by the choice of the second return time. Within each of the main secondary spikes smaller spikes can be observed that are generated by the first reflection site.

The two types of secondary spikes observed in figure 4.13 can only be distinguished clearly for particular choices of $t^1_{b,ms}$ and $t^2_{b,ms}$. In general, they become less distinguishable further
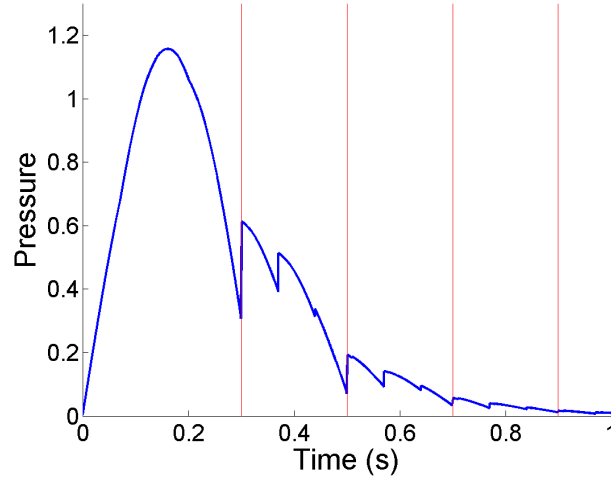
Figure 4.13: Main diastolic spikes, determined by second return time, are marked by red vertical lines. Second cardiac cycle. Choice of parameters: $s = 0.3$, $d = 0.7$, $\tau = 0.0001$, $R_D^1 = R_D^2 = 0.2$, $t_{b,ms}^1 = 70$, $t_{b,ms}^2 = 200$.

into diastole due to the superposition of an increasing number of reflected waves and the decreasing magnitude of all spikes. These phenomena can be observed in figure 4.14, especially in subfigures (c) and (d).

(a) $t_{b,ms}^1 = 70ms$ **(b)** $t_{b,ms}^1 = 95ms$ **(c)** $t_{b,ms}^1 = 120ms$

(d) $t_{b,ms}^1 = 145ms$ **(e)** $t_{b,ms}^1 = 170ms$ **(f)** $t_{b,ms}^1 = 195ms$
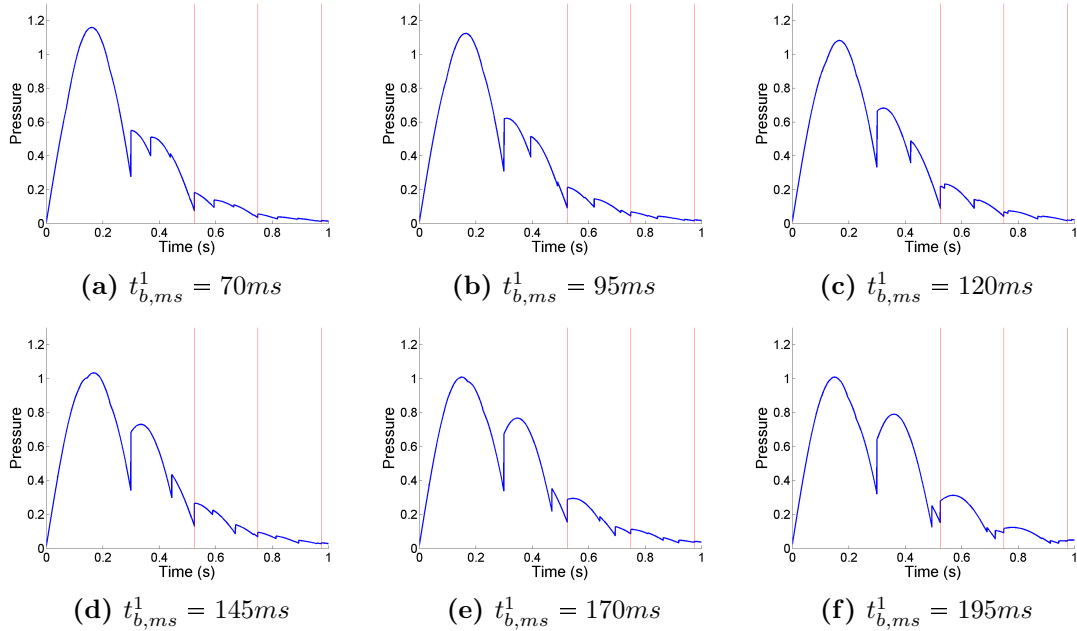
Figure 4.14: Different values of $t_{b,ms}^1$ and their influence on curve shape. Second cardiac cycle. Raturn time of second reflection site after end of systole indicated by red lines. Choice of parameters: $s = 0.3$, $d = 0.7$, $R_D^1 = R_D^2 = 0.2$, $t_{b,ms}^2 = 225ms$, $\tau = 0.0001$.

Additionally, in figure 4.14 it can be seen that the effects of the different reflection sites on the curve during diastole are most distinguishable if the difference $t_{b,ms}^2 - t_{b,ms}^1$ is either relatively large or very small. For a large difference the effects of the first site are negligible

compared to the effects of the second site, compare section 3.7.3. If the difference is small, the number of returning waves from the first and the second reflection site is the same with only a little time shift between them. This is mainly true for large values of $t_{b,ms}^2$ because in that case only a small number of reflected waves occurs during one cardiac cycle and even the accumulated time shift remains small. Interference of the waves produced by the two reflection sites is therefore limited.

Apart from the question of discriminability of reflection effects we observe that, as expected, influence of the reflection sites is similar to that in chapter 3.

Finally, we want to know if any of the reflection sites is dominating in the question of how realistic the generated curve looks. Figure 4.14 indicates that the return time from the first reflection site does play an important role. In figure 4.15, however, it becomes clear that the return time from the second reflection site is relevant too.

(a) $t_{b,ms}^2 = 120ms$ **(b)** $t_{b,ms}^2 = 145ms$ **(c)** $t_{b,ms}^2 = 170ms$

(d) $t_{b,ms}^2 = 195ms$ **(e)** $t_{b,ms}^2 = 220ms$ **(f)** $t_{b,ms}^2 = 245ms$
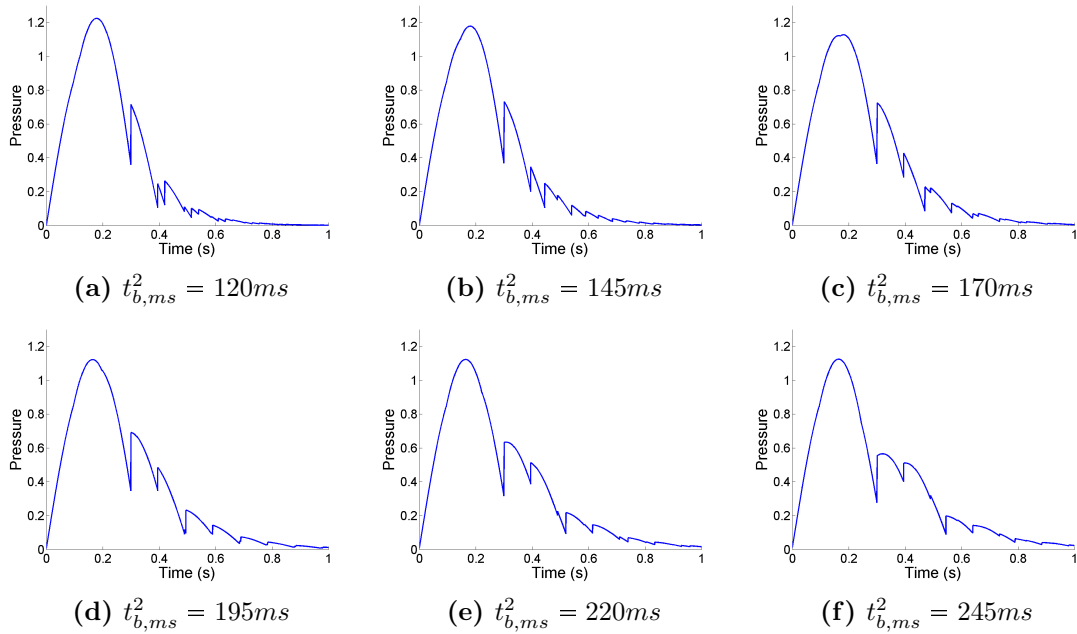
Figure 4.15: Different values of $t_{b,ms}^2$ and their influence on curve shape. Second cardiac cycle. Choice of parameters: $s = 0.3$, $d = 0.7$, $R_D^1 = R_D^2 = 0.2$, $t_{b,ms}^1 = 95ms$, $\tau = 0.0001$.

If we assume $R^{av} \equiv 1$ the effects are very similar. Discriminability of reflection effects is generally harder, see figure 4.16.
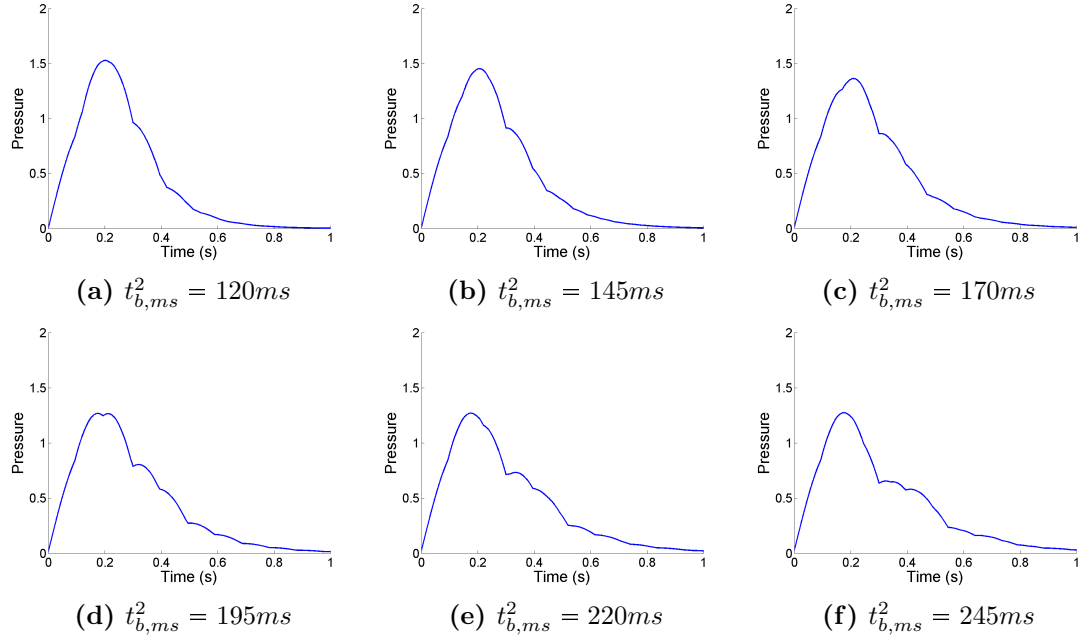
Figure 4.16: Different values of $t_{b,ms}^2$ and their influence on curve shape. Second cardiac cycle. Choice of parameters: $s = 0.3$, $d = 0.7$, $R_D^1 = R_D^2 = 0.2$, $t_{b,ms}^1 = 95ms$, $\tau = 0.0001$.

4.3.6 Influence of Step Size

As in the previous chapter, time step size τ is purely technical and does not represent any physiological phenomenon. We therefore expect the influence of τ on the model with two reflection sites to be the same as it is on the first model. Indeed, generating curves for several values of τ and comparing them to measured curves confirms this for both $R^{av} = \mathbb{1}_{diastole}$ and $R^{av} \equiv 1$.

4.4 Adding Reflection Sites

In the previous sections a blood pressure model with two distal reflection sites was discussed and compared to the model with only one distal reflection site. The superiority of the second model over the first one suggests that adding more reflection sites will further improve results. It has also been argued by Westerhof and Westerhof [55] that a single tube model with only one or two reflection sites is a poor representation of reality. In this section we will therefore generalize the model to include n distal reflection sites for some $n \in \mathbb{N}$. However, the arterial system will still be modeled as a single tube, see figure 4.17.

In order to describe reflected waves arising at n different reflection sites it is necessary to define n reflection coefficients $R_D^1, \ldots, R_D^n$ and return times $t_b^1, \ldots, t_b^n$. Without loss of generality we will assume $t_b^1 < t_b^2 < \ldots < t_b^n$. By splitting pressure into its forward and backward component, i.e. $P_k = P_k^f + P_k^b$, the difference equation system
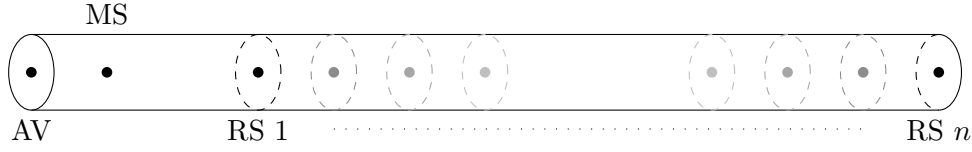
Figure 4.17: Tube model of the arterial system with n reflection sites as presented above. AV - aortic valve, MS - measuring site, RS 1, …, RS n - distal reflection sites.

Model 3

$$P_k^f = P_k^{in} + P_{k-2t_f}^b R_{k-t_f}^{av}, \tag{4.4a}$$

$$P_k^b = P_{k-t_b^1}^f R_D^1 + \ldots + P_{k-t_b^n}^f R_D^n \tag{4.4b}$$

can be derived. Inserting equation (4.4a) into (4.4b) and vice versa yields the two independent equations

$$
\begin{aligned}
P_k^f &= P_k^{in} + P_{k-2t_f-t_b^1}^f R_D^1 R_{k-t_f}^{av} + \ldots + P_{k-2t_f-t_b^n}^f R_D^n R_{k-t_f}^{av} \\
&= P_k^{in} + \sum_{l=1}^n P_{k-2t_f-t_b^l}^f R_D^l R_{k-t_f}^{av},
\end{aligned} \tag{4.5a}
$$

$$
\begin{aligned}
P_k^b &= P_{k-t_b^1}^{in} R_D^1 + P_{k-2t_f-t_b^1}^b R_D^1 R_{k-t_f-t_b^1}^{av} + \ldots + P_{k-t_b^n}^{in} R_D^n + P_{k-2t_f-t_b^n}^b R_D^n R_{k-t_f-t_b^n}^{av} \\
&= \sum_{l=1}^n P_{k-t_b^l}^{in} R_D^l + P_{k-2t_f-t_b^l}^b R_D^l R_{k-t_b^l-t_f}^{av}
\end{aligned} \tag{4.5b}
$$

of order $N = 2t_f + t_b^n$. Again, we know from standard literature [1, 11] that the initial value problems

$$
\begin{cases}
P_k^f = P_k^{in} + \sum_{l=1}^n P_{k-2t_f-t_b^l}^f R_D^l R_{k-t_f}^{av}, & k \in \mathbb{N}_{>2t_f+t_b^n}, \\
P_k^f = \bar{P}_k, & k = 1, \ldots, N
\end{cases}
$$

and

$$
\begin{cases}
P_k^b = \sum_{l=1}^n P_{k-t_b^l}^{in} R_D^l + P_{k-2t_f-t_b^l}^b R_D^l R_{k-t_f-t_b^l}^{av}, & k \in \mathbb{N}_{>2t_f+t_b^n}, \\
P_k^b = \hat{P}_k, & k = 1 \ldots, N,
\end{cases}
$$

defined by equations (4.5a) and (4.5b) and some initial values $\bar{P}_k$ and $\hat{P}_k$, have unique solutions. For the forward pressure the initial condition can be chosen as $P_k^f = P_k^{in}$ for

$k = 1, \ldots, N$. For the backward pressure it is

$$
P_k^b = \begin{cases}
0, & k = 1, \ldots, t_b^1, \\
P_{k-t_b^1}^{in} R_D^1, & k = t_b^1 + 1, \ldots, t_b^2, \\
\quad \vdots & \qquad \vdots \\
\displaystyle\sum_{l=1}^n P_{k-t_b^l}^{in} R_D^l, & k = t_b^n + 1, \ldots, N.
\end{cases}
$$

However, due to the increased complexity finding these solutions explicitly is not possible.
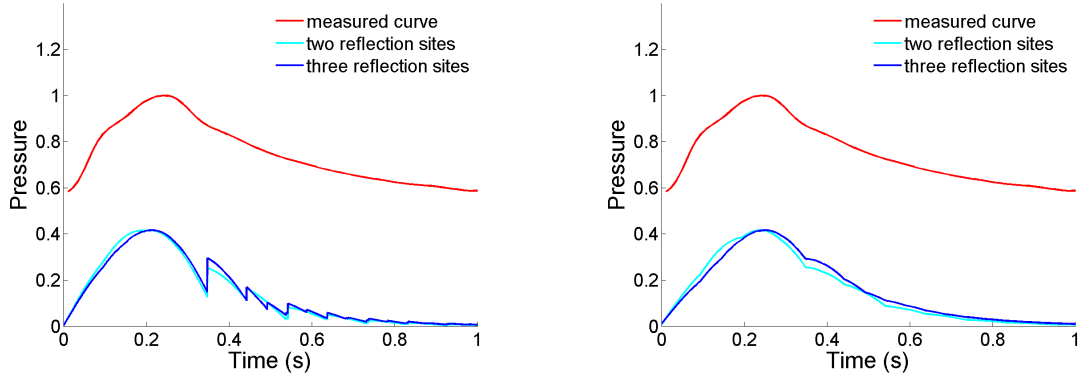
(a) $R^{av} = \mathbb{1}_{diastole}$. Second cardiac cycle. Choice of parameters for blue curve: $s = 0.348$, $d = 0.652$, $t_{b,ms}^1 = 95$, $t_{b,ms}^2 = 145$, $t_{b,ms}^3 = 195$, $R_D^1 = R_D^2 = 0.2$, $R_D^3 = 0.1$, $\tau = 0.0001$. Choice of parameters for cyan curve: $s = 0.348$, $d = 0.652$, $t_{b,ms}^1 = 95$, $t_{b,ms}^2 = 195$, $R_D^1 = R_D^2 = 0.2, \tau = 0.0001$.

(b) $R^{av} \equiv 1$. Second cardiac cycle. Choice of parameters for blue curve: $s = 0.348$, $d = 0.652$, $t_{b,ms}^1 = 95$, $t_{b,ms}^2 = 145$, $t_{b,ms}^3 = 195$, $R_D^1 = R_D^2 = 0.2$, $R_D^3 = 0.1$, $\tau = 0.0001$. Choice of parameters for cyan curve: $s = 0.348$, $d = 0.652$, $t_{b,ms}^1 = 95$, $t_{b,ms}^2 = 195$, $R_D^1 = R_D^2 = 0.2, \tau = 0.0001$.

Figure 4.18: Comparison of measured curve, a curve modeled with two reflection sites and a curve modeled with three reflection sites, normalized to same pulse pressure.

In figure 4.18 the model with three reflection sites is compared to a measured curve and the model with two reflection sites, both for (a) $R^{av} = \mathbb{1}_{diastole}$ and (b) $R^{av} \equiv 1$. The parameter values were found by trial and error. They were chosen such that the shape of the curve is as similar to the measured curve as possible. We can see that in particular for $R^{av} \equiv 1$ the model with three reflection sites is a better fit than the one with only two: The diastolic decay is a better approximation for the exponential decay that was presented in chapter 2.

Numerical analysis becomes more and more complex as the number of reflection sites increases. Since it would require the variation of each parameter separately, it goes beyond the scope of this thesis and will be left for further projects. We can, however, briefly compare the curves generated by the model with an increasing number of reflection sites while holding the sum of reflection coefficients constant, see figures 4.19 and 4.20. While the overall reflection remains the same it is distributed over more and more sites. Algo-

rithm 4.3.1 can easily be generalized to consider n reflection sites. In figure 4.19 we choose $R^{av} = \mathbb{1}_{diastole}$ and the following reflection sites:

(a) $R_D = 0.55$, $t_{b,ms} = 145ms$.

(b) $R_D^1 = 0.3$, $R_D^2 = 0.25$, $t_{b,ms}^1 = 95ms$, $t_{b,ms}^2 = 145ms$.

(c) $R_D^1 = 0.3$, $R_D^2 = 0.1$, $R_D^3 = 0.15$, $t_{b,ms}^1 = 95ms$, $t_{b,ms}^2 = 145ms$, $t_{b,ms}^3 = 195ms$.

(d) $R_D^1 = 0.2$, $R_D^2 = R_D^3 = 0.1$, $R_D^4 = 0.15$, $t_{b,ms}^1 = 95ms$, $t_{b,ms}^2 = 130ms$, $t_{b,ms}^3 = 145ms$, $t_{b,ms}^4 = 195ms$.

(e) $R_D^1 = 0.2$, $R_D^2 = R_D^3 = R_D^4 = 0.1$, $R_D^5 = 0.05$, $t_{b,ms}^1 = 95ms$, $t_{b,ms}^2 = 130ms$, $t_{b,ms}^3 = 145ms$, $t_{b,ms}^4 = 160ms$, $t_{b,ms}^5 = 195ms$.

(f) $R_D^1 = R_D^2 = R_D^3 = R_D^4 = R_D^5 = 0.1$, $R_D^6 = 0.05$, $t_{b,ms}^1 = 95ms$, $t_{b,ms}^2 = 110ms$, $t_{b,ms}^3 = 130ms$, $t_{b,ms}^4 = 145ms$, $t_{b,ms}^5 = 160ms$, $t_{b,ms}^6 = 195ms$.

(a) One reflection site. **(b)** Two reflection sites. **(c)** Three reflection sites.

(d) Four reflection sites. **(e)** Five reflection sites. **(f)** Six reflection sites.
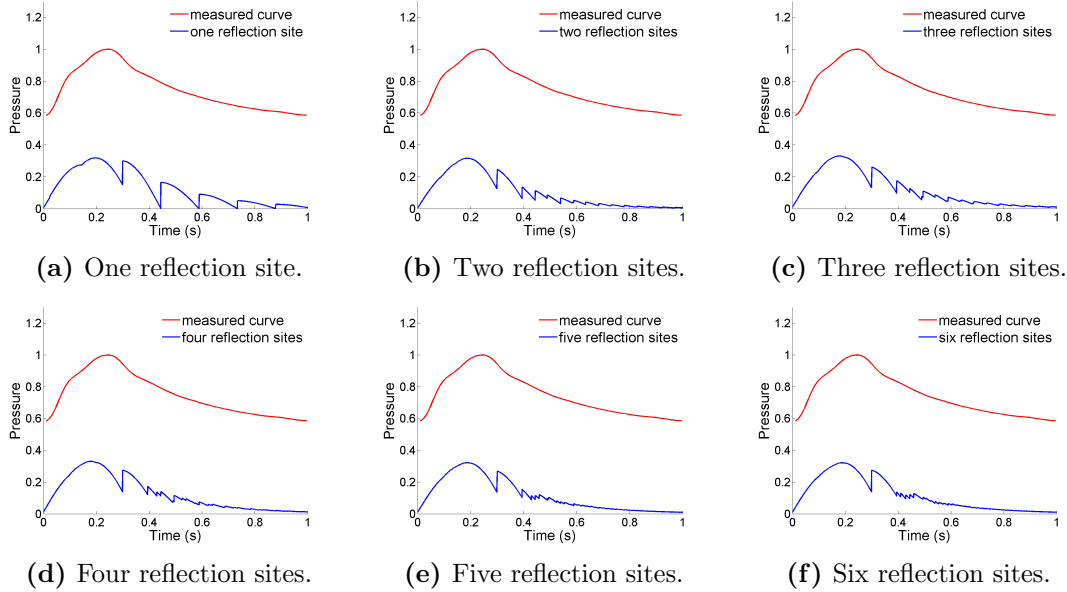
Figure 4.19: Comparison of measured curve and curves modeled with increasing number of reflection sites. Second cardiac cycle. $R^{av} = \mathbb{1}_{diastole}$. $\sum_{l=1}^{n} R_D^l = 0.55$. Choice of parameters: $s = 0.3$, $d = 0.7$, $\tau = 0.0001$.

We see that during diastole curves get smoother as the number of reflection sites increases. The main spike at the beginning of diastole, however, remains distinct. This can be explained by the discrete description of valve closure by $R^{av} = \mathbb{1}_{diastole}$. To optimize the shape of the curve further analysis is necessary that shall be done elsewhere.

In figure 4.20 we choose $R^{av} \equiv 1$ and the same reflection sites as in figure 4.19. Again, the curves become smoother as the number of reflection sites increases.

(a) One reflection site.

(b) Two reflection sites.

(c) Three reflection sites.

(d) Four reflection sites.

(e) Five reflection sites.

(f) Six reflection sites.
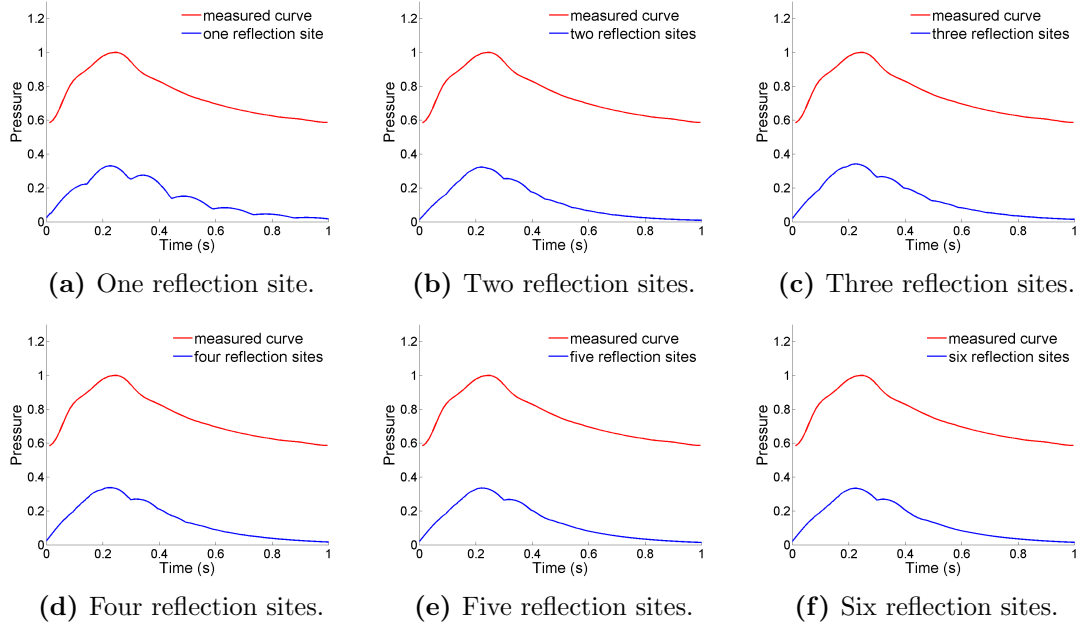
Figure 4.20: Comparison of measured curve and curves modeled with increasing number of reflection sites. Second cardiac cycle. $R^{av} \equiv 1$. $\sum_{l=1}^{n} R_D^l = 0.55$. Choice of parameters: $s = 0.3$, $d = 0.7$, $\tau = 0.0001$.

4.5   Conclusion

In this chapter the original model was extended to include more than one distal reflection site. Equations for a model with two reflection sites were given by (4.1a) and (4.1b). Finding explicit solutions was not possible but comparison with the previous model and a measured curve in section 4.2 showed that the model leads to a better fit than the original one. Numerical analysis revealed that interpretation of reflection coefficients and return times is more challenging in this model than before since the effects of the separate reflection sites interfere with each other. There are even more combinations of parameters to get a physiologically significant curve than before.

In section 4.4 the addition of further reflection sites was discussed. We concluded that even though using more than two reflection sites might add useful information to the curve, analyzing this model exceeds the scope of this thesis and shall be done elsewhere.

CHAPTER 5

Discussion

In this chapter we want to discuss the results of this thesis and their implications for further research. Since the results were already discussed in detail in chapters 3 and 4, we will not list all our findings. Instead, we want to give an overview and motivate further research.

5.1 Conclusion

The aim of the thesis was to develop a simple new model for blood pressure using difference equations that describes effects of wave reflection and analyze its properties. Overall it can be said that this goal has been accomplished. The model proposed in chapter 3 is simple enough that it is possible to solve the equations. Comparing modeled curves with curves measured in patients shows that indeed the model represents reality fairly well. Even though the curves produced by the model are less smooth than measured ones they display the main characteristics of a blood pressure curve. Also in terms of periodicity and boundedness the curves agree with reality.

Analyzing how changes at the heart influence the outcome shows the following: Intuitively one would assume that reflections at the heart depend on the timing within the cardiac cycle. Other researchers have reached the same conclusion [49]. The curves produced by the model, however, are smoother and a better representation of reality if the heart is assumed to be a total reflector throughout the entire cardiac cycle. Analysis of the influence of the different parameters that describe the vascular system further confirms that assuming the heart to be a total reflector throughout the cardiac cycle is the better choice. One reason for this might be the fact that a step function does not describe

the physiological process of the aortic valve closing. Closing of the valve involves not only the states "open" and "closed" but also intermediate states that are ignored by the step function. Another reason could be that even when the valve is open, arriving blood pressure waves are not absorbed completely. They are still reflected inside the ventricle, with a different reflection coefficient than with a closed valve.

Also, observed influences of the parameters agree with results from a variety of previous studies. Increasing the reflection coefficient that is connected to the arterial system impedance increases systolic, diastolic and pulse pressure [27]. Increasing heart rate increases DBP and decreases SBP and PP [57, 58]. The influence of return time that is found agrees with results about pulse wave velocity [5] and the relationship of body height and systolic blood pressure [18]. Effects of parameter variation on curve shape can be observed that have no counterpart in literature. They help understand the model better.

Unfortunately it is not possible to choose parameters such that both shape and absolute values match real curves. This inspires the introduction of further reflection sites.

The model that includes two different reflection sites is more difficult and cannot be solved directly anymore. Numerical analysis, however, shows that the fit to measured curves improves by using two reflection sites. Again, the curves look more realistic if the heart is assumed to be a total reflector throughout the cardiac cycle. Influence of the parameters is more complex and cannot be directly compared to results from literature anymore [4].

More than two reflection sites make the model so complex that a thorough analysis would exceed the scope of this thesis. It can be seen, though, that indeed increasing the number of reflection sites makes the curves smoother.

5.2 Outlook

Even though the model was thoroughly analyzed in the previous chapters, some questions are left open. One can therefore still improve understanding of the model by further studies. Also, applications of the model can be found.

Improvement of the model. The first problem that can be addressed is the question of reflection at the heart. All the functions compared in section 3.5.2 are extreme cases. Instead one could try the function

$$R^{av} = A \cdot \mathbb{1}_{diastole} + B \cdot \mathbb{1}_{systole} \tag{5.1}$$

with constants $A, B \in [0, 1]$ to include wave reflection inside the left ventricle. To better represent the time of valve closure one could substitute the step function given in (5.1) by a continuous function, see figure 5.1.

Another possibility is to find a new model that describes the ventricle, maybe a Windkessel
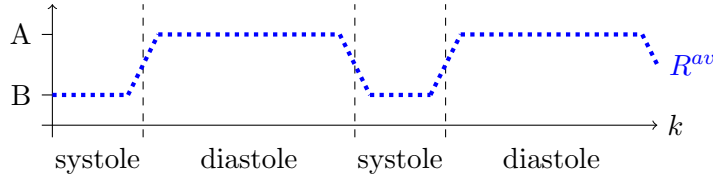
Figure 5.1: Alternative choice of R^{av} that includes valve closure.

model. During systole, this model is then linked with the arterial system. When the valve is closed during diastole, however, reflection at the heart is assumed to be total, as was presented in this thesis.

Next, more than two reflection sites can be assumed. The model can then be thoroughly studied to analyze influence and interdependence of parameters.

Applications of the model. There are several applications that could be developed with the help of the models presented here. We will only list a few of them.

First of all, one can try to *fit the model to measured curves* by choosing specific parameter values. This could be automated and implemented, for example in MATLAB, as follows. Preexisting algorithms can be used to find systole and diastole length and return times [3]. If the model is assumed to have only one reflection site and $t_f = 0$, the return time t_b can be found by using the shoulder point that is also used for calculating the augmentation index, see section 2.2.4. Next one needs to decide what functions to use for R^{av} and P^{in}. Using all these methods it will be possible to find the correct value of R_D by minimizing some error function. Depending on which error function is used the results will vary. The method can be refined by introducing more reflection sites.

Once the parameters to fit the model to a measured curve are known, the algorithm can be adapted to *separate the measured curve* into its forward and backward component. This can further be compared to traditional wave separation methods [20, 53].

A concept that has come up recently [2, 35] is that of *wave tracking*. The idea is that as an initial wave coming from the heart gets reflected and re-reflected at various reflection sites throughout the vascular system it multiplies. The number of waves (forward and backward) stemming from the initial wave grows exponentially. At a fixed site measured pressure at any point in time is therefore the sum of different "descendants" of several reflected waves. Wave tracking algorithms aim to separate these parts and attribute them to their respective heart beats. The model developed in this thesis could be adapted to find a new method to track waves.

Possibly more applications of the model can be found that have not been mentioned here. This confirms that the model is worth further studies.

A.1 Linear Difference Equations

This section aims to give an overview of the theory of difference equations used in sections 3.3.1 and 4.1. It is based on several books on difference equations [1, 11, 17].

In the following results the inhomogeneous linear system

$$u_{k+1} = Au_k + b_{k+1}, \qquad k \in \mathbb{N}_0 \tag{A.1.2}$$

and the corresponding homogeneous system

$$u_{k+1} = Au_k, \qquad k \in \mathbb{N}_0 \tag{A.1.3}$$

will be considered for some $N \in \mathbb{N}$, a nonsingular matrix $A \in \mathbb{R}^{N \times N}$ and $b_k \in \mathbb{R}^N$ for $k \in \mathbb{N}$. Usually, an initial condition $u_0 \in \mathbb{R}^N$ is prescribed.

A.1.1 Solution Theory

Definition A.1.1 *The **solution** of a system of type* (A.1.2) *or* (A.1.3) *is defined as a sequence of vectors $u_k \in \mathbb{R}^N$, $k \in \mathbb{N}_0$ such that the respective iteration is satisfied.*

For homogeneous systems, the solution can be found directly by taking powers of the system matrix A.

Theorem A.1.2 *The solution of the homogeneous system* (A.1.3) *with the initial condition u_0 is given by*

$$u_k = A^k u_0$$

for $k \in \mathbb{N}_0$.

Proof. See [1], theorem 2.6.1 for $k_0 = 0$ and constant A. □

Definition A.1.3 *Two solutions* $(u_k^{(1)})_{k \in \mathbb{N}_0}$ *and* $(u_k^{(2)})_{k \in \mathbb{N}_0}$ *of* (A.1.3) *are called* **linearly independent** *if*

$$au_k^{(1)} + bu_k^{(2)} = 0, \qquad \forall k \in \mathbb{N}_0$$

implies $a = b = 0$.

Theorem A.1.4 *The homogeneous system* (A.1.3) *has N linearly independent solutions*

$$(u_k^{(1)})_{k \in \mathbb{N}_0}, \ \ldots, \ (u_k^{(N)})_{k \in \mathbb{N}_0}.$$

Proof. See [11], theorem 2.18. □

Definition A.1.5 *Consider any N linearly independent solutions*

$$(u_k^{(1)})_{k \in \mathbb{N}_0}, \ \ldots, \ (u_k^{(N)})_{k \in \mathbb{N}_0}$$

of (A.1.3). *The matrix*

$$V_k = \left[u_k^{(1)}, \ldots, u_k^{(N)} \right], \qquad k \in \mathbb{N}_0$$

is called **fundamental matrix** *of the system.*

Multiplying the matrix V_k with a constant vector yields a fundamental matrix that satisfies a different initial condition.

Definition A.1.6 *Let U_k denote the* **principal fundamental matrix** *of* (A.1.3), *i.e.* $U_0 = I_n$.

Definition A.1.7 *The* **Green's matrix** *of* (A.1.3) *is defined by*

$$G(k, j) = U_k U_j^{-1}.$$

Theorem A.1.8 *There holds*

$$G(k, j) = A^{k-j}.$$

Proof. See [17], lemma 3.4. □

Theorem A.1.9 *The solution of the inhomogeneous system* (A.1.2) *with the initial con-*

dition u_0 is given by

$$u_k = U_k u_0 + \sum_{j=1}^{k} A^{k-j} b_{j-1}$$

for $k \in \mathbb{N}_0$.

Proof. Equation (3.2) in [17] gives

$$u_k = U_k u_0 + \sum_{j=1}^{k} U_k U_j^{-1} b_{j-1}.$$

Inserting definition A.1.7 and theorem A.1.8 completes the proof. □

A.1.2 Stability Theory

Definition A.1.10 *A solution $(u_k)_{k\in\mathbb{N}_0}$ of system (A.1.2) or (A.1.3) with the initial condition u_0 is called*

1. **stable** *if for all $\epsilon > 0$ there exists $\delta > 0$ such that for all solutions $(y_k)_{k\in\mathbb{N}_0}$ that satisfy the initial condition y_0 and $\|u_0 - y_0\| < \delta$ it follows $\|u_k - y_k\| < \epsilon$ for all $k \in \mathbb{N}_0$,*

2. **globally attractive** *if for all solutions $(y_k)_{k\in\mathbb{N}_0}$ of the system there holds $\lim_{k\to\infty} \|u_k - y_k\| = 0$,*

3. **globally asymptotically stable** *if it is both globally attractive and stable.*

Obviously the following theorem is true.

Theorem A.1.11 *If a solution $(u_k)_{k\in\mathbb{N}_0}$ of (A.1.2) or (A.1.3) is globally asymptotically stable, it is stable.*

Theorem A.1.12 *The following statements are equivalent:*

(a) *All solutions of the system (A.1.3) are globally asymptotically stable.*

(b) *There holds $\lim_{k\to\infty} \|u_k\| = 0$ for alle solutions of (A.1.3).*

If the above statements are true, it follows that there exists $c \in \mathbb{R}^+$ such that $\|U_k\| \leqslant c$ for all $k \in \mathbb{N}_0$.

Proof. See [17], theorem 4.2. □

Theorem A.1.13 *The following statements are equivalent:*

1. *All solutions of the inhomogeneous system* (A.1.2) *are globally asymptotically stable.*

2. *The trivial solution of the homogeneous system* (A.1.3) *is globally asymptotically stable.*

Proof.   See [17], lemma 4.1 and the remark on the following page.   □

Theorem A.1.14 *Consider the linear difference equations*

$$x_k = a_k x_{k-N} + h_k, \qquad k \in \mathbb{N}_{>N} \tag{A.1.4a}$$

$$y_k = b_k y_{k-N} + h_k, \qquad k \in \mathbb{N}_{>N} \tag{A.1.4b}$$

with the initial condition $x_k = y_k = c_k$ for $k = 1, \dots, N$. Assume $a_k \geqslant b_k$ for all $k > N$. Then there holds

$$x_k \geqslant y_k, \qquad \forall k \in \mathbb{N}.$$

Proof.   The claim can be proved by mathematical induction. The base $x_1 = y_1$ follows directly from the initial condition. Now assume $x_k \geqslant y_k$ for all $k \leqslant n$ with $n \geqslant N$. To prove $x_{n+1} \geqslant y_{n+1}$, consider

$$x_{n+1} = a_{n+1} x_{n+1-N} + h_{n+1} \geqslant a_{n+1} y_{n+1-N} + h_{n+1} \geqslant b_{n+1} y_{n+1-N} + h_{n+1} = y_{n+1}.$$

The equality signs follow directly from (A.1.4). The first $\geqslant$ follows from the induction hypothesis, the second one from $a_k \geqslant b_k$.   □

A.2   Thresholds

This appendix aims to illustrate the dependence of the threshold for significant differences in the influence of R_D^1 and R_D^2 on return times and the constant reflection coefficient that is mentioned in section 4.3.3. The tables are provided for completeness and would decrease readability if inserted in section 4.3.3 directly.

For the following computations the threshold was chosen as the lowest value $0 < c < 1$ such that

$$\frac{|SBP(R_D^1 = R_D^{const}, R_D^2 = c) - SBP(R_D^1 = c, R_D^2 = R_D^{const})|}{\max_{R_D^2} SBP(R_D^1 = R_D^{const}, R_D^2)} > 0.1.$$

First consider the case $R^{av} = \mathbb{1}_{diastole}$. Tables A.2.1 and A.2.2 illustrate the dependence of the threshold on $t_{b,ms}^2$ for several fixed values of $t_{b,ms}^1$. The two tables only differ in the

value of R_D^{const} that was chosen. In both tables it can be observed that even though the threshold does not depend on $t_{b,ms}^2$ monotonously, it has a tendency to decrease if $t_{b,ms}^2$ and with it the difference $t_{b,ms}^2 - t_{b,ms}^1$ increases. In fact, the difference seems to be more important than the actual values.

$t_{b,ms}^1 = 50ms$		$t_{b,ms}^1 = 75ms$		$t_{b,ms}^1 = 100ms$		$t_{b,ms}^1 = 125ms$	
$\mathbf{t_{b,ms}^2}$ (in ms)	**c**	$\mathbf{t_{b,ms}^2}$ (in ms)	**c**	$\mathbf{t_{b,ms}^2}$ (in ms)	**c**	$\mathbf{t_{b,ms}^2}$ (in ms)	**c**
75	0.93	100	0.96	125	> 1	150	> 1
100	0.90	125	0.99	150	> 1	175	0.95
125	0.93	150	0.90	175	0.95	200	0.99
150	0.90	175	0.94	200	0.89	225	0.87
175	0.92	200	0.96	225	0.92	250	0.85
200	0.89	225	0.88	250	0.93	275	0.89
225	0.91	250	0.91	275	0.92	300	0.89

Table A.2.1: Dependence of threshold for SBP on the difference $t_{b,ms}^2 - t_{b,ms}^1$. Choice of parameters: $s = 0.3$, $d = 0.7$, $R_D^{const} = 0.2$, $\tau = 0.0001$.

Comparing tables A.2.1 and A.2.2 shows that increasing R_D^{const} seems to generally lower the threshold values. For $R_D^{const} = 0.2$ for some combinations of return times the threshold is beyond the range of the varied reflection coefficient (indicated by > 1 in the table). For $R_D^{const} = 0.4$, however, threshold values are significantly below one for all studied combinations of return times.

$t_{b,ms}^1 = 50ms$		$t_{b,ms}^1 = 75ms$		$t_{b,ms}^1 = 100ms$		$t_{b,ms}^1 = 125ms$	
$\mathbf{t_{b,ms}^2}$ (in ms)	**c**	$\mathbf{t_{b,ms}^2}$ (in ms)	**c**	$\mathbf{t_{b,ms}^2}$ (in ms)	**c**	$\mathbf{t_{b,ms}^2}$ (in ms)	**c**
75	0.86	100	0.90	125	0.90	150	0.90
100	0.81	125	0.85	150	0.98	175	0.88
125	0.80	150	0.81	175	0.83	200	0.93
150	0.77	175	0.83	200	0.80	225	0.80
175	0.78	200	0.82	225	0.83	250	0.77
200	0.75	225	0.75	250	0.80	275	0.79
225	0.77	250	0.81	275	0.79	300	0.75

Table A.2.2: Dependence of threshold for SBP on the difference $t_{b,ms}^2 - t_{b,ms}^1$. Choice of parameters: $s = 0.3$, $d = 0.7$, $R_D^{const} = 0.4$, $\tau = 0.0001$.

Tables A.2.3 and A.2.4 illustrate the dependence of the threshold on $t_{b,ms}^1$ for several fixed values of $t_{b,ms}^2$. Again, they differ in the value of R_D^{const}. It can be observed that as $t_{b,ms}^1$ increases and therefore the difference $t_{b,ms}^2 - t_{b,ms}^1$ decreases the threshold values increase, a result that agrees with the previous one. As before, the difference seems to be more important than the actual values.

Comparing tables A.2.3 and A.2.4 shows that increasing R_D^{const} seems to generally lower the threshold values.

The same analysis can be done for $R^{av} \equiv 1$, with very similar results. Tables A.2.5 and A.2.6 illustrate the dependence of the threshold on $t_{b,ms}^2$ for several fixed values of $t_{b,ms}^1$. Again, the two tables only differ in the value of R_D^{const} that was chosen. In both tables it

$t^2_{b,ms} = 200ms$		$t^2_{b,ms} = 225ms$		$t^2_{b,ms} = 250ms$		$t^2_{b,ms} = 275ms$	
$\mathbf{t^1_{b,ms}}$ (in ms)	c	$\mathbf{t^1_{b,ms}}$ (in ms)	c	$\mathbf{t^1_{b,ms}}$ (in ms)	c	$\mathbf{t^1_{b,ms}}$ (in ms)	c
25	0.88	50	0.91	75	0.91	100	0.92
50	0.89	75	0.88	100	0.93	125	0.89
75	0.96	100	0.92	125	0.85	150	0.85
100	0.89	125	0.87	150	0.90	175	1.00
125	0.99	150	0.98	175	0.95	200	0.95
150	0.99	175	> 1	200	0.97	225	> 1
175	> 1	200	> 1	225	> 1	250	> 1

Table A.2.3: Dependence of threshold for SBP on the difference $t^2_{b,ms} - t^1_{b,ms}$. Choice of parameters: $s = 0.3$, $d = 0.7$, $R^{const}_D = 0.2$, $\tau = 0.0001$.

$t^2_{b,ms} = 200ms$		$t^2_{b,ms} = 225ms$		$t^2_{b,ms} = 250ms$		$t^2_{b,ms} = 275ms$	
$\mathbf{t^1_{b,ms}}$ (in ms)	c	$\mathbf{t^1_{b,ms}}$ (in ms)	c	$\mathbf{t^1_{b,ms}}$ (in ms)	c	$\mathbf{t^1_{b,ms}}$ (in ms)	c
25	0.75	50	0.77	75	0.81	100	0.79
50	0.75	75	0.75	100	0.80	125	0.79
75	0.82	100	0.83	125	0.77	150	0.78
100	0.80	125	0.80	150	0.78	175	0.88
125	0.93	150	0.88	175	0.86	200	0.87
150	0.87	175	> 1	200	0.93	225	> 1
175	> 1	200	> 1	225	> 1	250	> 1

Table A.2.4: Dependence of threshold for SBP on the difference $t^2_{b,ms} - t^1_{b,ms}$. Choice of parameters: $s = 0.3$, $d = 0.7$, $R^{const}_D = 0.4$, $\tau = 0.0001$.

can be observed that even though the threshold does not depend on $t^2_{b,ms}$ monotonously, it has a tendency to decrease if $t^2_{b,ms}$ and with it the difference $t^2_{b,ms} - t^1_{b,ms}$ increases. In fact, the difference seems to be more important than the actual values.

$t^1_{b,ms} = 50ms$		$t^1_{b,ms} = 75ms$		$t^1_{b,ms} = 100ms$		$t^1_{b,ms} = 125ms$	
$\mathbf{t^2_{b,ms}}$ (in ms)	c	$\mathbf{t^2_{b,ms}}$ (in ms)	c	$\mathbf{t^2_{b,ms}}$ (in ms)	c	$\mathbf{t^2_{b,ms}}$ (in ms)	c
75	0.95	100	0.97	125	0.97	150	0.98
100	0.93	125	0.94	150	0.95	175	0.96
125	0.91	150	0.93	175	0.94	200	0.95
150	0.90	175	0.92	200	0.93	225	0.93
175	0.89	200	0.91	225	0.92	250	0.93
200	0.89	225	0.90	250	0.91	275	0.92
225	0.88	250	0.89	275	0.90	300	0.91

Table A.2.5: Dependence of threshold for SBP on the difference $t^2_{b,ms} - t^1_{b,ms}$. Choice of parameters: $s = 0.3$, $d = 0.7$, $R^{const}_D = 0.2$, $\tau = 0.0001$.

As before, comparing tables A.2.5 and A.2.6 shows that increasing R^{const}_D seems to generally lower the threshold values.

Tables A.2.7 and A.2.8 illustrate the dependence of the threshold on $t^1_{b,ms}$ for several fixed values of $t^2_{b,ms}$. Again, they differ in the value of R^{const}_D. It can be observed that as $t^1_{b,ms}$ increases and therefore the difference $t^2_{b,ms} - t^1_{b,ms}$ decreases the threshold values increase, a result that agrees with the previous one. As before, the difference seems to be more

$t_{b,ms}^1 = 50ms$		$t_{b,ms}^1 = 75ms$		$t_{b,ms}^1 = 100ms$		$t_{b,ms}^1 = 125ms$	
$\mathbf{t_{b,ms}^2}$ (in ms)	c	$\mathbf{t_{b,ms}^2}$ (in ms)	c	$\mathbf{t_{b,ms}^2}$ (in ms)	c	$\mathbf{t_{b,ms}^2}$ (in ms)	c
75	0.93	100	0.95	125	0.96	150	0.97
100	0.90	125	0.92	150	0.93	175	0.94
125	0.87	150	0.89	175	0.91	200	0.92
150	0.85	175	0.88	200	0.89	225	0.91
175	0.84	200	0.86	225	0.88	250	0.89
200	0.83	225	0.85	250	0.87	275	0.88
225	0.83	250	0.85	275	0.86	300	0.87

Table A.2.6: Dependence of threshold for SBP on the difference $t_{b,ms}^2 - t_{b,ms}^1$. Choice of parameters: $s = 0.3$, $d = 0.7$, $R_D^{const} = 0.4$, $\tau = 0.0001$.

important than the actual values.

$t_{b,ms}^2 = 200ms$		$t_{b,ms}^2 = 225ms$		$t_{b,ms}^2 = 250ms$		$t_{b,ms}^2 = 275ms$	
$\mathbf{t_{b,ms}^1}$ (in ms)	c	$\mathbf{t_{b,ms}^1}$ (in ms)	c	$\mathbf{t_{b,ms}^1}$ (in ms)	c	$\mathbf{t_{b,ms}^1}$ (in ms)	c
25	0.75	50	0.77	75	0.81	100	0.79
50	0.75	75	0.75	100	0.80	125	0.79
75	0.82	100	0.83	125	0.77	150	0.78
100	0.80	125	0.80	150	0.78	175	0.88
125	0.93	150	0.88	175	0.86	200	0.87
150	0.87	175	> 1	200	0.93	225	> 1
175	> 1	200	> 1	225	> 1	250	> 1

Table A.2.7: Dependence of threshold for SBP on the difference $t_{b,ms}^2 - t_{b,ms}^1$. Choice of parameters: $s = 0.3$, $d = 0.7$, $R_D^{const} = 0.2$, $\tau = 0.0001$.

Comparing tables A.2.7 and A.2.8 shows that increasing R_D^{const} seems to generally lower the threshold values. For $R_D^{const} = 0.2$ for some combinations of return times the threshold is beyond the range of the varied reflection coefficient (indicated by > 1 in the table). For $R_D^{const} = 0.4$, however, threshold values are significantly below one for all studied combinations of return times.

$t_{b,ms}^2 = 200ms$		$t_{b,ms}^2 = 225ms$		$t_{b,ms}^2 = 250ms$		$t_{b,ms}^2 = 275ms$	
$\mathbf{t_{b,ms}^1}$ (in ms)	c	$\mathbf{t_{b,ms}^1}$ (in ms)	c	$\mathbf{t_{b,ms}^1}$ (in ms)	c	$\mathbf{t_{b,ms}^1}$ (in ms)	c
25	0.80	50	0.83	75	0.85	100	0.86
50	0.83	75	0.85	100	0.87	125	0.88
75	0.86	100	0.88	125	0.89	150	0.90
100	0.89	125	0.91	150	0.92	175	0.92
125	0.92	150	0.93	175	0.94	200	0.94
150	0.95	175	0.95	200	0.96	225	0.96
175	0.97	200	0.98	225	0.98	250	0.98

Table A.2.8: Dependence of threshold for SBP on the difference $t_{b,ms}^2 - t_{b,ms}^1$. Choice of parameters: $s = 0.3$, $d = 0.7$, $R_D^{const} = 0.4$, $\tau = 0.0001$.

ΔA_c	change in cross-sectional area	P^b	backward pressure
ΔP	change in blood pressure	P^f	forward pressure
ΔV	change in blood volume	P_k^{in}	pressure generated by heart at time k
η	viscosity of blood		
Γ	reflection coefficient	P_0	reflectionless pressure
ρ	density of blood	P_k	pressure at time k
τ	time step size	PP	pulse pressure
A_c	cross-sectional area of vessel	PWV	pulse wave velocity
AI	augmentation index	Q	blood flow
AP	late systolic boost	Q^b	backward flow
AV	aortic valve	Q^f	forward flow
bpm	beats per minute	Q_0	reflectionless flow
C	compliance	R	resistance
c_0	pulse wave velocity	r	tube radius
C_A	area compliance	R^{av}	reflection coefficient at aortic valve
DBP	diastolic blood pressure		
dI_w	wave intensity	R_D	reflection coefficient at distal reflection site
ECG	electrocardiogram		
I	inertance	RM	reflection magnitude
k	time variable	RS	distal reflection site
L	tube length	SBP	systolic blood pressure
$mmHg$	millimeters of mercury	t_b	number of time steps for pressure impulse to go to reflection site and back to measuring site
MS	measuring site		
P	blood pressure		

t_f	number of time steps for pressure impulse to go to aortic valve		ms
$t_{b,ms}$	return time from distal reflection site in ms	U	flow velocity
$t_{f,ms}$	travel time to the aortic valve in	Z	input impedance
		Z_0	characteristic impedance

Bibliography

[1] R.P. Agarwal. *Difference Equations and Inequalities*. Marcel Dekker Inc., New York, 1992.

[2] J. Alastruey, K.H. Parker, J. Peiro, and S.J. Sherwin. Analysing the pattern of pulse waves in arterial networks: a time-domain study. *Journal of Engineering Mathematics*, 64:331–351, 2009.

[3] A. Bauer, B. Hametner, T. Weber, and S. Wassertheurer. Method comparison and validation of the determination of ejection duration from oscillometric measurements. In *Preprints of the 9th Vienna International Conference on Mathematical Modelling*, Vienna, Austria, February 2018.

[4] D.S Berger, J.K.-J. Li, W.K. Laskey, et al. Repeated reflection of waves in the systemic arterial system. *American Journal of Physiology - Heart and Circulatory Physiology*, 264:H269–H281, 1993.

[5] J.C. Bramwell and A.V. Hill. Velocity of transmission of the pulse-wave. *The Lancet*, 199:891–892, 1922.

[6] E. Braunwald, S.J. Sarnoff, and W.N Stainsby. Determinants of duration and mean rate of ventricular ejection. *Circulation Research*, 6:319–325, 1953.

[7] R. Burattini and G Gnudi. Computer identification of models for the arterial tree input impedance: Comparison between two new simple models and first experimental results. *Medical and Biological Engineering and Computing*, 20:134–144, 1982.

[8] R. Burattini, G.G. Knowlen, and K.B. Campbell. Two arterial effective reflecting sites may appear as one to the heart. *Circulation Research*, 68:85–99, 1991.

[9] K.B. Campbell, L.C. Lee, H.F. Frasch, and A. Noordergraaf. Pulse reflection sites and effective length of the arterial system. *American Journal of Physiology - Heart and Circulatory Physiology*, 256:H1684–H1689, 1989.

[10] C.G. Caro et al. *The Mechanics of the Circulation*. Cambridge University Press, 2012.

[11] S.N. Elaydi. *An Introduction to Difference Equations*. Springer, New York, 1996.

[12] L. Formaggia, D. Lamponi, and A. Quarteroni. One-dimensional models for blood flow in arteries. *Journal of Engineering Mathematics*, 47:251–276, 2003.

[13] L. Formaggia, A. Quarteroni, and A. Veneziani, editors. *Cardiovascular Mathematics*. Springer, Milano, 2009.

[14] O. Frank. Die Grundform des arteriellen Pulses. *Zeitschrift für Biologie*, 37:483–526, 1899.

[15] S. Hildebrandt. *Analysis 1*. Springer, Berlin Heidelberg, 2nd edition, 2006.

[16] R. Kelly, C. Hayward, A. Avolio, and M.F. O'Rourke. Noninvasive determination of age-related changes in the human arterial pulse. *Circulation*, 80:1652–1659, 1989.

[17] U. Krause and T. Nesemann. *Differenzengleichungen und diskrete dynamische Systeme*. de Gruyter, Berlin/Boston, 2nd edition, 2012.

[18] C. Langenberg, R. Hardy, D. Kuh, and M.E.J. Wadsworth. Influence of height, leg and trunk length on pulse pressure, systolic and diastolic blood pressure. *Journal of Hypertension*, 21:537–543, 2003.

[19] R.D. Latham, N. Westerhof, J.P. Giolma, and S.A. Altobelli. Regional wave travel and reflections along the human aorta: a study with six simultaneous micromanometric pressures. *Circulation*, 1985.

[20] J.K.-J. Li. Time domain resolution of forward and reflected waves in the aorta. *IEEE Transactions on Biomedical Engineering*, 33(8):783–785, 1986.

[21] R.K. Mallik. Solutions of linear difference equations with variable coefficients. *Journal of Mathematical Analysis and Applications*, 222:79–91, 1998.

[22] S. Mendis, P. Puska, and B. Norrving, editors. *Global Atlas on cardiovascular disease prevention and control*. World Health Organization, 2011.

[23] C.J. Mills, I.T. Gabe, J.H. Gault, et al. Pressure-flow relationships and vascular impedance in man. *Cardiovascular Research*, 4:405–417, 1970.

[24] S. Mohanta, C. Yin, C. Weber, et al. Aorta atherosclerosis lesion analysis in hyperlipidemic mice. *Bio-protocol*, 6(11):e1833, 2016.

[25] J.P. Murgo, N. Westerhof, J.P. Giolma, et al. Aortic input impedance in normal man: Relationship to pressure wave forms. *Circulation*, 1980.

[26] J.P. Mynard and J.J. Smolich. Wave potential and the one-dimensional windkessel as a wave-based paradigm of diastolic arterial hemodynamics. *American Journal of Physiology - Heart and Circulatory Physiology*, 307:H307–H318, 2014.

[27] W.W. Nichols, M.F. O'Rourke, and C. Vlachopoulos. *McDonald's Blood Flow in Arteries, Sixth Edition: Theoretical, Experimental and Clinical Principles*. 2011.

[28] OERservices: Anatomy and physiology II. Circulatory pathways. Online resource: https://courses.lumenlearning.com/suny-ap2/chapter/circulatory-pathways/. Accessed: March 1, 2018.

[29] M.F. O'Rourke. The arterial pulse in health and disease. *American Heart Journal*, 82:687–702, 1971.

[30] M.F. O'Rourke and M.G. Taylor. Input impedance of the systemic circulation. *Circulation Research*, 20:365–380, 1967.

[31] G.L. Papageorgiou and N.B. Jones. Wave reflection and hydraulic impedance in the healthy arterial system: a controversial subject. *Medical and Biological Engineering and Computing*, 26:237–242, 1988.

[32] H.-C. Pape et al., editors. *Physiologie*. Georg Thieme Verlag, 7th edition, 2014.

[33] K. H. Parker. Arterial reservoir pressure, subservient to the McDonald lecture, Artery 13. *Artery Research*, 7:171–185, 2013.

[34] K.H. Parker. An introduction to wave intensity analysis. *Medical and Biological Engineering and Computing*, 47:175–188, 2009.

[35] K.H. Parker. The reservoir-wave model. *Artery Research*, 18:87–101, 2017.

[36] S. Parragh, B. Hametner, M. Bachler, et al. Non-invasive wave reflection quantification in patients with reduced ejection fraction. *Physiological Measurement*, 36:179–190, 2015.

[37] P. Segers, J. De Backer, D. Devos, et al. Aortic reflection coefficients and their association with global indexes of wave reflection in healthy controls and patients with Marfan's syndrome. *American Journal of Physiology - Heart and Circulatory Physiology*, 290(6):H2385–H2392, 2006.

[38] S.J. Sherwin, V. Franke, J. Peiro, and K.H. Parker. One-dimensional modelling of a vascular network in space-time variables. *Journal of Engineering Mathematics*, 47:217–250, 2003.

[39] Y. Shi, P. Lawford, and R. Hose. Review of zero-d and 1-d models of blood flow in the cardiovascular system. *BioMedical Engineering OnLine*, 10(33), 2011. doi:10.1186/1475-925X-10-33.

[40] P. Sipkema, N. Westerhof, and O.S. Randall. The arterial system characterised in the time domain. *Cardiovascular Research*, 14:270–279, 1980.

[41] H. Smulyan, S.J. Marchais, B. Pannier, et al. Influence of body height on pulsatile arterial hemodynamic data. *Journal of the American College of Cardiology*, 31:1103–1109, 1998.

[42] Statistik Austria. Todesursachen gesamt. Online resource: http://www.statistik.at/web_de/statistiken/menschen_und_gesellschaft/gesundheit/todesursachen/todesursachen_im_ueberblick/index.html. Accessed: April 13, 2018.

[43] N. Stergiopulos, B.E. Westerhof, and N. Westerhof. Total arterial inertance as the fourth element of the windkessel model. *American Journal of Physiology - Heart and Circulatory Physiology*, 276:H81–H88, 1999.

[44] L. Stoner, J.M. Young, and S. Fryer. Assessments of arterial stiffness and endothelial function using pulse wave analysis. *International Journal of Vascular Medicine*, 2012, 2012.

[45] M.G. Taylor. An approach to an analysis of the arterial pulse wave I. Oscillations in an attenuating line. *Physics in Medicine and Biology.*, 1:258–269, 1957.

[46] M.G. Taylor. An approach to an analysis of the arterial pulse wave II. Fluid oscillations in an elastic pipe. *Physics in Medicine and Biology*, 1:321–329, 1957.

[47] M.G. Taylor. The influence of the anomalous viscosity of blood upon its oscillatory flow. *Physics in Medicine and Biology*, 3:273–290, 1959.

[48] F.N. van den Vosse and N. Sterigopulos. Pulse wave propagation in the arterial tree. *Annual Review of Fluid Mechanics*, 43:467–499, 2011.

[49] J.J. Wang and K.H. Parker. Wave propagation in a model of the arterial circulation. *Journal of Biomechanics*, 37:457–470, 2004.

[50] T. Weber, J. Auer, M.F. O'Rourke, et al. Arterial stiffness, wave reflections, and the risk of coronary artery disease. *Circulation*, 109:184–189, 2004.

[51] B.E. Westerhof, J.P van den Wijngaard, J.P. Murgo, and N. Westerhof. Location of a reflection site is elusive. *Hypertension*, 52:478–483, 2008.

[52] N. Westerhof, J.-W. Lankhaar, and B.E. Westerhof. The arterial windkessel. *Medical and Biological Engineering and Computing*, 47:131–141, 2009.

[53] N. Westerhof, P. Sipkema, G.C. van den Bos, and G. Elzinga. Forward and backward waves in the arterial system. *Cardiovascular Research*, 6:648–656, 1972.

[54] N. Westerhof, N. Stergiopulos, and M.I.M Noble. *Snapshots of Hemodynamics*. Springer, 2005.

[55] N. Westerhof and B.E. Westerhof. Crosstalk proposal: Forward and backward pressure waves in the arterial system do represent reality. *The Journal of Physiology*, 591(5):1167–1169, 2013.

[56] I.B. Wilkinson, S.A. Fuchs, I.M Jansen, et al. Reproducibility of pulse wave velocity and augmentation index measured by pulse wave analysis. *Journal of Hypertension*, 16:2079–2084, 1998.

[57] I.B. Wilkinson, H. MacCallum, L. Flint, et al. The influence of heart rate on augmentation index and central arterial pressure in humans. *The Journal of Physiology*, 525.1:263–270, 2000.

[58] I.B. Wilkinson, N.H. Mohammad, S. Tyrrell, et al. Heart rate dependency of pulse pressure amplification and arterial stiffness. *American Journal of Hypertension*, 15:24–30, 2002.

[59] J.R. Womersley. Oscillatory flow in arteries: the constrained elastic tube as a model of arterial flow and pulse transmission. *Physics in Medicine and Biology*, 2:178–187, 1957.